A systems approach to dissecting immune gene regulatory networks in the modulation of brain function

A Dissertation Presented

By

Yang Xu

Submitted to the Faculty of the

University of Massachusetts Graduate School of Biomedical Sciences, Worcester

In partial fulfillment of the requirements for the degree of

DOCTOR OF PHILOSOPHY

October, 20th 2017

Biomedical Sciences

A systems approach to dissecting immune gene regulatory networks in the modulation of brain function

A Dissertation Presented

By

Yang Xu

This work was undertaken in the Graduate School of Biomedical Sciences

(Interdisciplinary Graduate Program)

Under the mentorship of

Vladimir Litvak, Thesis Advisor

Leslie Berg, Member of Committee

Egil Lien, Member of Committee

Ann Rittenhouse, Member of Committee

Juan Fuxman Bass, External Member of Committee

Timothy Kowalik, Chair of Committee

Anthony Carruthers, Ph.D.

Dean of the Graduate School of Biomedical Sciences

October, 20th 2017

Dedication

This thesis is dedicated to my parents, Ping and Zhenhua, and my fiancé, Kostas, for their endless support, encouragement and patience.

Acknowledgements

An exciting moment after any important milestone in life is to look back in the past and commemorate all the people who supported you to achieve your goal.

First off, I would like to express my utmost gratitude to my thesis Advisor, Vladimir Litvak, for his guidance, patience, and encouragement throughout my four years in his lab. Vladimir was always encouraging during these years and willing to discuss not only scientific topics and but also personal concerns. It goes without saying that the tremendous scientific and professional support of my collaborator, Professor Jonathan Kipnis, also played a catalytic role in the success of my studies and is sincerely appreciated. I also want to express my greatest gratitude to Professor Leslie Berg, who was the first mentor/advisor I had when I started my PhD at the University of Massachusetts. Leslie has been extremely supportive during my graduate studies and without her precious pieces of advice my career path would have been totally different.

I would like to express the deepest appreciation to my family, as without their permanent support I would have never been able to complete my studies. In addition, many thanks go to my dearest friends Larisa, Alejandro, Juan, Katherine, Vana, Jocelyn, Jill, Monika, Will, Gaia, Maria, Ioannis, Nasia and Nikos for the fun time I had with them here in Massachusetts.

Of high importance was also the support of my past group mate, Aaron, and the whole crew of the Kipnis and the Brass labs. The past and current members of the Brass lab have been there for me constantly and without them

my PhD studies would be very lonely. Last but not least, I wanted to specifically thank Noel, Jim, Tony and Ioanna from the Kipnis lab for the long scientific discussion we had over the years. These discussions were the recipe for the great scientific work we did and published together.

I would also like to acknowledge the big support from the MaPS Department. MaPS has really provided a world-class environment for me to grow both professionally and personally. My acknowledgements would not be completed without expressing my sincere appreciation to the members of my final exam committee: Prof. Tim Kowalik, Prof. Leslie Berg, Prof. Egil Lien, Prof. Ann Rittenhouse, Prof. Juan Fuxman Bass.

Abstract

Although the central nervous system was long perceived as the ivory tower without immune entities, there is growing evidence that the immune and nervous systems are intimated connected. These two systems have been shown to communicate both cellularly and molecularly under physiological and pathological conditions. Despite our increasing understanding of the interplay between these two systems, there are still numerous open questions. In this thesis, I address such unanswered questions related to: the role of microglia and their mechanism in contributing to pathologies in Rett syndrome; the beneficial effects of T-cell secreted cytokines in supporting social brain function; the evolutionary link of the interactions between the nervous and immune systems; the transcription regulation of a subset of microglia population in common neurodegenerative diseases.

Collectively, the current thesis is focused on the joint frontier of bioinformatics and experimental work in neuroimmunology. A multifaceted approach, that includes transcriptomics, genomics and other biomolecular modules, was implemented to unearth signaling pathways and mechanisms underlying the presenting biological phenomena. The findings of this thesis can be summarized as follows: 1) MeCP2 acts as a master regulator in the transcriptional repression of inflammatory stimuli in macrophages; 2) T-cell secreted IFN-γ supports social brain function through an evolutionally conserved interaction between the immune and nervous systems; 3) The APOE-TREM2

pathway regulates the microglia phenotype switch in neurodegenerative diseases. Provided that recent technologies allow for readily manipulating the immune system, the findings presented herein may create new vistas for therapeutic interventions in various neurological disorders.

Table of Contents

List of Figures

CHAPTER I INTRODUCTION

Overview of neuro-immune interactions

The central nervous system (CNS), composed of the brain and spinal cord, was long considered to be an immune privileged unit that is protected by the blood-brain-barrier and blood-cerebrospinal barrier. The interaction of the immune and nervous systems was often mentioned in the context of neuroinflammation, degeneration, injury and autoimmunity. As such, the detection of immune entities was often perceived as a hallmark of pathology (Villoslada et al., 2008, Shechter et al., 2013, Schwartz and Kipnis, 2011).

It has recently become clear that the immune system is also crucial for tissue maintenance and homeostasis (Ricklin et al., 2010). Consistent immune surveillance in the CNS does exist and although it is tightly regulated, it depends on specialized sentinels within the anatomical niches (Brynskikh et al., 2008, Derecki et al., 2012, Filiano et al., 2016, Kipnis, 2016, Schwartz and Kipnis, 2011). The CNS contains a large repertoire of immune cells, including the parenchymal resident microglia, macrophages, dendritic cells and T cells in the meninges, choroid plexus and perivascular spaces (Herz et al., 2017). Together, these immune cells can mount robust responses to eliminate threats and facilitate tissue recovery when necessary. Furthermore, the immune and nervous systems interact intimately. Communication between the two systems is essential for proper brain function, and endeavors to understand this complex dialogue will

open new doors to treating neurological disorders through targeting the wide repertoire of immune cells and molecules.

Microglia function under homeostasis and disease

Microglia are the brain's most prominent immune cells and one of the most well studied cells in terms of its effect on neurons (Schafer et al., 2012, Paolicelli et al., 2011, Zhan et al., 2014). Situated within the brain parenchyma, microglia serve as the tissue-resident macrophages in the CNS and participate in important processes in both brain development and functions. Such processes include constructions of neuronal circuits, monitor of synaptic function and control of synaptogenesis (Prinz et al., 2011, Roumier et al., 2004, Schafer et al., 2012). Developed from the primitive yold-sac derived macrophages, microglia colonize the brain during early embryonic development, and proliferate locally within the parenchyma without penetration from peripheral monocytes (Gomez Perdiguero et al., 2015, Ajami et al., 2007, Ginhoux et al., 2010).

Microglia play a significant role in synaptic pruning in both development and maintenance of homeostasis in adulthood. Synaptic pruning can be attributed to microglia receptors, such as CX3CR1 and CR3, or TREM2/DAP12 recognizing ligands on the neuronal membrane (Hoshiko et al., 2012, Paolicelli et al., 2011, Schafer et al., 2012). During postnatal development, microglia have been shown to be critical in sculpting the visual circuit by pruning synapses of the developing lateral geniculate nucleus via CR3-mediated complement process

(Schafer et al., 2012). Disruption of microglia-specific CR3/C3 signaling causes impaired synaptic pruning and connectivity (Schafer et al., 2012). Similarly, such interaction between microglia-specific complement receptor and its ligands on developing neurons is also observed in CX3CR1-mediated synaptic pruning. Mice lack *Cx3cr1* exhibit reduced number of microglia and decreased synapse pruning (Paolicelli et al., 2011). A recent study (Zhan et al., 2014) revealed the functional effects of microglia Cx3cr1-mediated synaptic pruning on brain circuitry. CX3CR1-deficient mice exhibited weaker synaptic transmission, decreased functional connectivity, and deficits in social behavior associated with autism spectrum disorder (Zhan et al., 2014).

To understand the roles of microglia beyond development, researchers have employed both genetic and pharmacological approaches to delete microglia from the adult brain. Parkhurst and co-workers used an $Cx3cr1^{CreER/+}::R26^{iDTR/+}$ genetic mouse model to specifically delete microglia upon diphtheria toxin administration (Parkhurst et al., 2013), while Elmore et al. followed an alternative approach to eliminate microglia using a colony-stimulating factor 1 receptor (CSF1R) antagonist (Elmore et al., 2014). However, these drastic approaches of eliminating microglia in short term produced mild phenotypes (Parkhurst et al., 2013) or no behavioral effects whatsoever (Elmore et al., 2014). Interestingly, microglia depletion longer-term using genetic approaches resulted in synapse degeneration and visual deficits (Wang et al., 2016). These studies suggest that

microglia play a major role in normal brain physiology in both development and adulthood (Figure I-1).

Microglia constantly sample their environment by their dynamic processes, and can be vulnerable to subtle changes/stimuli in the surrounds and become dysfunctional in CNS diseases. The role of microglia in CNS pathologies has been well-documented. For instance, obsessive-compulsive grooming in mice and Rett syndrome have been associated with mutations in HoxB8 (Chen et al., 2010) and MeCP2 (Cronk et al., 2015, Derecki et al., 2012), respectively. These findings demonstrate that microglia dysfunction contributes significantly to structural and functional deficiencies of the CNS. Intriguingly, activation and proliferation of microglia are reported in several neurodegenerative conditions, including Alzheimer's disease (AD) and Amyotrophic lateral sclerosis (ALS). Recent studies showed that elimination of these dysfunctional microglia is beneficial, and prevented synaptic degeneration (Hong and Stevens, 2016) and mitigated cognitive impairments independent of Aβ levels.

In summary, numerous seminal studies have provided evidence about the distinct roles of microglia in synaptic pruning and sculpting brain circuitry in development and maintenance of homeostasis in adulthood. On the other hand, it has also been demonstrated that microglia become dysfunctional and have a delirious impact under conditions of neuronal death and aging-mediated inflammation (Figure I-1).

In the current thesis, Chapter II describes microglia and macrophage-intrinsic signaling pathways that are disturbed in a Rett syndrome mouse model. Our study provided the mechanism underlying microglia and macrophage phenotypes in the absence of MeCP2. Similar to Chapter II, Chapter IV addresses microglia phenotype switching under neurodegenerative conditions.

Immune secreted molecules on behavior

The adaptive immune system, particular through T cells, affects brain function under physiological conditions. Previous work demonstrated that severe combined immunodeficiency (SCID) mice, which lack T cells and B cells, show deficits in several learning and memory behavioral tasks (Derecki et al., 2010). Notably, learning is not affected in mice that specifically lack B cells (Radjavi et al., 2014), but can be rescued by reconstituting the T cells compartment (Brynskikh et al., 2008). These observations indicated the specific role of T cells on cognition. Other studies have implicated T cell influence on other brain functions, and lack of T cells in mice resulted in heightened susceptibility in a model of post-traumatic stress disorder (Cohen et al., 2006), compulsive grooming (Rattazzi et al., 2013) and impaired maternal behavior (Quinnies et al., 2015).

A question that can be legitimately posed is how T cells affect behavior and brain functions under physiological conditions. Although the mechanism of underlying T-cell influence on normal brain function was unknown before we

published our study, seminal studies had provided great insights on the ability of meningeal T cells in affecting behavior in healthy brain. Pharmacological inhibition of T-cell homing (anti-VLA4 antibody) to meninges reproduced learning deficits as seen in SCID mice (Derecki et al., 2010). Meningeal T cells situated in the space between the pia, arachnoid, and dura, although proximate, they do not enter the brain parenchyma under homeostasis (Figure I-2) (Derecki et al., 2010, Filiano et al., 2016). How meningeal T cells affect brain function without entering the brain tissue still remains enigmatic. One plausible scenario is that T cell-secreted soluble cytokines (such as IFN-γ, IL4, IL13, IL17, IL10 and TGF-β) can directly target neurons and other cells in the brain through paracrine signaling. Based on this, the work of this thesis attempts to address the effect of T-cell-mediated cytokine signaling on brain behavior.

A pathogen-versus-host competition

The effect of immune cells and their secreted molecules on human's behavior is well studied in the context of sickness behavior. When pathogens invade the body, they trigger robust immune responses, such as activation of innate immune cells and lymphocytes, and increased production of proinflammatory cytokines (Bluthe et al., 2000, Dantzer, 2009, Kelley et al., 2003). As a result, our behavior also changes in order to promote clearance of pathogens and increases the chance for host survival. Such behavior changes include: social withdrawal, increased sleep and decreased appetite etc. (Hart, 1988, Shakhar and Shakhar,

2015). This collection of behaviors is called sickness behavior and constitutes one of the most prominent behavioral response to an infection. Several theories have been proposed previously regarding the evolution of sickness behavior. A dominant theory in the field was proposed by Hart, who suggested that sickness behavior is not a maladaptive response to infection but rather an organized, evolved behavioral strategy to combat the infection (Hart, 1988). Recently, a contesting theory was proposed claiming that sickness behavior is a result of altruism and kin selection, and provides an evolutionary advantage to survival of the herd (Shakhar and Shakhar, 2015). Intriguingly, one study reported that if pathogen infections do not cause apparent or no symptoms of the hosts, there is increased social interaction mediated by the pathogen to facilitate transmission, as opposed to social withdrawal being a component of sickness behavior (Reiber et al., 2010). If pathogen-driven social aggregation cannot fully explain social withdrawal caused by pathogen infection, in Chapter III we propose a plausible theory wherein pathogen-driven prosocial and host induced sickness behavior are evolutionary connected and can be regarded as the result of a ‘arms-race’ between the host and pathogens (Filiano et al., 2017, Filiano et al., 2016, Kipnis, 2016).

Systems biology approaches

Biology has advanced explosively since the discovery of DNA and protein in the early 1960s. Biologists have examined the functions and properties of each part

painstakingly, and thanks to that, our understanding on these individual units such as cell types, transcription factors and proteins has increased significantly (Lienert et al., 2014). However, little is known about the activities across the whole organism system. Understanding the output of an organism requires systems-level analyses as the same protein/gene may not function the same across all cell types and conditions, and the precise function of these individual units are dependent on the microenvironment of the organism such as cell types, spatiotemporal dynamics, and epigenetic landscape (Ideker et al., 2001). Advances in molecular biology, particularly in genome sequencing and high-throughput technologies, have made it feasible to measure a good swatch of this complexity in a workable way, which has boosted the development of a new field in biology- systems biology. Systems approach to an area can be defined as a broad strategy to understand certain outputs as a whole (Davis et al., 2017). It focuses on understanding a system's structure and dynamics, behavior and relationships of all the elements (Ideker et al., 2001). This powerful approach has resulted in the discovery of previously unknown relationships and phenomena and provided important insights into human diseases and mouse models of diseases (Davis et al., 2017, Ideker et al., 2001, Kitano, 2002).

Systems approach in immunology

The most feasible application in systems biology research is to focus on signal transduction cascades and molecules to provide system-level insights. One of

the major successes in systems immunology is to elucidate signaling pathways that are important in the immune system (Davis et al., 2017). This has resulted not only in better understanding of these signaling pathways, but also in the creation of efficient, reliable models to mimic and predict important aspects of innate immune responses (Litvak et al., 2009, Litvak et al., 2012, Ramsey et al., 2008, Schoggins et al., 2014). This approach has become possible owing to the large amount of data generated per experiment and the corresponding advances in sequencing technology. In combination, it has greatly enhanced our understanding on chromatin and gene regulation, protein interactions and complex gene regulatory networks controlling the whole system (Lienert et al., 2014).

Tools used in systems approaches

The generation of genomic and genomic-wide expression data comes with the important challenge to develop robust tools to analyze such data, and to translate them so that they provide an expansive view of the underlying biological phenomena. Initial work in this field focused on the development of techniques for accurate identification of differentially expressed genes using various statistical methods. However, the main difficulty does not lie in the identification of these genes, but in the interpretation of the underlying processes. Trying to understand individual genes from the significant list of differentially expressed genes is laborious and ineffective as the significant lists from different studies

can vary greatly. Moreover, it can be confusing when a pathway of interest shows moderate effect that does not appear in the top of the list (Tian et al., 2005). Therefore, recent efforts have focused on the development of robust tools and methods to analyze biological pathways rather than individual gene functions.

Two main types of approaches for analyzing biological pathways are discussed in the literature: 1) the over-representation approach using Gene Ontology (GO) and 2) the Gene Set Enrichment Analysis (GSEA).

In the GO approach, predefined pathways representing various biological process, molecular function and cellular components, are used to identify significant pathways that are overly represented in the biological condition under study (Khatri and Draghici, 2005, Khatri et al., 2002). In this approach, the statistically significant differential expression gene list is first sorted out by one of the many statistical methods available. Then, the significant list, containing the top genes correlated to the biological condition under study, is examined against all GO categories in the database. To examine the evidence of association with any GO category, a number of statistical models, including Fisher's exact test based on the hypergeometric distribution (Cho et al., 2001) or its large-sample approximation X^2 test, are typically implemented (Man et al., 2000). Since its development, this approach has found favor among biologists and has been widely applied for functional profiling in many microarray and genome-wide expression studies (Goeman et al., 2003, Ashburner et al., 2000, Oshlack et al.,

2010). Currently, there are more than 20 existing tools (stand-alone or web-based) for this type of analysis, most often using GO as the source of gene sets. Popular tools include David (Huang da et al., 2009), Gorilla (Eden et al., 2009), g:Profiler (Reimand et al., 2016) and BiNGO (Maere et al., 2005). Despite its wide application, this approach has a few major drawbacks, such as 1) the significant gene list may be too short to use in ontological analysis due to the modest biological differences and the inherent noise of genome-wide expression technology; 2) the gene list may be too long and the difference between the more significant and less significant genes is substantial. Interpretation of these cases can be inaccurate and ad hoc, since the order of the genes is not taken into consideration; 3) when independent groups study the same biological phenomena, the gene list from these studies may be inconsistent.

To address the limitations of the GO approach, an alternative and more robust analytical method-Gene Set Enrichment Analysis (GSEA) was developed (Mootha et al., 2003, Subramanian et al., 2005). This approach takes into consideration the pathway signature in all of the genes in an experiment and provides a more accurate calculation of the statistical significance by permuting the class labels. GSEA is the main tool used in this work for genome-wide expression analysis. This method is implemented to predict signaling pathways disturbed in the biological systems, and to integrate transcriptomes derived from different platforms. In combination with additional information, such as genetics

and gene-regulatory networks, GSEA offers potential insights into the logic of dynamic neuroimmune networks at a systems level.

The current dissertation is focused on the joint frontier of bioinformatics and experimental work in the field of neuroimmunology. Transcriptomes downloaded from publicly available databases or generated in our research groups were used for pathways analysis, promoter analysis and construction of gene regulatory networks. The objective of this research is two-fold: 1) The development of a transcriptome analysis pipeline that improves our mechanistic understanding of the biological system of interest and the interactions of its biomolecular modules. 2) The use of a systems approach to study the complexity of biological systems by building and studying them in a context isolated from their high degree of natural interconnectivity. This allows for efficiently and inexpensively generating testable hypotheses to drive new sets of experiments.

The ensuing thesis is organized as follows:

- Chapter I discusses the emerging questions in the field of neuroimmunology and introduces an approach to address these questions.
- Chapter II presents an RNA-seq analysis and experimental validation of microglia and macrophages phenotypes disturbed in a Rett syndrome mouse model, MeCP2-null mice. A previous study had demonstrated that brain resident microglia contribute to pathologies in the MeCP2-null mice.

However, the mechanism of how microglia become dysfunctional and contribute to Rett phenotypes is unknown. To define the functional role of MeCP2 in microglia and macrophages (which were also found to be reduced in numbers in certain tissues), we performed global gene-expression profiling and pathway analysis. We show that macrophages responses to three stimuli are all intrinsically impaired in the absence of MeCP2, suggesting MeCP2 as a master regulator in gene expression in macrophages.

- In Chapter III, the communication of T cell-secreted cytokines and brain-circuit mediated behaviors is explored. Despite being ‘immune-privileged’, the CNS uses the assistance of the immune system both under homeostasis and in diseased conditions (Filiano et al., 2017). T cell and its secreted cytokines have been previously reported to play a critical role in spatial learning (Derecki et al., 2010). Lack of T cells are linked with other behavioral deficits. To uncover the role of T-cell and its secreted cytokines in regulating various brain functions and behaviors, we performed meta-analysis of transcriptomes downloaded from a public database. We discovered an unexpected novel connection between T-cells mediated IFN-γ responses and brain transcriptomes exposed to social environment enrichment. Following experiments done at our collaborator’s lab using genetic mouse models and behavioral assays, we validated this prediction and identified the mechanism underlying such a connection. we further

provided evidence that the novel role of IFN-γ in supporting social behavior is also conserved in rat, zebrafish and flies. These findings allow us to propose a plausible hypothesis regarding the evolution of sickness behavior.

- Chapter IV focuses on microglia phenotype switching in neurodegenerative diseases, a hotly debated field. Modern RNA-seq analysis shows that microglia transcriptome exhibits an unique transcriptional signature under homeostasis, and this homeostatic microglia is tightly controlled by the TGFβ pathway (Butovsky et al. 2013; Gautier et al. 2012; Hickman et al. 2013). However, microglia become dysfunctional and lose their homeostatic signature in CNS diseases. To study microglia phenotype switches in pathological conditions, we performed meta-analysis of microglia transcriptome under various conditions that were deposited in the public database. We were able to identify a unique microglia subset, dubbed MGnD, that are shared among several neurodegenerative diseases conditions. Pathway analysis revealed the signaling pathways regulating MGnD signature. In combination with promoter analysis and transcriptional factor binding site cluster analysis, we constructed the gene regulatory network orchestrating the microglia phenotype switch in neurodegenerative conditions.

- Chapter V describes in detail the novel approach of GSEA-driven meta-analysis method that I developed and applied in the work of Chapters II, III, IV.
- Chapter VI provides a brief summary of the conclusions and main contributions of the present dissertation and proposes potential vistas of future research.

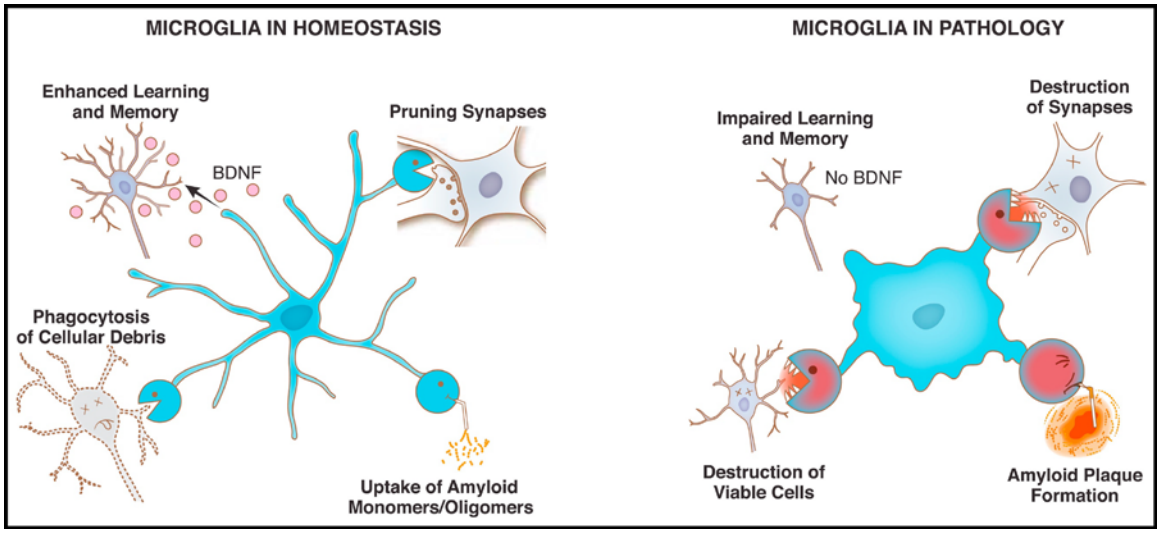

Figure adopted from (Herz et al., 2017).

Figure I-1 CNS modulating roles of microglia.
Microglia not only contribute to neuronal health but also participate in neuronal dysfunction and morphologic abnormalities. Left: the neuro-supportive role of microglia is regulated by the secretion of trophic factors, such as BDNF and the participation of pruning as part of the normal developmental program. The phagocytic activity is important for the cleanup of senescent cells and debris and slowing the toxic effect of amyloid-β. Right: In the absence of vital microglia, the CNS loses a necessary facilitator of neuronal synaptic function. Interactions with neurons promote plasticity, but aberrant activity can enable intense inflammatory reactions that lead to CNS pathology. Phagocytic pursuit declines with age and can promote the progression of pathology and give rise to cognitive regression.

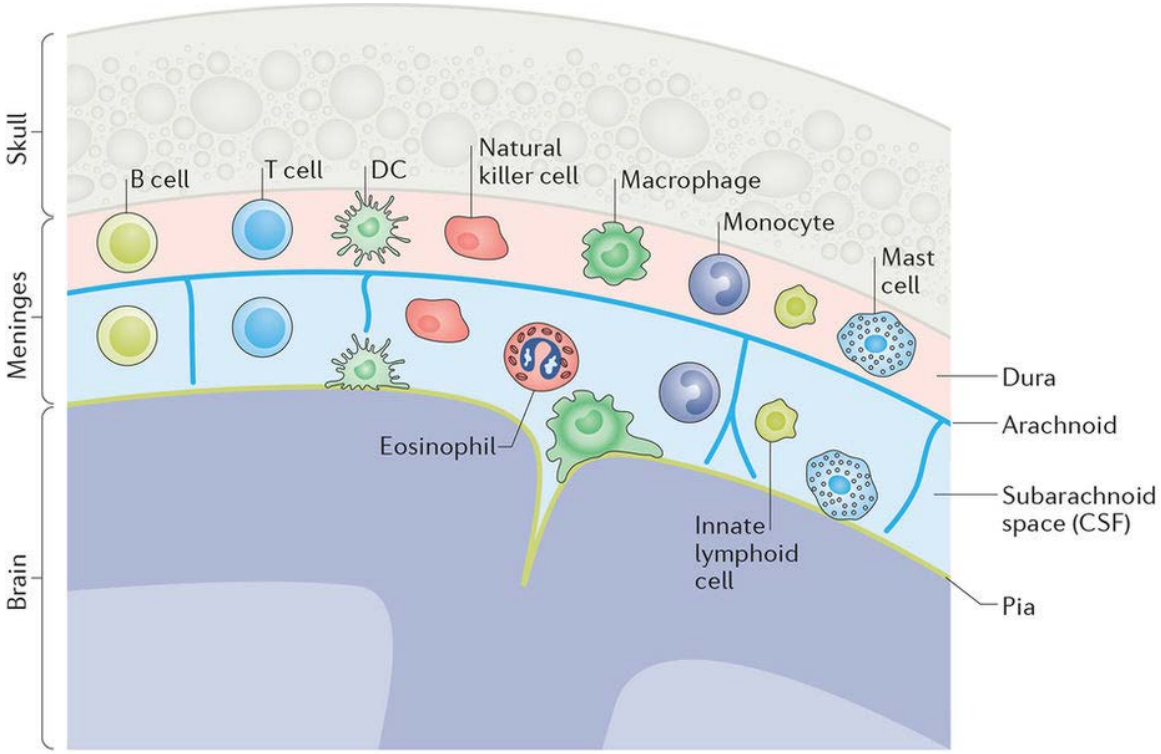

Figure adopted from (Filiano et al., 2017).

Figure I-2 Immune cells reside in meningeal spaces.
A schematic representation of the three membranes that comprise the meninges: the dura, arachnoid and pia. A full complement of immune cells has been observed in the dura and subarachnoid layers of the meninges and in the cerebrospinal fluid (CSF). DC, dendritic cell.

CHAPTER II METHYL-CPG BINDING PROTEIN 2 REGULATE MICROGLIA AND MACROPHAGE GENE EXPRESSION IN RESPONSE TO INFLAMMATORY STIMULI

The work presented in this chapter has been published as:

James C. Cronk, Noel C. Derecki, Emily Ji, **Yang Xu**, Aaron Lampano, Igor Smirnov, Wendy Baker, Geoffrey T. Norris, Ioanna Martin, Nathan Coddington, Yochai Wolf, Stephan Turner, Alan Aderem, Alexander L. Klibanov, Tajie H. Harris, Steffen Jung, Vladimir Litvak, and Jonathan Kipnis (2015). Methyl-CpG binding protein 2 regulates microglia and macrophage gene expression in response to inflammatory stimuli. **Immunity** *42*, 679-91.

My contribution to this work include RNA-seq analysis, functional pathways analysis and experimental validations for the predicted pathways.

Chapter II Methyl-CpG binding protein 2 regulate microglia and macrophage gene expression in response to inflammatory stimuli

Summary

Mutations in MECP2, encoding the epigenetic regulator methyl-CpG-binding protein 2, are the predominant cause of Rett syndrome, a disease characterized by both neurological symptoms and systemic abnormalities. Microglia dysfunction is thought to be contributing to the disease pathogenesis, and here we found microglia become activated and subsequently lost with disease progression in Mecp2-null mice. Mecp2 was found to be expressed in peripheral macrophage and monocyte populations, several of which also became depleted in Mecp2-null mice. RNA-seq revealed increased expression of glucocorticoid- and hypoxia-induced transcripts in Mecp2-deficient microglia and peritoneal macrophages. Furthermore, Mecp2 was found to regulate inflammatory gene transcription in response to TNF stimulation. Postnatal re-expression of Mecp2 using Cx3cr1^{creER} increased the lifespan of the otherwise Mecp2-null mice. These data suggest that Mecp2 regulates microglia and macrophage responsiveness to environmental stimuli to promote homeostasis. Dysfunction of tissue-resident macrophage might contribute to the systemic pathologies observed in Rett syndrome.

Introduction

Rett syndrome, caused primarily by mutations in methyl-CpG binding protein 2 (MeCP2) (Amir et al., 1999), features prominent neurologic sequelae (Chahrour and Zoghbi, 2007); accordingly, efforts to understand the function of MeCP2 have been focused largely on its role in neurons (Chahrour and Zoghbi, 2007). Recent reports have found expression and roles for Mecp2 in astrocytes (Ballas et al., 2009, Lioy et al., 2011, Yasui et al., 2013), oligodendrocytes (Nguyen et al., 2013), and microglia (Derecki et al., 2012, Maezawa and Jin, 2010). In addition, Mecp2 is expressed in many tissues (Shahbazian et al., 2002). Thus, mutations in MeCP2 likely affect multiple organ systems and cell types, which is indeed reflected in the complexity of symptoms associated with Rett syndrome (Chahrour and Zoghbi, 2007, Dunn and MacLeod, 2001). While neurological symptoms are prominent, most girls with Rett syndrome also suffer from somatic impairments, including stunted growth, osteopenia, scoliosis, and digestive difficulties (Chahrour and Zoghbi, 2007, Dunn and MacLeod, 2001).

Many tissue-resident macrophages, including microglia, originate during embryonic hematopoiesis, beginning in the yolk sac and moving to the fetal liver. These precursor cells disseminate throughout tissues during embryogenesis, engraft within nearly every organ system, and form self-renewing populations(Ginhoux et al., 2010, Kierdorf et al., 2013, Schulz et al., 2012, Yona et al., 2013)). Other populations of tissue-resident macrophages, such as intestinal lamina propria intestinal macrophages, are constantly replenished by

circulating monocytes (Bain et al., 2013, Varol et al., 2009). The functional roles of tissue-resident macrophages vary greatly and are dependent upon location and context (Davies et al., 2013). However, all tissue-resident macrophages appear to be unified by their role as provisioners of homeostatic maintenance (Davies et al., 2013). Further, monocyte-derived inflammatory non-resident macrophages are critical for effective response to infection and injury. In this context, these cells rely on a carefully balanced network of skewing paradigms, which direct macrophage function including the initiation and resolution of inflammation, clearance of debris and pathogens, and assistance in the healing process (Sica and Mantovani, 2012). Notably, mice lacking macrophage colony stimulating factor 1 receptor (CSF-1R) are deficient in all macrophages and are characterized by multiple organ failures and shortened lifespan (Dai et al., 2002), emphasizing the critical importance of macrophages in support of bodily tissues.

Our previous work demonstrated that engraftment of wild-type monocytes into the brains of Mecp2-null mice (through bone marrow transplantation) extends lifespan by several months and improves neurologic and behavioral outcomes (Derecki et al., 2012). In addition, phagocytosis of apoptotic cells in vitro is impaired in Mecp2-null microglia. Although brain engraftment by monocytes with bone-marrow transplant is crucial for significant lifespan extension in Mecp2-null mice (Derecki et al., 2012), we did not explore the possibility that Mecp2 might be important for the normal function of other mononuclear phagocytes.

Here we demonstrated that numerous populations of macrophages and monocytes expressed Mecp2, and that Mecp2- null mice become deficient in several macrophage populations, including microglia. We next showed that postnatal re-expression of Mecp2 under a Cx3cr1-inducible promoter resulted in a lifespan increase in otherwise Mecp2-null mice. In order to elucidate mechanisms behind the macrophage defects in the context of Mecp2-deficiency, we demonstrated by RNA-Seq that acutely isolated Mecp2-null microglia and peritoneal macrophages displayed changes in specific signaling pathways, suggesting that Mecp2 is an important regulator of microglia and macrophage gene expression. Further in vivo and in vitro validation studies confirmed that Mecp2 is important for proper transcriptional regulation of multiple gene-expression programs in macrophages. Overall, these results demonstrated that Mecp2 is an important epigenetic regulator of macrophage response to stimuli and stressors.

Methods

Animals

Male and female C57Bl/6J, B6.129P2(C)-Mecp2$^{tm1.1Bird}$/J, B6.129P2-Mecp2^{tm2Bird}/J, and B6.129P-Cx3cr1^{tm1Litt}/J mice were purchased from Jackson Laboratories and/or bred in house using stock obtained from Jackson Laboratories. Cx3cr1creER mice were kindly provided by S. Jung (Weizmann Institute of Science) and were maintained in our laboratory on C57Bl/6J background. All animals were housed in temperature and humidity controlled rooms, and maintained on a 12 hr/12 hr light/dark cycle (lights on at 7:00). All strains were kept in identical housing conditions. Mice were scored for pathology based on a 3-point scale across four categories: hind-limb-clasping, tremors, gait, and general appearance. For each category, 3 = wild-type, 2 = mid-phenotypic, and 1 = late-phenotypic. Mice that scored in-between 3 and 2 were considered early/pre-phenotypic. Approximate ages for prephenotypic mice were 4–5 weeks, and for late-phenotypic 8–12 weeks; however, all experiments were performed and labeled based on actual phenotype of the mice. All procedures complied with regulations of the Institutional Animal Care and Use Committee at The University of Virginia.

Tamoxifen treatment

Tamoxifen (Sigma T5648) was solubilized in corn oil (Sigma) at 10 mg/ml. Mice were injected three times, subcutaneously, between the shoulder blades, at 48 hr intervals at a dose of 100 mg/kg. For tamoxifen feeding, mice were placed on

tamoxifen diet TD.130856 (Harlan Laboratories) for up to 3 months before analysis, while controls were left on normal mouse chow (Harlan Laboratories).

RNA-Seq analysis

Total RNA was extracted using the RNeasy mini kit (QIAGEN). RNA-seq was performed by Hudson Alpha Genomic Services Laboratory. Statistical analysis and data post-processing were performed with in-house developed functions using Matlab (Litvak et al. 2009; Litvak et al. 2012). For transcriptome analysis of wild-type and Mecp2-null microglia and peritoneal macrophages, genes were selected for inclusion on the basis of filtering for minimum log2 expression intensity (>4).

Gene set enrichment analysis

Gene set enrichment analysis (GSEA) is an analytical tool for relating differentially regulated genes to transcriptional signatures and molecular pathways associated with known biological functions (Subramanian et al., 2005). The statistical significance of the enrichment of known transcriptional signatures in a ranked list of genes was determined as described (Subramanian et al., 2005). To assess the phenotypic association with Mecp2 deficiency, we used the list of genes that was ranked according to differential gene expression in Mecp2-null and wild-type microglia. We used 4,722 gene sets from the Molecular Signature Database C2 version 4.0 and 32 custom gene sets including hypoxia and glucocorticoid-stimulated gene sets.

Quantitative chromatin immunoprecipitation analysis

For ChIP analysis, formalin-fixed cells were sonicated and processed for immunoprecipitation essentially as described (Ning et al., 2011). In brief, 1.5 $x10^7$ BMMs were cross-linked for 10 min in 1% paraformaldehyde, washed, and lysed. Chromatin was sheared by sonication (5 cycles x 60 sec each cycle at 30% maximum potency) to fragments of approximately 150 bp. For Mecp2 ChIP, the sheared chromatin was incubated with anti-Mecp2 antibodies (ABE171) (Millipore), and then immunoprecipitated using anti-rabbit immunoglobulin G (IgG) Dynabeads (Invitrogen) pre-conjugated with anti-Chicken IgY antibodies (ab6877) (Abcam), washed, and eluted. For acH4 ChIP, the sheared chromatin was incubated with anti-rabbit IgG Dynabeads (Invitrogen) pre-conjugated with antibodies acH4 (06-598) (Upstate) or Isotype control IgG1 (BD Pharmigen), washed, and eluted. Eluted chromatin was reverse-cross-linked, and DNA was purified using phenol/chloroform/isoamyl extraction.

For quantitative ChIP, immunoprecipitated DNA samples were amplified with Fkbp5-promoter-specific primers (Forward: TGCACTGCCTATGCAAATGA and Reverse: AGCTTCCTCCATCCCTCTT) using TaqMan quantitative PCR analysis. PCR samples from IgY-ChIPs served as a negative control.

Accession numbers

The Gene Expression Omnibus (GEO) accession number for the RNA-seq data reported in this paper is GSE66211, and the Gene Expression Omnibus (GEO) accession number for the ChIP-seq data reported in this paper is GSE66501.

Results

Microglia become activated and subsequently depleted with disease progression in Mecp2-Null mice

Previous data (Derecki et al. 2012) showing a role for microglia in disease pathogenesis of Mecp2-deficient mice led us to study in greater detail the role of Mecp2 in microglia and developmentally related peripheral tissue-resident macrophages. Wild-type microglia were found to express Mecp2, as examined by intracellular flow cytometric labeling (Figure II-1A) or by in situ immunofluorescence (Figure II-1B). This is in line with previously reported results (Maezawa and Jin, 2010). We next investigated how loss of Mecp2 affects microglia in vivo. Using a thinned-skull technique, we performed intravital two-photon imaging on pre- and late-phenotypic Mecp2-null and wild-type mice. We observed that pre-phenotypic Mecp2- null microglia had significantly smaller somas (similar to Mecp2-null neurons and astrocytes), whereas late-phenotypic. Mecp2-null microglia soma were larger in size as compared to wild-type (Figure II-1C and 1D), suggestive of microglia activation(Maezawa and Jin, 2010). In addition, in situ Sholl analysis demonstrated that while pre-phenotypic Mecp2-null microglia were not different from wild-type, microglia from late-phenotypic mice displayed significantly reduced process complexity in three examined brain areas (hippocampus, neocortex, and cerebellum; Figure II-1E). Together, the findings of increased soma size and decreased process complexity suggested that Mecp2-null microglia became activated with disease progression. Indeed,

qRT-PCR of acutely isolated Mecp2-null microglia from pre- and late-phenotypic mice showed increased Tnf mRNA encoding the pro-inflammatory cytokine tumor necrosis factor (TNF) (Figure II-1F) while Tgfb1 transcription, required for microglia maintenance (Butovsky et al., 2014), was decreased in late-phenotypic microglia (Figure II-1G).

We next examined Mecp2-null microglia by flow cytometry, which revealed a progressive loss of microglia in Mecp2-null mice from pre- to late-phenotypic stage (Figure II-1H and 1I). Loss of microglia was found throughout the brain Figure II-1J). The loss was also observed in brains of late-phenotypic Mecp2-null mice by immunohistochemistry. Further, immunohistochemical staining for Iba1, a microglial marker, and for cleaved caspase 3 (CC3), a marker of apoptotic cells, revealed sporadic $CC3^{+}$ microglia in late-phenotypic Mecp2-null brains. In sum, these data suggest that in the context of Mecp2-deficiency, microglia become activated and are lost with disease progression.

Meningeal macrophages are lost with disease progression in Mecp2-Null mice

When analyzing microglia by intravital two-photon microscopy, we also observed significant morphologic disruption of *Cx3cr1*$^{GFP/+}$ meningeal macrophages in vivo in late-phenotypic Mecp2-null mice suggestive of reactive phenotype (Figure II-2A). To assess meningeal macrophages in further detail, we performed immuno- fluorescent labeling of meninges from pre-, mid-, and late-phenotypic

Mecp2-null mice using antibodies against CD163 and F4/80. A progressive loss of macrophages at the late-phenotypic state was evident in Mecp2-null mice (Figure II-2B and 2C). Perivascular macrophages in the meninges are F4/80^{+}CD163^{+}, whereas a separate meningeal macrophage population is F4/80^{+}CD163^{-} (Davies et al., 2013). When we analyzed these populations separately, we found that perivascular macrophages (F4/80^{+}CD163^{+}) were progressively lost in Mecp2- null mice (Figure II-2D), whereas non-perivascular meningeal macrophages (F4/80^{+} CD163^{-}) were not significantly depleted (Figure II-2E).

Peripheral monocytes and macrophages express Mecp2, and some are lost in Mecp2-Null mice

Given the phenotype of meningeal macrophages and microglia, we decided to expand our analysis to additional populations of peripheral macrophages. Many tissue-resident macrophages, including microglia, originate from similar progenitor pools during embryogenesis (Ginhoux et al., 2010, Hoshiko et al., 2012, Kierdorf et al., 2013, Schulz et al., 2012, Yona et al., 2013), and might therefore share pathologies in the context of Mecp2-deficiency. We found that all tested tissue-resident macrophages expressed Mecp2 (Figure II-3A and 3B). In addition, Ly6c^{lo} monocytes, which represent a longer-lived resident population in the blood (Yona et al., 2013) also expressed Mecp2 (Figure II-3B). In contrast,

Ly6c^{hi}CCR2^{+} monocytes and neutrophils expressed low or undetectable amounts of Mecp2 (Figure II-3C).

As expected, based on the microglia and meningeal macrophage results described above, we found reductions of other peripheral macrophage populations in Mecp2-null mice. Unlike microglia, CD64^{+}F4/80^{+}CD11b^{+} macrophages from the small intestine were reduced in both pre- and late-phenotypic Mecp2-null mice (Figure II-3D and 3E). Circulating Ly6c^{lo} monocytes were also reduced in number in both pre- and late-phenotypic Mecp2-null mice (Figure II-3F and 3G).

Because both CD64^{+} F4/80^{+} CD11b^{+} intestinal macrophages and Ly6c^{lo} monocytes share their derivation from Ly6c^{hi} monocytes (Bain et al., 2013, Varol et al., 2009, Yona et al., 2013), it is possible that the reductions seen in these populations even in pre-phenotypic Mecp2-null mice might reflect their common origin. To this end, we tested whether Ly6c^{hi} monocytes from bone marrow were impaired in their ability to differentiate and/or proliferate as macrophages in response to MCSF in vitro. We found that Mecp2-null Ly6c^{hi} monocytes differentiated into macrophages with similar kinetics to wild-type and produced similar numbers of macrophages per monocyte, making it an unlikely possibility that Mecp2 is directly necessary for Ly6c^{hi} monocyte differentiation or macrophage proliferation in the absence of other factors.

Although Mecp2 did not affect differentiation or proliferation in vitro, we hypothesized that Mecp2 might play a role in monocyte/macrophage responses

within the context of the full disease caused by whole-animal Mecp2-deficiency. To test this possibility, we depleted monocytes and macrophages using intravenous (i.v.) clodronate liposomes in wild-type and Mecp2- null littermates (mid-phenotypic, 6 weeks to allow for immune system maturation but prior to the peak of disease) and measured the repopulation of resident monocytes. DiI liposomes were injected i.v. 2 days after clodronate liposome injection, similar to published protocols (Sunderkotter et al., 2004). Ly6chi monocytes released from the bone marrow become DiI labeled and can be tracked in their differentiation to Ly6clo monocytes. On day 5 post-clodronate injection (day 3 post DiI), wild-type and Mecp2-null mice had, as expected, begun to reconstitute their circulating monocyte populations, with a non-significant trend toward fewer total (Figures II.3H and 3I). However, when total monocytes were examined, Mecp2-null mice had significantly fewer resident Ly6clo monocytes as compared to wild-type (Figure II-3J). In addition, when only DiI+ monocytes were examined (representing only the circulating monocytes present on day 2 post-clodronate injection), DiI+ monocytes in wild-type mice had almost completely differentiated into Ly6clo resident monocytes, whereas Mecp2-null mice displayed a deficit in Ly6clo monocyte differentiation (Figure II-3K). The fact that some populations were deficient in the pre-phenotypic state (resident monocytes and intestinal macrophages), but others were lost progressively (microglia and meningeal perivascular macrophages) led us to hypothesize that Mecp2 is likely playing a complex role in macrophage biology which is not limited to macrophage survival

and/ or death. Of note, we did not observe any difference in F4/80+CD163– meningeal macrophages (Figure II-2E) or splenic red pulp macrophages (data not shown), which also express Mecp2 (Figure II-3A and 3B), further suggesting that the role of Mecp2 in macrophages is complex or upstream of cell loss and/or death, because not all macrophage populations were equally affected by Mecp2-deficiency. In addition, our data regarding microglia suggested inflammatory activation (Figure II-1–1G), implicating Mecp2-deficiency in processes beyond simple loss of microglia/macrophages. Overall, the data suggested a complex role for Mecp2 in macrophages, consistent with its previously described role in other cell types as an epigenetic regulator, affecting a multitude of genes (Guy et al., 2011).

Postnatal expression of Mecp2 via Cx3cr1creER in the otherwise Mecp2-Deficient mice increases lifespan

Previously we showed that transplantation of Mecp2-null mice with wild-type bone marrow increases lifespan, and that engraftment of microglia-like cells into the brain is important for this effect (Derecki et al., 2012). More recently, Cx3cr1^{creER} mice have become available (Goldmann et al., 2013, Yona et al., 2013), and microglia are among a subset of macrophages with high expression of CX3CR1 during adulthood (Jung et al., 2000). Thus, the Cx3cr1^{creER} mouse can be used to efficiently target microglia, in addition to other CX3CR1-expressing monocytes and macrophages. Therefore, we crossed Cx3cr1^{creER}

mice with Mecp2Lox-stop mice and their offspring (Cx3cr1$^{creER/+}$ Mecp2$^{Lox\text{-}stop/y}$) were treated with tamoxifen (~9 weeks of age), when symptoms just started to appear. In line with our previous finding with bone-marrow transplantation (Derecki et al., 2012), the lifespan of tamoxifen-treated Cx3cr1$^{creER/+}$ Mecp2$^{Lox\text{-}stop/y}$ mice was significantly extended (Figure II-4A) and weight loss was reversed as compared to oil-treated controls (Figure II-4B), supporting the importance of microglia and macrophages in the arrest of pathology. In order to test for specificity of Mecp2 expression after tamoxifen treatment, we placed Cx3cr1$^{creER/+}$ Mecp2$^{Lox\text{-}stop/y}$ mice on a tamoxifen diet for 3 months to maximize expression in any cells that would have the potential to recombine. As expected, we found no significant expression of Mecp2 in T or B cells, and partial re-expression in monocytes (Figure II-4C), as previously reported (Yona et al., 2013). In the spleen, we found a small percentage of Mecp2-expressing red pulp macrophages (~20%) (Figure II-4D), consistent with the fact that red pulp macrophages do not express high amounts of CX3CR1. However, CD64^{+}F4/80^{+} intestinal macrophages and microglia, in which CX3CR1 is highly expressed, had nearly 100% Mecp2 recombination (Figure II-4E and 4F). Non-microglia cells in the CNS displayed no Mecp2 recombination (Figure II-4G). Together, these results support that Mecp2-deficiency in microglia/macrophages contributes to pathology and that restoring Mecp2-mediated regulation of transcriptional responses has the potential to mediate benefits in the context of whole-body Mecp2-deficiency.

Mecp2 regulates glucocorticoid and hypoxia responses in microglia and peritoneal macrophages

In order to define the functional role of Mecp2 in macrophages, we examined the global gene-expression profile in microglia and peritoneal macrophages derived from Mecp2-null mice. We detected increased expression of glucocorticoid-induced transcriptional signature genes in Mecp2-null cells when compared to their wild-type counterparts, suggesting that Mecp2 functions as a repressor of this pathway (Figure II-5A-5D). Among the dysregulated genes in Mecp2-null microglia and peritoneal macrophages, Fkbp5, a canonical glucocorticoid target gene, was strongly upregulated (Figure II-5A and 5C). A number of studies have demonstrated that Mecp2 directly represses the Fkbp5 gene (Nuber et al., 2005, Urdinguio et al., 2008). Using chromatin immunoprecipitation (ChIP) analysis, we demonstrated Mecp2 binding to the Fkbp5 gene promoter in bone marrow-derived macrophages (BMDM) (Figure II-5E). Furthermore, Mecp2 deletion resulted in increased amounts of histone H4 acetylation at cis-regulatory regions of Fkbp5 gene under basal conditions (Figure II-5F). These results suggest that Mecp2 restrains Fkbp5 gene expression through epigenetic mechanisms. ChIP analysis demonstrated the binding of nuclear receptor co-repressor 2 (Ncor2) and histone deacetylase 3 (Hdac3) to the promoter region at the Fkbp5 gene. These results are consistent with the well-established role of Mecp2 in the recruitment of the Ncor2 and Hdac3 complex to target genes (Ebert et al., 2013,

Lyst et al., 2013). We next examined the Fkbp5 gene-expression pro- file in dexamethasone-treated wild-type and Mecp2-null macrophages. Our results revealed that Mecp2 controls the sensitivity of the Fkbp5 gene to glucocorticoid stimulation. Mecp2 deletion resulted in the upregulation of Fkbp5 gene expression under dexamethasone stimulation at a low dose normally incapable of triggering Fkbp5 gene expression (Figure II-5G).

We noticed that the glucocorticoid-induced gene set contains a number of hypoxia-inducible genes. Furthermore, our gene set enrichment analysis demonstrated significantly increased expression of a subset of hypoxia-inducible genes in Mecp2-null microglia (Figure II-5H and 5I). To validate the cell intrinsic role for Mecp2 in the negative regulation of these hypoxia-inducible genes, we cultured BMDM under either normoxia or hypoxia conditions (1% O2) and examined their mRNA using quantitative PCR analysis. We validated increased expression of three canonical hypoxia-inducible genes, *Hif3a, Ddit4*, and *Cyr61* in Mecp2-null macrophages cultured under hypoxia conditions when compared to their wild-type counterparts (Figure II-5J), confirming a role for Mecp2 in regulation of at least a subset of hypoxia-induced gene transcripts.

Mecp2 restrains inflammatory responses in macrophages

Our RNA-seq analysis revealed increased expression of Tnf induced transcriptional signature genes in Mecp2-null microglia cells when compared to their wild-type counterparts. These results indicate that Mecp2-deficiency leads

to dysregulation of inflammatory responses in microglia and macrophages. To validate this finding, we examined the role of Mecp2 in the regulation of TNF-induced inflammatory responses in macrophages. We observed increased expression of *Il6, Tnf, Cxcl2, Cxcl3*, and *Csf3* genes in TNF-stimulated Mecp2-null BMDM when compared to wild-type counterparts (Figure II-6A). In order to corroborate these findings in vivo, we examined the inflammatory response of resident peritoneal macrophages. Mice were injected intraperitoneally with TNF, allowed to respond for 6 hr, and then peritoneal cells were collected by lavage. Cells from peritoneal lavage were positively selected for $F4/80^{+}$ macrophages via AutoMACS. Peritoneal macrophages from Mecp2- null mice injected with TNF displayed an altered transcriptional response as compared to wild-type (Figure II-6B), including both over- and under-expression of multiple TNF response genes. No differences in baseline expression were evident in peritoneal macrophages from mice after saline treatment. Targets observed in vitro with TNF stimulated BMDMs were also overexpressed in peritoneal macrophages stimulated with TNF in vivo, suggesting that Mecp2 has consistent transcriptional roles across macrophage populations (Figure II-6A and 6B). *Csf3*, the gene encoding granulocyte-colony stimulating factor (GCSF), was overexpressed in TNF-stimulated Mecp2-null macrophages both in vitro and in vivo (Figure II-6A and 6B). Late-phenotypic Mecp2-null mice without any manipulation also displayed increased GCSF protein in serum (Figure II-6C). Because a well-established effect of GCSF is to stimulate neutrophil production (Bendall and

Bradstock, 2014), we examined neutrophil numbers in Mecp2-null mice. Indeed, we found that Mecp2-null mice develop severe neutrophilia. In addition, GCSF is known to drive the egress of hematopoietic stem cells (HSC) from the bone marrow (Bendall and Bradstock, 2014) and as expected, late-phenotypic Mecp2-null mice also became progressively deficient in bone marrow HSC with disease progression. In order to test whether or not neutrophilia and HSC loss play a role in the disease, we treated Mecp2-null mice with a neutralizing anti-GCSF antibody beginning at age 6-7 weeks (a mid-phenotypic time-point). Flow cytometric analysis revealed rescue of neutrophilia (Figure II-6D) and prevention of HSC loss. The treatment also moderately increased the lifespan of Mecp2-null mice (Figure II-6E). Together, these findings implicate Mecp2 in control of the macrophage inflammatory response, which might have downstream implications for complex disease processes in the context of Mecp2-deficiency.

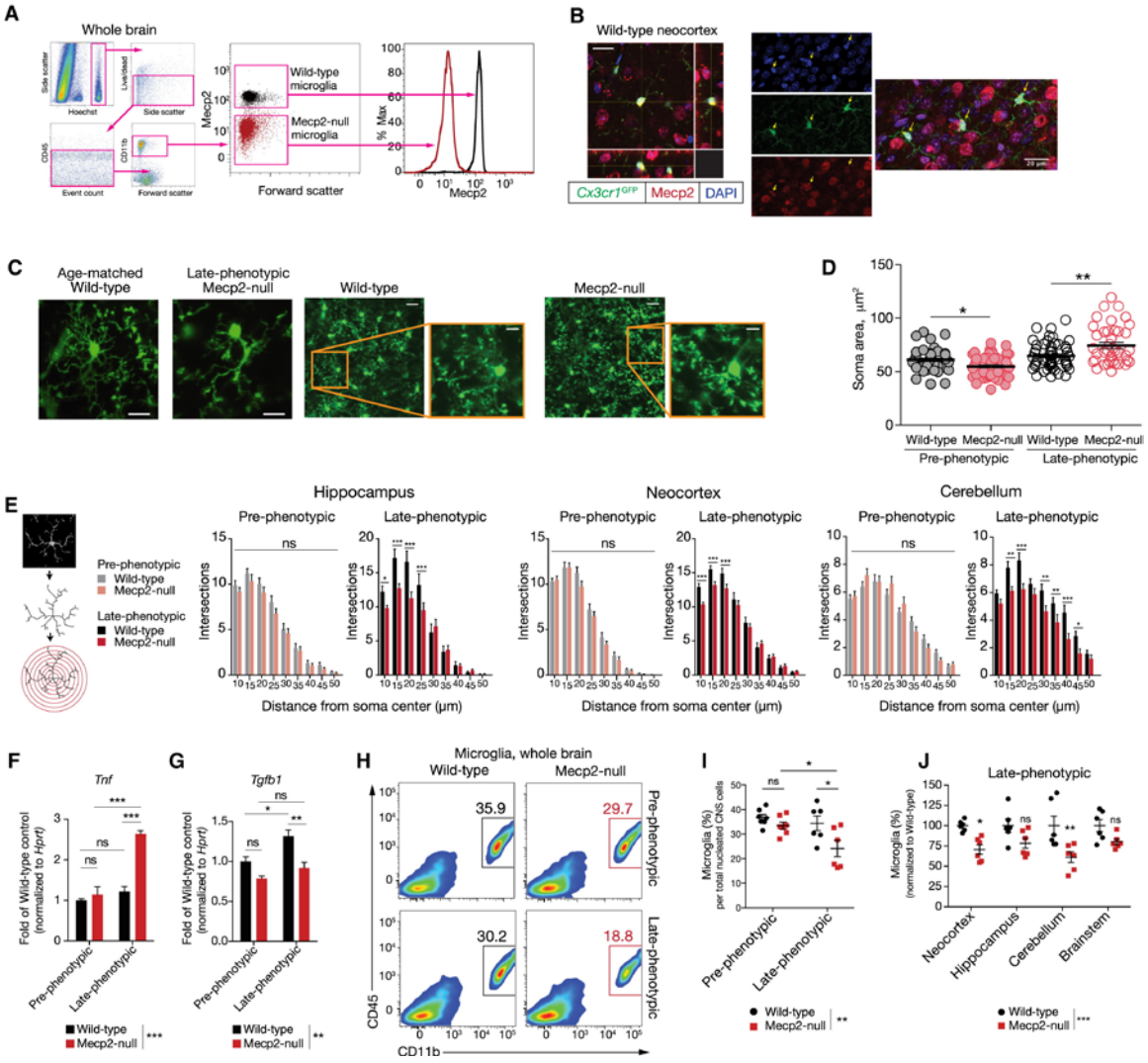

Figure II-1 Microglia become activated and subsequently depleted with disease progression in Mecp2-null mice.

(A) Flow cytometry demonstrating Mecp2 expression in microglia from whole brain. (B) Cryosections from $Cx3cr1^{GFP/+}$ wild type mice demonstrating Mecp2 expression in microglia (scale bar, 20 µm). Images were cropped from larger images to allow for better visualization of Mecp2 localization within microglia. (C) Representative stills from 2-photon live-imaging of late-phenotypic $Cx3cr1^{GFP/+}$ wild type and $Cx3cr1^{GFP/+}$ Mecp2-null microglia. (D) Quantitative assessment of microglial soma size measured by two-photon intravital microscopy in pre- and late-phenotypic $Cx3cr1^{GFP/+}$ wild type and $Cx3cr1^{GFP/+}$ Mecp2-null mice (*, $p < 0.05$; **, $p < 0.01$; two-way ANOVA with Bonferroni post-test; n = 3 mice per group. Error bars represent SEM). (E) Sholl profiles for pre- and late-phenotypic wild type and Mecp2-null microglia in hippocampus and neocortex showing intersections; (***, $p<0.001$; **, $p<0.01$; *, $p<0.05$; two-way ANOVA with Bonferroni post-test, n = 3 mice per group with 3 separate areas from slices

from identical brain structures analyzed per each genotype. Data are presented as mean ±SEM). (F,G) qRT-PCR of Tnf (F) and Tgfb1 (G) from pre- and late-phenotypic Mecp2-null mice and their age-matched wild type controls (*, $p < 0.05$; **, $p < 0.01$; two-way ANOVA with Bonferroni post-test, n = 3 mice for all groups except late-phenotypic wild type for which n = 5. Data are presented as mean ± SEM). (H) Flow cytometric analysis demonstrating the percentage of microglia in whole brain preparations in Mecp2-null mice with increasing disease severity. Numbers show the percentage of Hoechst+ (nucleated) singlet CNS cells that are $CD45^{lo}CD11b^{+}$ microglia. (I) Quantification of microglia in pre- and late- phenotypic Mecp2-null mice as compared to age-matched wild type controls. Cells were gated on $Hoechst^{+}$ (nucleated cells), Singlets, Size, and $CD45^{lo/neg}$ to exclude peripheral immune cells. (Two-way ANOVA with Bonferroni post-test; pre-phenotypic, not significant. Late-phenotypic; *, $p<0.05$. Pre-phenotypic vs. late-phenotypic Mecp2-null; *, $p < 0.05$. Overall main effect wild type vs. Mecp2-null; **, $p < 0.01$. n = 7 pairs of wild type and Mecp2-null mice pooled from 3 independent experiments for pre-phenotypic groups and n = 6 pairs of wild type and Mecp2-null mice pooled from 4 independent experiments for late-phenotypic groups. Error bars represent SEM). (J) Brain region-specific microglia percentages as measured by flow cytometry in late-phenotypic Mecp2-null mice and age-matched wild type controls (*, $p < 0.05$; **, $p < 0.01$; ***, $p < 0.001$; two-way ANOVA; n = 6 mice per group. Error bars represent SEM).

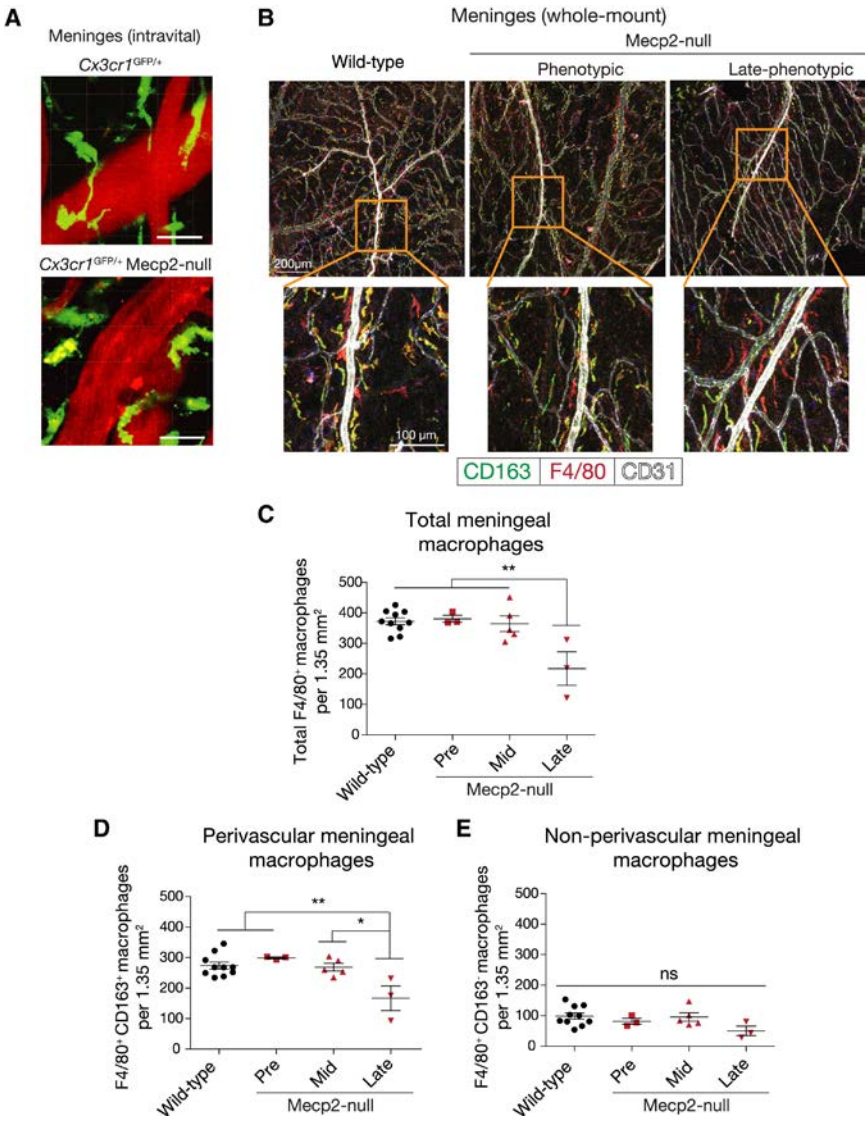

Figure II-2 Meningeal macrophages are lost with disease progression in Mecp2-null mice. (A) Representative stills from intravital two-photon microscopy of phenotypic Mecp2-null meningeal macrophages demonstrating abnormal/activated morphology. (B) Representative images of wild type, mid and late-phenotypic Mecp2-null meningeal macrophages. Upper panels, scale bar = 200μm. Lower panels, scale bar = 100μm. (C) Quantification of total meningeal macrophages in late-phenotypic Mecp2-null mice as compared to wild type, pre- and mid-phenotypic Mecp2-null (One-way ANOVA with Bonferroni post-test; **, $p < 0.01$. Error bars represent SEM). (D) Quantification of $F4/80^{+}CD163^{+}$ perivascular meningeal macrophages in late-phenotypic Mecp2-null mice as compared to wild type, pre and mid-phenotypic Mecp2-null (One-way ANOVA with Bonferroni post-test; *, $p < 0.01$; **, $p < 0.01$. Error bars represent SEM). (E) Quantification of $F4/80^{+}CD163^{-}$non-perivascular meningeal macrophages in Mecp2-

null mice as compared to wild type (One-way ANOVA with Bonferroni post-test. Error bars represent SEM).

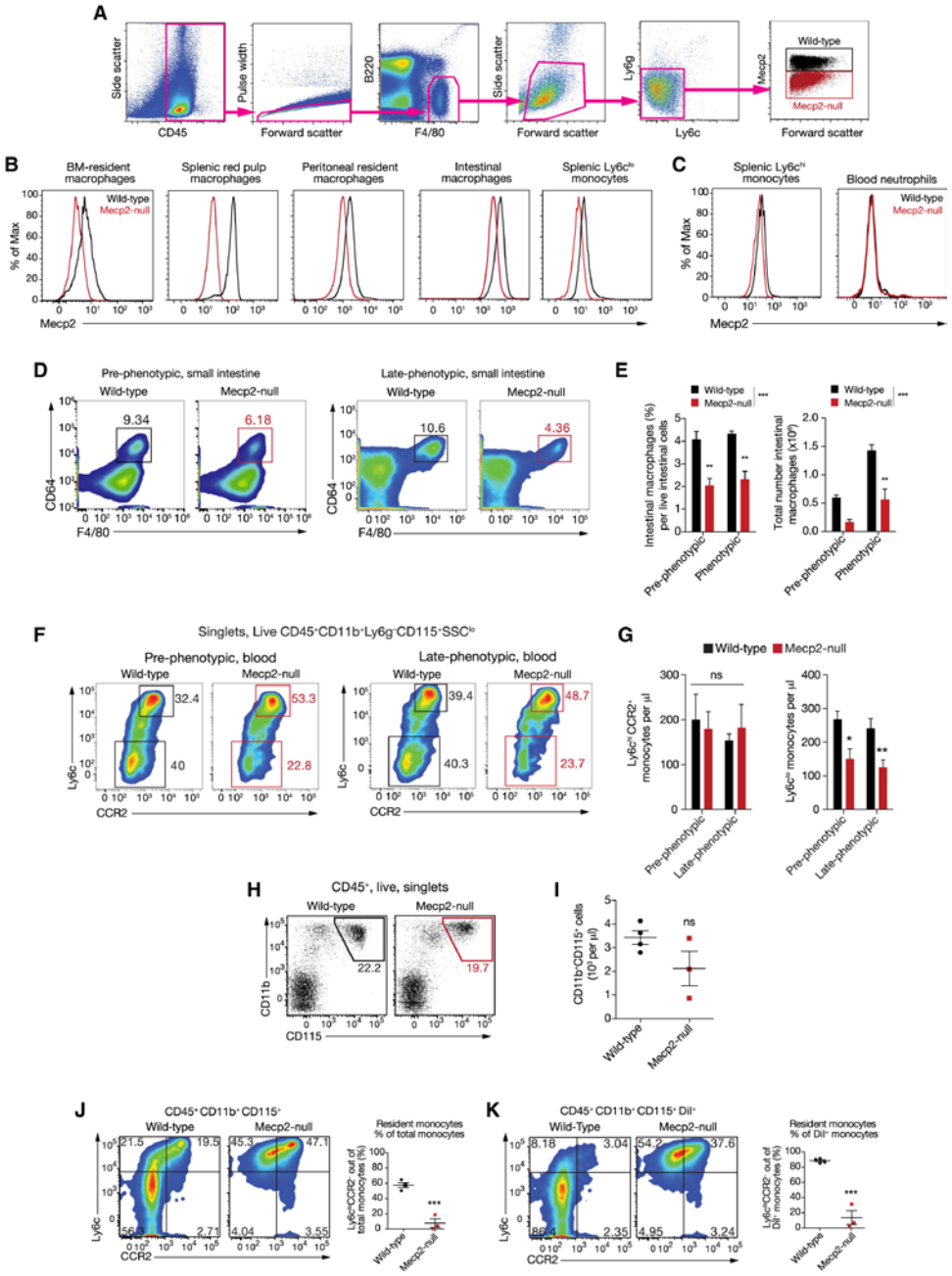

Figure II-3 Peripheral monocytes and macrophages express Mecp2, and some are lost in Mecp2-null mice.

(A) Example gating strategy for Mecp2 expression; shown are red pulp macrophages from spleen. (B) Mecp2 expression in macrophage and monocyte populations as measured by intracellular flow cytometric staining in wild type and Mecp2-null mice. Gating: Bone marrow (BM)-resident macrophages- size, $CD45^{+}$, Singlets, $Ly6c^{-}$, $F4/80^{+}$, $CD11b^{lo}$, $CD3^{-}$, SSC^{lo}; Splenic red pulp

macrophages- $CD45^+$, Singlets, $F4/80^+$, $B220^-$, Size, SSC^{lo}, $Ly6g^-$, Ly6c; Peritoneal resident macrophages- Size, Singlets, $CD45^+$, $CD11b^+$, $F480^{hi}$; Intestinal macrophages- Singlets, viability, $CD45^+$, $CD11b^+$, $CD64^+$; Splenic $Ly6c^{lo}$ monocytes, $CD45^+$, Singlets, $CD115^+$, SSC^{lo} $Ly6c^{lo}$. (C) Flow cytometric Mecp2 staining in inflammatory monocytes ($Ly6c^{hi}CCR2^+$) and neutrophils ($Ly6g^{hi}CD11b^+$). Gating: Splenic $Ly6c^{hi}CCR2^+$ monocytes-$CD45^+$, Singlets, $CD115^+$, SSC^{lo}, $Ly6c^{hi}$; Neutrophils- Singlets, $CD45^+$, $CD11b^+$, $Ly6g^+$. (D, E) Flow cytometric analysis of resident intestinal macrophages in Mecp2-null mice as compared to wild type control. (D) Representative flow cytometry plots showing the percentage of $CD64^+F4/80^+$ out of all $CD45^+$ intestinal cells in pre- and late-phenotypic Mecp2-null mice as compared to age-matched wild type controls. (E) Quantification of $CD64^+CD11b^+$ intestinal macrophages as measured by both percentage of total live intestinal cells (Two-way ANOVA with Bonferroni post-test; **, $p < 0.01$; ***, $p < 0.001$) and absolute cell counts per animal (Two-way ANOVA with Bonferroni post-test; **, $p < 0.01$; ***, $p < 0.001$). Data is representative of two independent experiments for phenotypic mice. Data are presented as mean ±SEM. (F) Flow cytometry plots of $Ly6c^{hi}CCR2^+$ and $Ly6c^{lo}$ blood monocytes in pre- and late-phenotypic Mecp2-null mice as compared to age-matched wild type controls. Numbers represent percentage of cells out of Singlets, Live, $CD45^+CD11b^+Ly6g^-CD115^+SSC^{lo}$ monocytes. (G) Quantification of numbers of circulating $Ly6c^{hi}CCR2^+$ and $Ly6c^{lo}$ monocytes (*, $p<0.05$; **, $p<0.01$; Two-way ANOVA with Bonferroni post-test; n = 6–8 mice per group. Error bars represent SEM). (H) Representative plots of $CD11b^+CD115^+$ total monocytes from blood of wild type and Mecp2-null mice on day 5 post clodronate liposome injection. (I) Monocyte count from peripheral blood of Mecp2-null and wild type controls on day 5 post clodronate liposome injection (unpaired two-tailed Student's t-test, not significant. Error bars represent SEM). (J) Representative flow cytometry plots displaying differentiation of $Ly6c^{hi}CCR2^+$ monocytes to $Ly6c^{lo}$ monocytes and quantification of $\%Ly6c^{lo}CCR2^-$ resident monocytes on day 5 post clodronate liposome injection; representative of two independent experiments. (***, $p<0.001$, unpaired two-tailed Student's t-test. Error bars represent SEM). (K) Same as (J), except only DiI^+ monocytes are shown (cells labeled on day 2 post clodronate injection via DiI liposome injection); representative of two independent experiments. ***, $p<0.001$ (unpaired two-tailed Student's t-test. Error bars represent SEM).

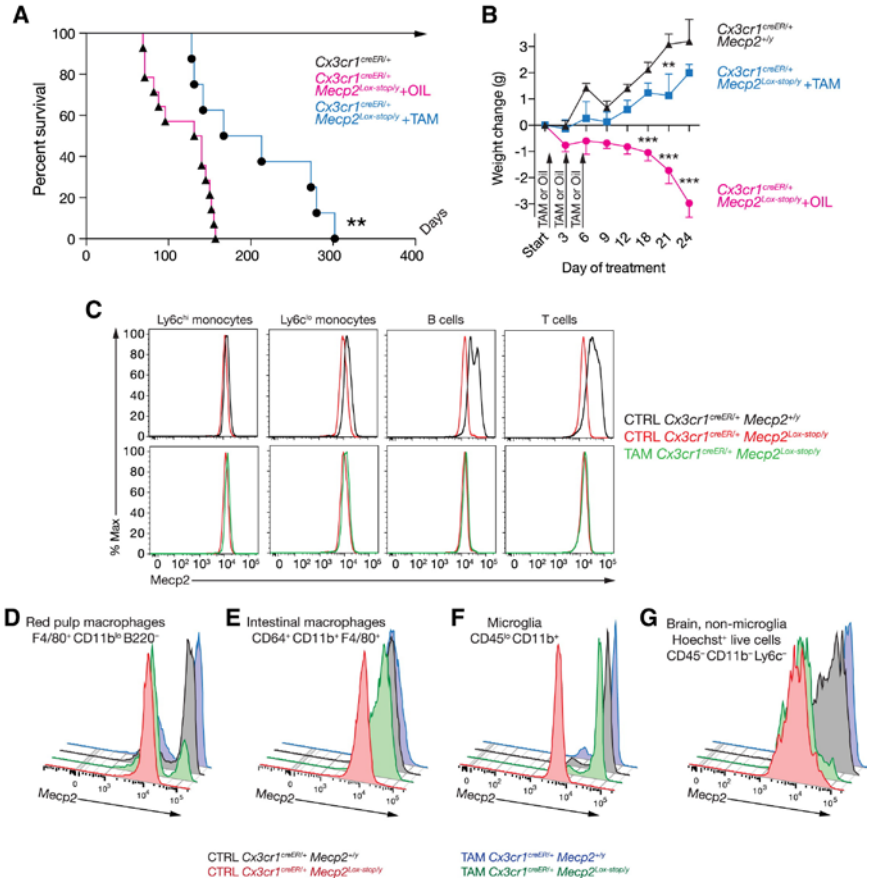

Figure II-4 Postnatal expression of Mecp2 viaCx3cr1^{creER} in otherwise Mecp2-deficient mice increases lifespan.

(A) Cx3cr1$^{creER/+}$Mecp2$^{Lox\text{-}stop/y}$ mice after postnatal tamoxifen or oil control treatment in phenotypic mice (**, p<0.01; log-rank Mantel-Cox test; tamoxifen treated n = 8, oil treated n = 12). (B) Weight change after postnatal tamoxifen or oil control treatment in phenotypic Cx3cr1$^{creER/+}$Mecp2$^{Lox\text{-}stop/y}$ mice (**, p < 0.01; ***, p<0.001. Two-way ANOVA with Bonferroni post-test; n = 5 oil and n = 3 tamoxifen treated Cx3cr1$^{creER/+}$Mecp2$^{Lox\text{-}stop/y}$. n = 7 Cx3cr1$^{creER/+}$Mecp2$^{+/y}$ tamoxifen treated. Asterisks over Cx3cr1$^{creER/+}$Mecp2$^{Lox\text{-}stop/y}$ oil-treated indicate comparisons to Cx3cr1$^{creER/+}$Mecp2$^{Lox\text{-}stop/y}$ tamoxifen-treated. Asterisks over Cx3cr1$^{creER/+}$Mecp2$^{Lox\text{-}stop/y}$ tamoxifen-treated indicate comparisons to Cx3cr1$^{creER/+}$Mecp2$^{+/y}$. Data are presented as mean ± SEM). (C-G) Analysis of Mecp2 re-expression in tamoxifen treated mice. Mice were fed tamoxifen food for 3 months to maximize possible recombination and analyzed by flow cytometry. Flow cytometry plots displaying Mecp2 expression in Cx3cr1$^{creER/+}$Mecp2$^{Lox\text{-}stop/y}$ mice with or without tamoxifen treatment in (C) circulating monocytes, B, and T cells; (D) red pulp macrophages; (E) intestinal macrophages; (F) microglia and (G) total non-microglia nucleated cells in the CNS.

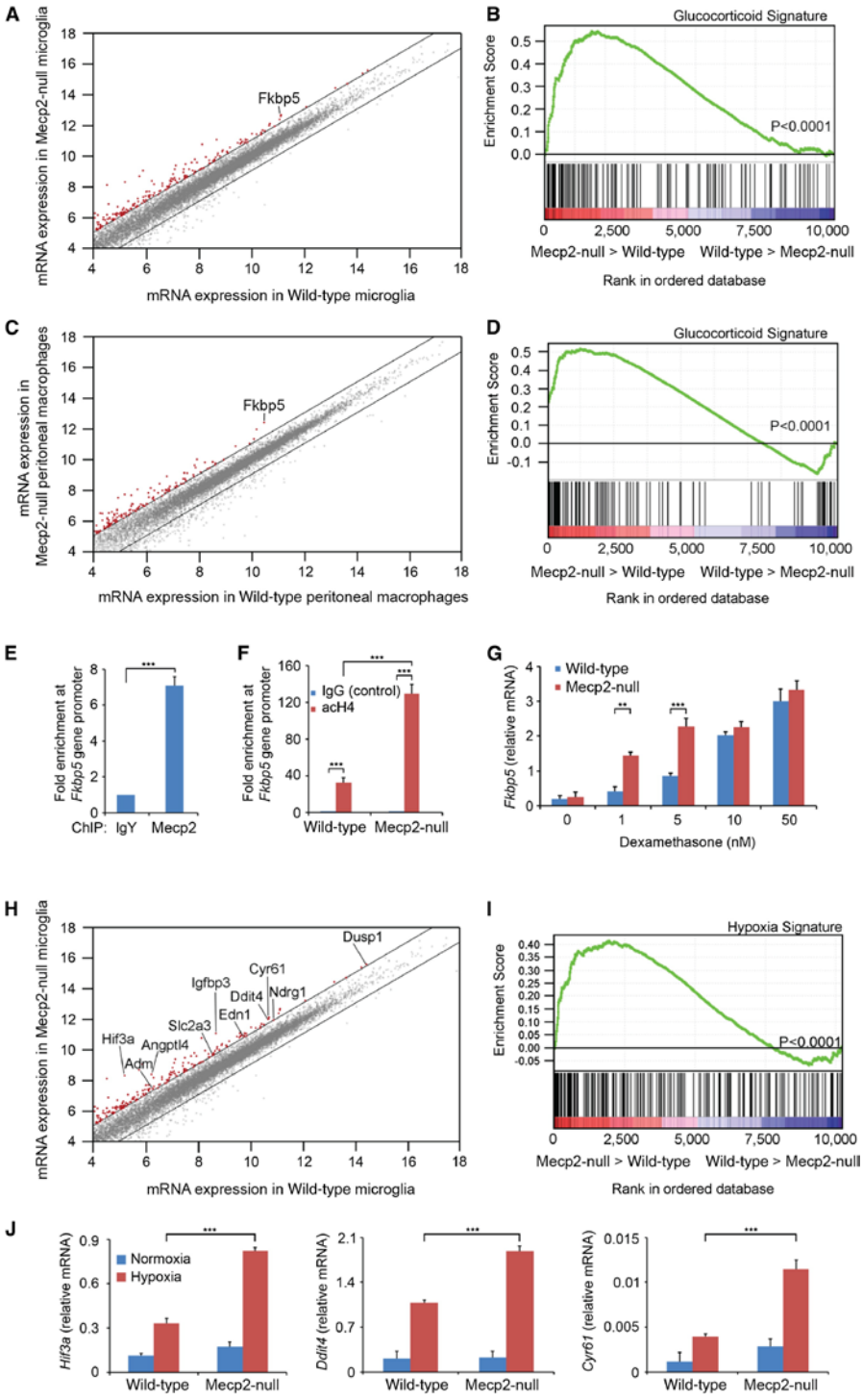

Figure II-5 Mecp2 regulates glucocorticoid and hypoxia responses in microglia and peritoneal macrophages.

Scatter plot comparing global gene expression profiles between wild type and Mecp2-null microglia. The black lines indicate a 2-fold cut-off for the difference in gene expression levels. Data represent the average of 6 wild type and 3 Mecp2-null samples, with each sample representing 3 pooled mice (thus, 18 mice and 9 mice respectively). mRNA expression is shown on a log2 scale. (B) Gene set enrichment analysis (GSEA) reveals the over-representation of glucocorticoid transcription signature genes in Mecp2-null microglia. The middle part of the plot shows the distribution of the genes in the glucocorticoid transcription signature gene set ('Hits') against the ranked list of genes. Data represent the average of 6 wild type and 3 Mecp2-null samples. (C) Scatter plot comparing global gene expression profiles between wild type and Mecp2-null peritoneal macrophages as in (A). Data represent the average of 6 pooled wild type and 6 pooled Mecp2-null mice. (D) Global gene expression in wild type and Mecp2-null peritoneal macrophages was analyzed as in (B). Data represent the average of 6 pooled wild type and 6 pooled Mecp2-null mice. (E) ChIP of Mecp2 from unstimulated wild type macrophages showing binding of Mecp2 to the promoter region of the Fkbp5 gene. Data were normalized to IgY (negative control). Data represent the average of three independent experiments. *** $p < 0.001$ and ** $p < 0.01$, (unpaired two-tailed Student's t-test. Data are presented as mean ±SEM). (F) ChIP analysis of histone H4 acetylation at the Fkbp5 gene promoter in wild type and Mecp2-null macrophages. Data represent the average of three independent experiments (*** $p < 0.001$ and ** $p < 0.01$; unpaired two-tailed Student's t-test. Data are presented as mean ± SEM). (G) Dexamethasone-stimulation of wild type and Mecp2-null macrophages was associated with a significant increase in Fkbp5 mRNA levels. Dexamethasone induction of Fkbp5 mRNA was significantly increased in Mecp2-null macrophages. Data represent the average of three independent experiments (*** $p < 0.001$ and ** $p < 0.01$; unpaired two-tailed Student's t-test. Data are presented as mean ± SEM). (H) Scatter plot comparing global gene expression profiles between wild type and Mecp2-null microglia. The black lines indicate a 2-fold cut-off for the difference in gene expression levels. Data represent the average of 6 wild type and 3 Mecp2-null samples, with each sample representing 3 pooled mice (18 and 9 mice respectively). mRNA expression levels are on a log2 scale. (I) Gene-set enrichment analysis (GSEA) reveals the over-representation of hypoxia signature genes in unstimulated Mecp2-null microglia. (J) Wild type and Mecp2-null macrophages were grown in hypoxia or normoxia for 24 hrs. mRNA levels of Hif3a Ddit4, and Cyr61 were measured using qRT-PCR. Results are representative of three independent experiments (average of three values ± SEM; *** $p < 0.001$ by unpaired two-tailed Student's t-test).

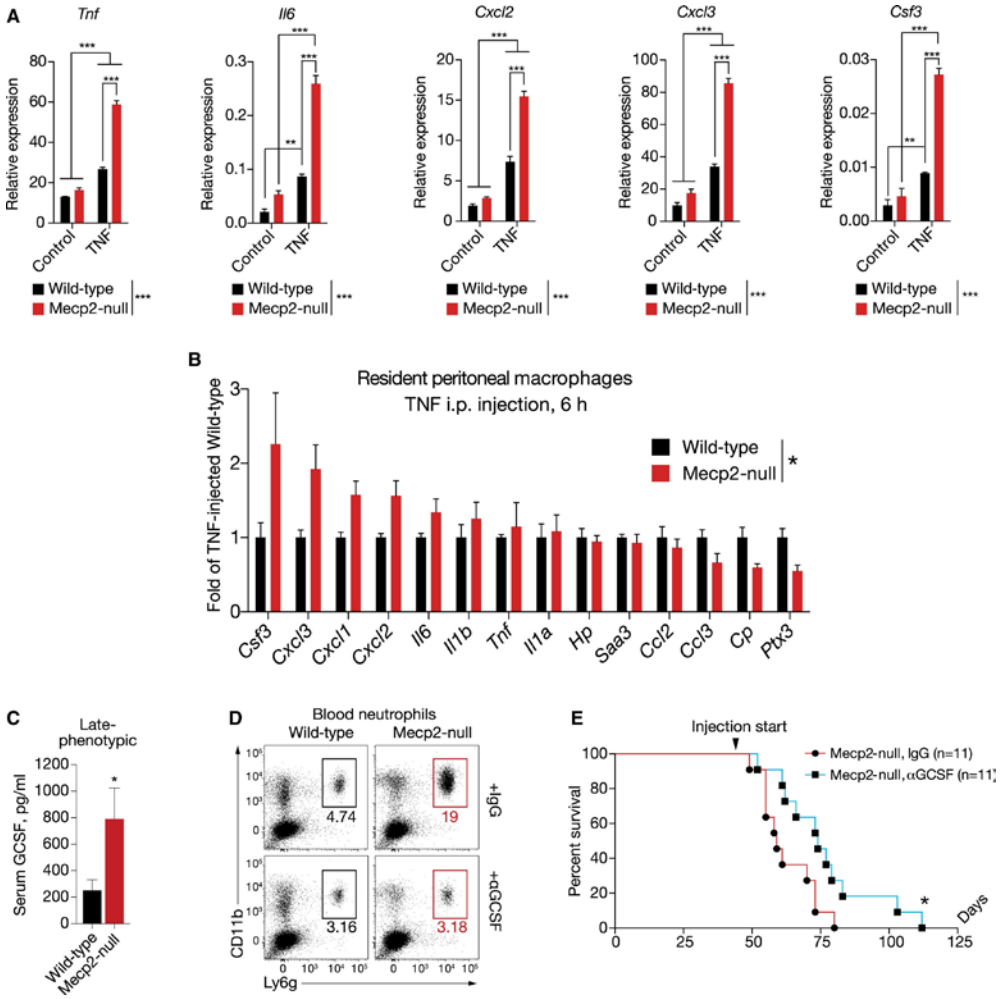

Figure II-6 Mecp2 restrains inflammatory responses in macrophages.
(A) Wild type and Mecp2-null macrophages were treated for 6 hr with TNF and subjected to quantitative real time PCR (qRT-PCR) for Tnf Il6 Cxcl2 Cxcl3, and Csf3. Data are representative of three experiments (average of three values ± SEM; ***, $p < 0.001$ and ** $p < 0.01$; Two-way ANOVA with Bonferroni post-test). (B) Mecp2-null or age-matched wild type mice were injected with intraperitoneal TNF and allowed to respond for 6 hr. Resident peritoneal macrophages were collected by lavage and subsequent AutoMACS sort for F4/80$^+$ cells. RNA was collected and qRT-PCR performed for the indicated genes (*, $p < 0.05$; Two-way ANOVA with Bonferroni post-test. Interaction for Genotype and Gene; *, $p = 0.01$. N = 3 wild type and 4 Mecp2-null. Data are presented as mean ± SEM). (C) Granulocyte colony-stimulating factor (GCSF) ELISA of serum from late-phenotypic Mecp2-null mice and wild type controls (*, $p < 0.05$; Mann-Whitney two-tailed; n = 9 per group. Data are presented as mean ± SEM). (D) Representative flow cytometry plots of Mecp2-null and wild type mice treated with anti-GCSF neutralizing or isotype antibodies showing percentage of neutrophils out of all CD45$^+$ circulating blood cells. Plots are representative of two independent experiments performed with n = 2 mice for all groups, analyzed 1–2 weeks post start of injections. (E) Survival of Mecp2-null mice treated with either

anti-GCSF neutralizing or isotype antibodies (*, $p < 0.05$; log-rank Mantel-Cox test; $n = 11$ per group).

CHAPTER III UNEXPECTED ROLE OF INTERFERON-Γ IN REGULATING NEURONAL CONNECTIVITY AND SOCIAL BEHAVIOUR

The work presented in this chapter has been published as:

Anthony J. Filiano, **Yang Xu**, Nicholas J. Tustison, Rachel L. Marsh, Wendy Baker, Igor Smirnov, Christopher C. Overall, Sachin P. Gadani, Stephen D. Turner, Zhiping Weng, Sayeda Najamussahar Peerzade, Hao Chen, Kevin S. Lee, Michael M. Scott, Mark P. Beenhakker, Vladimir Litvak & Jonathan Kipnis (2016). Unexpected role of interferon-γ in regulating neuronal connectivity and social behavior. **Nature** *535*, 425-429

My contribution to this work include RNA-seq analysis, meta-analysis of publicly available transcriptomes of mice, rat, zebrafish and drosophila flies.

Chapter III Unexpected role of interferon-γ in regulating neuronal connectivity and social behavior

Summary

Immune dysfunction is commonly associated with several neurological and mental disorders. Although the mechanisms by which peripheral immunity may influence neuronal function are largely unknown, recent findings implicate meningeal immunity influencing behaviour, such as spatial learning and memory (Derecki et al., 2010). Here we show that meningeal immunity is also critical for social behaviour; mice deficient in adaptive immunity exhibit social deficits and hyper-connectivity of fronto-cortical brain regions. Associations between rodent transcriptomes from brain and cellular transcriptomes in response to T-cell-derived cytokines suggest a strong interaction between social behaviour and interferon-gamma (IFN-γ)-driven responses. Concordantly, we demonstrate that inhibitory neurons respond to IFN-γ and increase GABAergic (γ-aminobutyric-acid) currents in projection neurons, suggesting that IFN-γ is a molecular link between meningeal immunity and neural circuits recruited for social behaviour. Meta-analysis on the transcriptomes of a range of organisms reveals that rodents, fish, and flies elevate IFN-γ/JAK-STAT-dependent gene signatures in a social context, suggesting that the IFN-γ signalling pathway could mediate a co-evolutionary link between social/aggregation behaviour and an efficient anti-pathogen response. This study implicates adaptive immune dysfunction, in particular IFN-γ, in disorders characterized by social dysfunction and suggests a

co-evolutionary link between social behaviour and an anti-pathogen immune response driven by IFN-γ signalling.

Methods

Mice

All mice (C57BL/6) were either bred in-house or purchased from the Jackson Laboratory. For each individual experiment, the control mice were obtained from the same institution as test mice. In the case that mice were purchased, they were maintained for at least 1 week to habituate before manipulation/experimentation. When possible, mice used for experiments were littermates. These include all electrophysiology experiments, all cohorts using *Stat1*$^{fl/fl}$ mice, experiments analysing induced seizures, experiments counting c-fos^{+} neurons, and experiments using *Il4*$^{-/-}$ mice. Experiments assessing the social behaviour of SCID mice using the three-chamber assay included mice bred in-house and mice purchased from the Jackson Laboratory. All other experiments used mice purchased from the Jackson Laboratory. Experimental groups were blinded and randomly assigned before the start of experimentation and remained blinded until all data were collected. Mice were housed under standard 12 h light/dark cycle conditions in rooms equipped with control for temperature and humidity. Unless stated otherwise, male mice were tested at 8–10 weeks of age. Sample sizes were chosen on the basis of a power analysis using estimates from previously published experiments. All experiments were approved by the Institutional Animal Care and Use Committee of the University of Virginia.

Behaviour

For cohorts tested with multiple behavioural assay, the elevated plus-maze was performed first and then followed by the open field before any other assay. Before all experiments, mice were transported to the behaviour room and given 1 h to habituate. All behavioural testing was conducted during daylight hours.

Elevated plus-maze

Mice were placed into the centre hub and allowed to explore the plus-maze for 10 min. Video tracking software (CleverSys) was used to quantify time spent in the open arms.

Open field

Mice were placed into the open field (35 cm × 35 cm) and allowed to explore for 15 min. Total distance and time spent in the centre (23 cm × 23 cm) were quantified using video tracking software (CleverSys).

Rotarod

Mice were placed on an accelerating rotarod (MedAssociates) that accelerated from 4.0 to 40 rpm over 5 min. Infrared beams were used to quantify the latency of a mouse to fall off the rod. Mice were given six trials with a 4-h break between trials 3 and 4.

Three-chamber sociability assay

The three-chamber sociability test was conducted as previously described (Moy et al., 2004). Briefly, mice were transported to the testing room and habituated for at least 1 h. The room was maintained in dim light and a white noise generator

used to mitigate any unforeseen noises. Test boxes were fabricated, in-house, by a machine shop. Test mice were placed in the centre chamber with the two outer chambers containing empty wire cages (Spectrum Diversified Designs) and allowed to explore for 10 min (habituation phase). After the habituation phase, mice were returned to the centre chamber. A novel mouse (an 8- to 10-week-old male C57BL/6J, ~18–22g) was placed under one cup and an object placed under the other. Before testing, the novel mouse was habituated to the cup by being placed under the cup for 10 min, three times a day for 5 days. Mice were allowed to explore for an additional 10 min (social phase). A video tracking system (CleverSys) was used to quantify the time spent around each target. For three-chamber experiments comparing social behaviour between wild-type and SCID mice, data collected using males and females were combined because no significant effects were found between genders. When females were tested, juvenile C57BL/6J male (approximately 4 weeks old) mice were used as novel demonstrators.

Novel/social environment

Mice were single housed and maintained unmanipulated for 5 days, then placed in a novel/social environment with a mouse (opposite sex and identical *scid* genotype) under video surveillance as previously described (Filiano et al., 2013). After 2 h, mice were killed and prepared for immunohistochemistry as described below. The time spent interacting was measured by a blinded observer for 5 min at the 30, 60, and 90 min post-introduction time points.

Resting-state fMRI

The protocol for rsfMRI was adapted from Zhan *et al.* (Zhan et al., 2014). Mice were maintained under light anaesthesia with (1–1.25%) isoflurane and images were acquired on a 7.0 T MRI Clinscan system (Bruker, Etlingen, Germany) using a 30-mm inner-diameter mouse whole-body radiofrequency coil. High-resolution structural images were acquired by collecting 16 0.7-mm-thick coronal slices using TR/TE 5,500/65 ms and an 180° flip angle. A BOLD rsfMRI time series of 16 0.7-mm-thick coronal slices was collected using TR/TE 4,000/17 ms and a 60° flip angle. For analysis, a structural template was custom labelled using *The Mouse Brain* by Paxinos and Franklin as reference (Johnson et al., 2010). The non-rigid transformation between the template and each individual mouse was estimated using the open source Advanced Normalization Tools (ANTs) package that was then used to propagate the regional labels to each subject (Avants et al., 2011). Cleaning of the bold fMRI data was performed using tools available in ANTsR—a statistical and visualization interface between ANTs and the R statistical project (Avants et al., 2015). fMRI preprocessing consisted of motion correction (Power et al., 2012), bandpass filtering (frequency = 0.002–0.1) and CompCor estimation (Behzadi et al., 2007). The correlation matrix was determined from the clean fMRI data using the regions labels. To determine whether the functional connectivity between sample groups was significantly different, we tested for the equality of their corresponding correlation matrices. First, an aggregate correlation matrix was constructed for

each group by calculating the median value for each connection, and then the aggregate matrices were compared using the Jennrich test, as implemented in the cortest.jennrich function in the R psych package. To create a functional connectivity network for a sample group, a correlation threshold was applied to the connections between regions of interest. If a connection strength was above the threshold, it was kept as an edge in the network, otherwise it was discarded. When comparing networks from multiple sample groups, the threshold was determined by calculating the maximum threshold that left one of the networks connected (that is, it was possible to reach any node in the network from any other node).

Immunohistochemistry

Mice were killed under Euthasol then transcardially perfused with PBS with heparin. Brains were removed and drop fixed in 4% PFA for 48 h. After fixation, brains were washed with PBS, cryoprotected with 30% sucrose, then frozen in O.C.T. compound (Sakura Finetek) and sliced (40 μM) with a cryostat (Leica). Free-floating sections were maintained in PBS + Azide (0.02%) until further processing. Immunohistochemistry for c-fos (1:1,000 dilution; Millipore) on free-floating sections was performed as previously described (Palop et al., 2011).

Depletion of meningeal T cells

A rat monoclonal antibody to murine VLA4 (clone PS/2) was affinity purified from hybridoma supernatants and was used with the permission of K. Ley (La Jolla Institute of Allergy and Immunology, San Diego, CA). Mice were given two

separate injections (intraperitoneal; 0.2 mg in saline per mouse), 4 days apart, of either anti-VLA4 or rat anti-HRP for control (clone HRPN; BioXcell), then tested 24 h after final injection.

Dissection of meninges and flow cytometry

Meninges were dissected as previously described (Derecki et al., 2010). Briefly, after killing and perfusing, skulls caps were removed by making an incision along the parietal and squamosal bones. The meninges were removed from the internal side of the skull cap and gently pressed through a 70 µm nylon mesh cell strainer with sterile plastic plunger (BD Biosciences) to isolate a single cell suspension. Cells were then centrifuged at 300*g* at 4 °C for 10 min, resuspended in cold FACS buffer (pH 7.4; 0.1 M PBS; 1 mM EDTA; 1% BSA), and stained for extracellular markers using the following antibodies at a 1:200 dilution: CD45 PerCP-Cyanine5.5 (eBioscience), TCR BV510 (BD Bioscience), CD4 FITC (eBioscience), L/D Zombie NIR (BioLegend). To measure intracellular IFN-γ single-cell isolates from meninges were maintained in T-cell isolation buffer (RPMI + 2% FBS, 2 mM L-glutamine, 1 mM sodium pyruvate, 10 mM HEPES, 1× non-essential amino acids, and 1× Antibiotic-Antimycotic (Thermo Fisher) and stimulated with PMA/ionomycin (Cell Stimulation Cocktail – eBioscience) + 10 µg/ml brefeldin A at 37°C before extracellular staining as stated above. Cells were then permeabilized with Cytofix/Cytoperm (BD Biosciences) and stained with IFN-γ APC (eBioscience; clone XMG1.2).

To measure expression of IFN-γ receptors, brains were removed and placed in Neurobasal media containing 10% fetal bovine serum. The meninges were removed from the brain and the frontal cortex was micro-dissected under a dissection microscope. Using a 2 ml dounce homogenizer, brains were homogenized in Neurobasal media with 50 U/ml Dnase I. The homogenate was passed through a 70 μm nylon filter and washed with cold FACS buffer. IFNGR were labelled with anti-IFNGR1 Biotin (BD Pharmingen; GR20) or rabbit anti-IFNGR2 (Santa Cruz; M-20). Cells were washed with FACS buffer and incubated with FITC conjugated streptavidin or 488 conjugated chicken anti-rabbit. Next, cells were washed again then incubated with CD11B PE-Cyanine7 (eBioscience), L/D Zombie NIR (BioLegend), and Hoechst for 45 min. Cells were washed, then permeabilized and fixed with Cytofix/Cytoperm (BD Biosciences). After another wash with permeabilization wash buffer (PBS with 10% fetal bovine serum, 1% sodium azide, and 1% saponin; pH 7.4), cells were incubated overnight with NeuN PE (Millipore). Cells underwent a final wash and again passed through a 70 μm nylon filter. Samples were run on a flow cytometer Gallios (Beckman Coulter) then analysed using FlowJo software (Treestar).

SCID repopulation

SCID mice were repopulated with cells from spleen and lymph nodes (axillary, brachial, cervical, inguinal, and lumbar). Spleen and lymph nodes were collected from a 3- to 4-week-old donor and passed through a 70 μm nylon mesh cell strainer with a sterile plastic plunger. ACK buffer was used to lyse red blood cells

before washing with saline. Cells were counted on an automated cell counter (Nexcelom) and injected (intravenously) at 5×10^6 cells in 250 µl of saline (control mice were injected with 250 µl of saline only). For injections, the animal technician was blinded to the genotype of the mice and the content of the injection. Thus, all groups were handled identically. Mice aged 3–4 weeks were carefully placed into a tail vein injection platform. Their tails were briefly warmed using a heating pad and saline with cells or saline alone was slowly injected into the tail vein using a 28-gauge needle. After the injection, mice were returned to their home cage.

IFN-γ injections

Mice were anaesthetized with a ketamine/xylazine (ketamine (100 mg/kg) and xylazine (10 mg/kg)) injection (intraperitoneal) or isoflurane (2%), then placed into a stereotaxic frame with the head at an approximately 45° angle. The skin above the cisterna magna was cleaned and sanitized before a 1 cm incision was made. The underlying muscles were separated with forceps, retracted, and a small Hamilton syringe (33-gauge) was used to slowly inject 1 µl of saline or IFN-γ (20 ng; eBioscience) into the cisterna magna. After injection the syringe was held in place for 5 min to avoid back-flow of CSF. After the syringe was removed, muscles were put back in place and skin was sutured. Mice were placed on a heating pad and given ketoprofen and baytril for recovery.

Induced seizures

IFN-γ was injected into the CSF through the cisterna magna as described above, 24 h before inducing seizures. Control mice were injected with the same volume of saline. To induce seizures, mice were injected with PTZ (40 mg/kg; intraperitoneally). After injection, mice were placed into an empty housing cage and recorded for video analysis. Seizures were analysed by a blinded observer using a behaviour scoring system previously published (Li et al., 2014b).

Diazepam treatment

Diazepam (1.25 mg/kg) was delivered intraperitoneal for 30 min before testing for social behaviour.

Fluorescence *in situ* hybridization

Mice were euthanized then transcardially perused with PBS with heparin followed by 4% PFA. Brains were then removed and drop fixed in 4% PFA for 24 h, frozen in OCT, and 12 μM sections were cut on a cryostat. Fluorescence *in situ* hybridization was performed using RNA ISH tissue assay kits (Affymetrix) following the manufacturer's protocol. Tissues were treated with protease for 20 min at 40 °C. Images at 63× magnification were acquired on a Leica TCS SP8 confocal system (Leica Microsystems) using LAS AF Software.

AAV delivery

AAV1.hSyn.HI.eGFP–Cre.WPRE.SV40 and AAV1.hSyn.eGFP.WPRE.bGH were purchased from Penn Vector Core. IFNGR1$^{fl/fl}$ mice were purchased from the Jackson Laboratory. After 1 week of habituation, mice were anaesthetized with

2% isoflurane and injected bilaterally with 2×10^{10} genome copies of AAV virus in 1 µl at stereotaxic coordinates +2.5 µm bregma A/P, 0.25 µm lateral, 1.25 µm deep.

Measuring inhibitory currents

Visualized whole-cell patch-clamp recordings were performed on layer II/III prefrontal cortical neurons prepared from acute brain slices (adult) using the protective recovery method (Ting et al., 2014). Recordings were performed in 34 °C artificial cerebrospinal fluid (ACSF) containing (in mM) 131.5 NaCl, 25 $NaHCO_3$, 12 D-glucose, 2.5 KCl, 1.25 NaH_2PO_4, 2 $CaCl_2$, and 1 $MgCl_2$. ACSF also contained 3 mM kynurenic acid to block synaptic excitation and 2.5 mM NO-711 to enhance tonic inhibition (Nusser and Mody, 2002). Slices were incubated in this ACSF for 5–10 min before placement in the recording chamber. The patch pipette solution with elevated chloride contained (in mM) 140 CsCl, 4 NaCl, 1 $MgCl_2$, 10 HEPES, 0.05 EGTA, 2 Mg-ATP, and 0.4 Mg-GTP. Once recordings equilibrated, baseline holding current in ACSF was measured for 3.5 min, after which ACSF containing IFN-γ (20 pg/ml) was applied for 8.5 min and then washed. Data presented show the mean holding current during the last minute of control (ACSF) and drug (ACSF + IFN-γ) conditions.

RNA isolation and sequencing

Eight-week-old male mice were purchased from the Jackson Laboratory and housed in standard housing boxes with either four mice per cage or isolated for 6 days. Mice were euthanized as described above and the PFC was

microdissected under a dissection microscope. RNA was isolated using an RNAeasy mini kit (Qiagen) and a cDNA library was generated with a TruSeq Stranded mRNA Library Prep Kit (Illumina) with Agencourt AMPure XP beads for PCR cleanup. Samples were loaded onto a NextSeq 500 High-output 75 cycle cartridge and sequenced on a NextSeq 500 (Illumina).

Transcriptome analysis

Raw FASTQ sequencing reads were chastity filtered to remove clusters having outlying intensity corresponding to bases other than the called base. Filtered reads were assessed for quality using FastQC. Reads were splice-aware aligned to the UCSC mm9 genome using STAR (Dobin et al., 2013), and reads overlapping UCSC mm9 gene regions were counted using featureCounts (Liao et al., 2014b). The DESeq2 Bioconductor package (Love et al., 2014) in the R statistical computing environment was used for normalizing count data, performing exploratory data analysis, estimating dispersion, and fitting a negative binomial model for each gene comparing the expression from the PFC of mice in a social environment versus isolation. After obtaining a list of differentially expressed genes, log (fold changes), and *P* values, Benjamini–Hochberg false discovery rate procedure was used to correct *P* values for multiple testing. A gene set enrichment analysis (GSEA) algorithm (Subramanian et al., 2005) was applied to identify the enrichment of transcriptional signatures and molecular pathways in PFC transcriptomes of mice exposed to group and isolation housing conditions. Four thousand seven hundred and twenty-six publicly available

transcriptional signatures were obtained from the molecular Signature Database C2 version 4.0, and GSEA was used to examine the distribution of these curated gene sets in lists of genes ordered according to differential expression between group and isolation housing conditions. We analysed statistics by evaluating nominal *P* value and normalized enrichment score (NES) on the basis of 1,000 random sample permutations.

Meta-analysis

The custom-made IFN-γ and pathogen-induced transcriptional signatures were generated by retrieving genes upregulated at least twofold following IFN-γ stimulation or pathogen infection. All custom signatures were derived from publicly available transcriptomes downloaded from Gene Expression Omnibus (GEO). Specifically, mammalian IFN-γ transcriptional signatures were derived from transcriptomes GSE33057, GSE19182, GSE36287, GSE9659, GSE1432, and GSE6353. Zebrafish IFN-γ transcriptional signature was used as described (Lopez-Munoz et al., 2009). *Drosophila* pathogen-induced JAK/STAT-dependent transcriptional signatures were derived from transcriptomes GSE54833 and GSE2828.

A GSEA algorithm was applied to identify the enrichment of custom-made mammalian IFN-γ transcriptional signatures in the publicly available brain cortex transcriptomes of mice and rats exposed to social aggregation, sleep deprivation, stress, psychostimulants (DOI, cocaine, amphetamine, methamphetamine, methylphenidate, caffeine, nicotine, and modafinil), antipsychotics (olanzapine,

haloperidol, and risperidone), anticonvulsants (levetiracetam, phenytoin, ethosuximide, and oxcarbazepine), and antidepressants (iproniazid, moclobemide, paroxetine, and phenelzine). In total, 41 transcriptomes were analysed as indicated in Supplementary Table 2. We analysed statistics by evaluating nominal *P* value and NES on the basis of 1,000 random sample permutations.

Zebrafish are social fish that aggregate into shoals (Engeszer et al., 2007, Krause et al., 2000, Miller and Gerlai, 2007, Saverino and Gerlai, 2008). Various zebrafish strains differ in their preference for social interaction and novelty, resembling the phenotypic variation of inbred mouse strains (Barba-Escobedo and Gould, 2012, Moy et al., 2004). Notably, domesticated zebrafish strains demonstrate higher social interaction and social novelty preference (Moretz et al., 2007, Zala et al., 2012) compared with wild zebrafish strains. Therefore, a GSEA algorithm was used to identify the enrichment of zebrafish IFN-γ transcriptional signature in the publicly available whole-brain transcriptomic profiles of behaviourally distinct strains of domesticated and wild zebrafish. The brain transcriptomic profiles of domesticated (Scientific Hatcheries (SH) and Transgenic Mosaic 1 (TM1)) and wild (Nadia, Gaighata) zebrafish strains were derived from publicly available transcriptome data set GSE38729. We analysed statistics by evaluating nominal *P* value and NES on the basis of 1,000 random gene set permutations.

Social interactions in *Drosophila melanogaster* flies play an important role in courtship, mating, egg-laying, circadian timing, food search, and even lifespan determination (Levine et al., 2002, Mery et al., 2009, Ruan and Wu, 2008, Sarin and Dukas, 2009, Sokolowski, 2010). Notably, a number of studies have demonstrated that social isolation leads to an aggressive behaviour in *Drosophila* flies, whereas group housing suppresses the aggressiveness (Hoffmann, 1987, Kamyshev et al., 2002, Wang et al., 2008). Therefore, we employed a GSEA algorithm to identify the enrichment of JAK/STAT-dependent transcriptional signatures in the publicly available brain transcriptomes of *Drosophila* populations that were socially-induced or genetically-selected for low-aggressive (that is, social) behaviour. The transcriptomic profiles were derived from publicly available transcriptome data sets GSE5404 and GSE6994. We analysed statistics by evaluating nominal *P* value and NES on the basis of 1,000 random gene set permutations.

Promoter motif analysis

A GSEA algorithm was used to identify genes that are differentially expressed in brain transcriptomes of mice and rats exposed to social aggregation, domesticated zebrafish strains, and low-aggressive *Drosophila melanogaster* populations, compared with their control counterparts. High-scoring differentially expressed ‘leading-edge’ social genes were selected on the basis of their presence in the IFN-γ and pathogen-induced transcriptional signatures. Specifically, as shown in Figure III-3, we have identified 31, 48, 14, and 53

leading-edge genes in brain transcriptomes of mice and rats exposed to social aggregation, domesticated Zebrafish strain, and low-aggressive *Drosophila melanogaster* population, respectively. We next extracted promoter sequences of 200 bp upstream of transcription start sites of these 'leading-edge' genes using UCSC Genome Browser (https://genome.ucsc.edu/). The MEME suite was then used to discover overrepresented transcription factor binding motifs, as described (Bailey et al., 2009). MEME parameters used were any number of motif repetitions per sequence, with a minimum motif width of 5 bases and maximum motif width of 15 bases. The discovered MEME motifs were compared using Tomtom analysis. In this case, the Tomtom motif similarity analysis ranks the MEME motif most similar to the vertebrates *in vivo* and *in silico*. The statistics were determined using Euclidean distance.

Circos plot

A GSEA algorithm was applied to identify the enrichment of IFN-γ, IL-4/IL-13, IL-17, and IL-10/TGF-β signalling pathways in the brain transcriptomes of rodent animals exposed to social aggregation, stress, psychostimulants, antipsychotics, and antidepressants. All custom signatures were derived from publically available rodent transcriptomes downloaded from Gene Expression Omnibus. Statistical significance of GSEA results was assessed using 1,000 sample permutations. A NES greater than 1.5 and a nominal *P* value less than 0.05 was used to determined pairwise transcriptome connectivity. A Circos graph was generated using circos package 0.68.12 (Krzywinski et al., 2009).

Statistics

Data were analysed using the statistical methods stated in each figure legend. For the three-chamber assay, a two-way ANOVA was performed using genotype/treatment and sociability as main effects, followed by applying a Sidak's post hoc comparison to assess if the group had a significant social preference. Before running an ANOVA, an equality of variance was determined by using a Brown–Forsythe test. Bars display the means, and error bars represent ranges of the standard error of the mean. For rsfMRI, data were analysed using a one-way ANOVA followed by a post hoc Tukey's test. The box and whisker plots extend to the 25th and 75th percentiles and the centre line indicates the mean. The whiskers represent the min and max data points. Data for seizure latency were analysed using a two-way ANOVA with repeated measures followed by Sidak's post hoc test.

Results

Meningeal T-cell compartment is necessary for supporting neuronal connectivity and social behaviour

Social behaviour is beneficial for many processes critical to the survival of an organism, including foraging, protection, breeding, and, for higher-order species, mental health (Cacioppo et al., 2014, Bourke, 2014). Social dysfunction manifests in several neurological and mental disorders such as autism spectrum disorder, frontotemporal dementia, and schizophrenia among others (Kennedy and Adolphs, 2012). Likewise, imbalance of cytokines, a disparity of T-cell subsets, and overall immune dysfunction is often associated with the above-mentioned disorders (Ashwood et al., 2011, Gupta et al., 1998, Waisman et al., 2015). However, the fundamental mechanisms by which dysfunctional immunity may interfere with neural circuits and contribute to behavioural deficits remain unclear.

To test whether adaptive immunity is necessary for normal social behaviour, we tested SCID mice (deficient in adaptive immunity) using the three-chamber sociability assay (Moy et al., 2004). This assay quantifies the preference of a mouse for investigating a novel mouse versus object, and has been used to identify deficits in multiple mouse models of disorders that present with social dysfunction (Silverman et al., 2010). Unlike wild-type mice, SCID mice lacked social preference for a mouse over an object (Figure III-1a). Importantly, SCID mice did not show anxiety, motor, or olfactory deficits. We confirmed that

SCID mice have social deficits by analysing social interactions in a home cage (data not shown). To test whether social deficits were reversible, we repopulated 4-week-old SCID mice with wild-type lymphocytes and measured social behaviour 4 weeks after transfer. SCID mice repopulated with lymphocytes, unlike those injected with the vehicle, showed social preference indistinguishable from wild-type mice (Figure III-1b).

Recent clinical findings indicate disturbed circuit homeostasis, resulting in hyper-connectivity, is a feature of children with autism spectrum disorder (Nelson and Valakh, 2015). Imaging studies using task-free resting state fMRI (rsfMRI), revealed hyper-connectivity among frontal cortical nodes in patients with autism spectrum disorder (Supekar et al., 2013). Disturbances in resting state connectivity are also observed in mice with social deficits (Zhan et al., 2014). rsfMRI is an unbiased technique used to assess synchrony between brain regions over time by comparing spontaneous fluctuations in blood oxygenation level-dependent (BOLD) signals (Shen, 2015). To assess the influence of adaptive immunity on functional connectivity, we analysed resting-state BOLD signals from wild-type and SCID mice. SCID mice exhibited hyper-connectivity between multiple frontal and insular regions (Figure III-1c and 1d) implicated in social behaviour and autism spectrum disorder. Notably, repopulating SCID mice with lymphocytes rescued aberrant hyper-connectivity observed in vehicle-treated SCID controls (Figure III-1c and 1d). Interestingly, other functionally connected regions, not directly implicated in social function, such as

interhemispheric connectivity between motor and somatosensory cortex, were not affected by a deficiency in adaptive immunity. Using another approach to analyse neuronal activation in a task-based system, we demonstrated that SCID mice exposed to a social stimulus exhibited hyper-responsiveness in the prefrontal cortex (PFC; increased number of c-fos^{+} cells in PFC; Figure III-1e and 1f) but not the hippocampus.

We previously demonstrated that T cells influence learning behaviour and exert their beneficial effects presumably from the meninges (Brynskikh et al., 2008, Derecki et al., 2010) To address the role of meningeal T cells in social behaviour, we decreased the extravasation of T cells into the meninges of wild-type mice using antibodies against VLA4 (Yednock et al., 1992), an integrin expressed on T cells (among other immune cells) required for CNS homing. Partial elimination of T cells from meninges was sufficient to cause a loss in social preference (Figure III-1g) . Despite their proximity to the brain, meningeal T cells do not enter the brain parenchyma, suggesting their effect is mediated by soluble factors. To identify which T-cell-mediated pathways are involved in regulating social behaviour, we used gene set enrichment analysis (GSEA) to search for T-cell-mediated response signatures (IFN-γ, IL-4/IL-13, IL-17, Il-10, TGF-β) in 41 transcriptomes from mouse and rat brain cortices. GSEA assesses whether the expression of a previously defined group of related genes is enriched in one biological state. In this case, we used GSEA to identify which cytokine-induced response signatures were enriched in the transcriptomes of

mice and rats exposed to different stimuli. The stimuli included social aggregation, sleep deprivation, stress, psychostimulants, antidepressants, anticonvulsants, and antipsychotics. Transcriptomes from cortices of animals exposed to social aggregation and psychostimulants were enriched for IFN-γ regulated genes (Figure III-1h).

IFN-γ supports proper neural connectivity and social behaviour

A substantial number of meningeal T cells are capable of expressing IFN-γ (41.95% ± 6.34 of TCR^+ cells) and recent work has proposed a role for IFN-γ in T-cell trafficking into meningeal spaces (Kunis et al., 2013). To assess the potential role of IFN-γ in mediating the influence of T cells on social behaviour, we first examined the social behaviour of IFN-γ-deficient mice and determined that they had social deficits (Figure III-2a). Importantly, IFN-γ-deficient mice did not show anxiety or motor deficits (data not shown). Similar to SCID mice, IFN-γ-deficient mice also exhibited aberrant hyper-connectivity in fronto-cortical/insular regions (Figure III-2b and 2c). While repopulating SCID mice with lymphocytes from wild-type mice restored a social preference, repopulating SCID mice with lymphocytes from *Ifng*$^{-/-}$ mice did not have such an effect (data not shown). Remarkably, a single injection of recombinant IFN-γ into the cerebrospinal fluid (CSF) of *Ifng*$^{-/-}$ mice was sufficient to restore their social preference when tested 24 h after injection (Figure III-2d) and reduce overall hyper-connectivity in the PFC (data not shown). To further validate a role for IFN-γ signalling in social

behaviour, we tested mice deficient for the IFN-γ receptor (*Ifngr1*$^{-/-}$ mice) and found that they had a similar social deficit as *Ifng*$^{-/-}$ mice (data not shown), which, as expected, was not rescued by injecting recombinant IFN-γ into the CSF (data not shown). On the basis of our previous demonstration of a role for IL-4 produced by meningeal T cells in spatial learning behaviour (Filiano et al., 2016), we assessed whether deficiency in IL-4 would also result in social deficits. IL-4-deficient mice did not demonstrate social deficits; in fact, they spent more time investigating a novel mouse than a novel object compared with wild-type mice (data not shown).

To determine which cell types in the brain responding to IFN-γ, we analysed mouse PFC for the expression of IFN-γ receptor subunits 1 and 2 and found that both neurons and microglia express mRNA and protein for R1 and R2 subunits of the IFN-γ receptor (Figure III-2e and 2f). Microglia are CNS resident macrophages and are known to express the IFN-γ receptor (Prieto et al., 1994). However, genetically deleting STAT1, the signalling molecule downstream of the IFN-γ receptor, from microglia (and other cells of myeloid origin), did not disturb normal social preference (data not shown). These results led us to focus on neuronal responses to IFN-γ as they relate to social behaviour.

To directly assess if IFN-γ can drive inhibitory tone in the PFC, we measured inhibitory currents in layer II/III pyramidal cells from acutely prepared brain slices from wild-type mice. In addition to receiving phasic inhibitory synaptic input, these cells are also held under a tonic GABAergic current that serves to

hyperpolarize their resting membrane potential (Figure III-2i). Tonic GABAergic currents are extra-synaptic and can yield long-lasting network inhibition (Olah et al., 2009). We observed that IFN-γ augmented tonic current (Figure III-2i and 2j), suggestive of elevated levels of ambient GABA during application of IFN-γ. Deleting the IFN-γ receptor from inhibitory neurons (*Vgat*^{Cre}::*Ifngr1*$^{fl/fl}$ mice) prevented IFN-γ from augmenting tonic inhibitory current. Given that IFN-γ promotes inhibitory tone, we tested whether IFN-γ could prevent aberrant neural discharges by injecting IFN-γ into the CSF and then chemically inducing seizures with the GABA type A receptor antagonist pentylenetetrazole (PTZ). Mice injected with IFN-γ were less susceptible to PTZ-induced seizures: IFN-γ delayed seizure onset and lowered seizure severity (Figure III-2k). Further, to test whether over-excitation causes social deficits in IFN-γ-deficient mice, we treated *Ifng*$^{-/-}$ mice with diazepam to augment GABAergic transmission[20]. Diazepam successfully rescued social behaviour of *Ifng*$^{-/-}$ mice, similar to the effect observed with recombinant IFN-γ treatment (Fig III. 2l), suggesting that social deficits, caused by a deficiency in IFN-γ, may arise from inadequate control of GABAergic inhibition by IFN-γ.

IFN-γ transcriptional signature genes in social behaviour-associated brain transcriptomes of rat, mouse, zebrafish, and Drosophila

It is intriguing that IFN-γ, predominately thought of as an anti-pathogen cytokine, can play such a profound role in maintaining proper social function. Since social

behaviour is crucial for the survival of a species and aggregation increases the likeliness of spreading pathogens, we hypothesized that there was co-evolutionary pressure to increase an anti-pathogen response as sociability increased, and that the IFN-γ pathway may have influenced this co-evolution. To test this hypothesis, we analyzed metadata of publically available transcriptomes from multiple organisms including the rat, mouse, zebrafish, and fruit flies. Using GSEA, we determined that transcripts from social rodents (acutely group-housed) are enriched for an IFN-γ responsive gene signature (Figure III-3a and 3b). Conversely, rodents that experienced social isolation demonstrated a dramatic loss of the IFN-γ responsive gene signature. Zebrafish and flies showed a similar association between anti-pathogen and social responses (Figure III-3c and 3d). We observed that immune response programs were highly enriched in the brain transcriptomes of flies selected for low aggressiveness traits (a physiological correlate for socially experienced flies; Figure III-3d). We next analyzed the promoters of these highly upregulated social genes and found them to be enriched for STAT1 transcription factor binding motifs (Figure III-3a–d). These data suggest, even in the absence of infection, an IFN-γ gene signature is upregulated in aggregated organisms. This is consistent with an interaction between social behaviour and the anti-pathogen response, a dynamic that could be mediated by the IFN-γ pathway. Since low-aggressive flies upregulate genes in the JAK/STAT pathway (canonically downstream of IFN-γ receptors in higher species), yet lack IFN-γ or T cells, it is intriguing to speculate that T-cell-derived

IFN-γ may have evolved in higher species to more efficiently regulate an anti-pathogen response during increased aggregation of individuals.

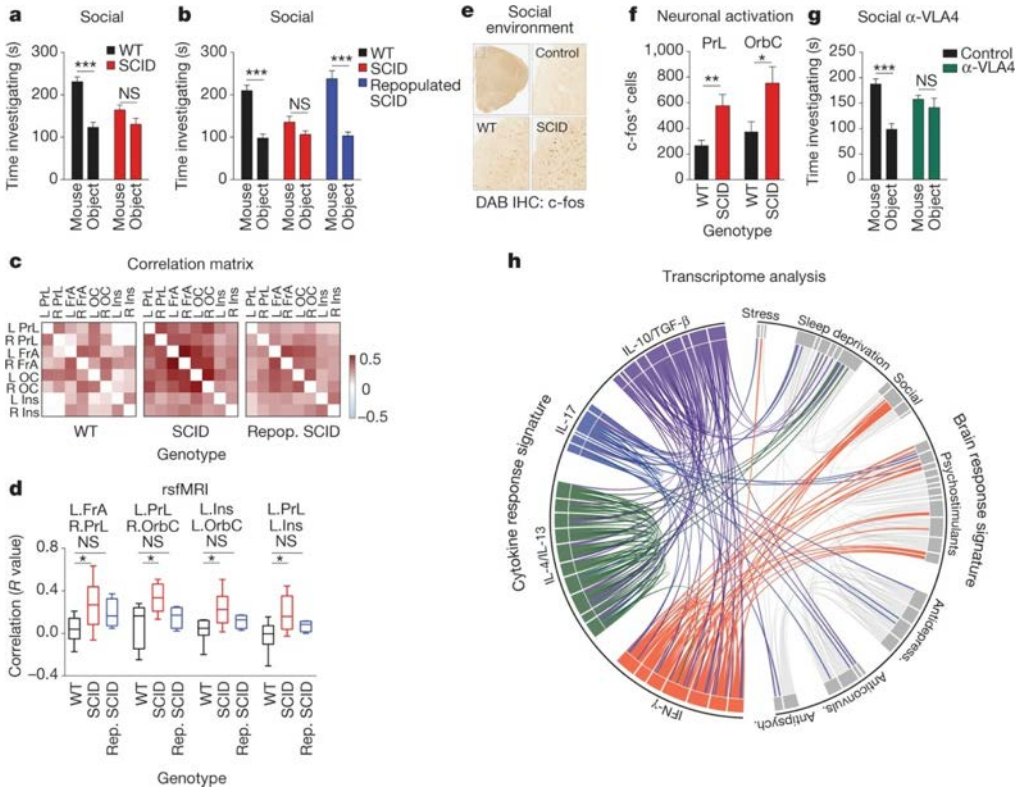

Figure III-1 Meningeal T cell compartment is necessary for supporting neuronal connectivity and social behavior.

a, Wild-type mice exhibit social preference that is absent in SCID mice (ANOVA for genotype ($F(1, 26)$) = 6.370, P = 0.0181; n = 14 mice per group; **P < 0.01 Sidak's post-hoc; pooled 2 independent experiments). b, Repopulating the adaptive immune system in SCID mice restored normal social behavior (n = 17;16;15 mice per group; ANOVA for genotype ($F(2, 45)$) = 8.282, P = 0.0009 and interaction ($F(2, 45)$) = 9.146, P = 0.0005; ***P < 0.001; **P < 0.01 Sidak's post-hoc; pooled 3 independent experiments). c, Correlation matrices from wild-type, SCID, and repopulated (Repop.) SCID mice were generated by rsfMRI. Abbrev.: L=left; R=right; FrA=frontal association area; PrL=prelimbic cortex; Ins=insula; OrbC=orbital cortex. d, Correlation values from rsfMRI. The box and whisker plots extend to the 25th and 75th percentiles with the center-line showing the mean. The whiskers represent the min and max data points. (n = 8;9;4 mice per group; ANOVA < 0.05; *P < 0.05 Sidak's post-hoc; pooled 2 independent experiments). e, Immunohistochemistry of c-fos in the PFC. f, Elevated c-fos+ cells in the prefrontal and orbital cortices of SCID compared to wild-type mice (n = 9;10 mice per group; **P < 0.01; *P < 0.05 t-test; single experiment). g, Acute partial depletion of meningeal T cells caused social deficits (n = 12;13 mice per group; ANOVA for interaction ($F(1, 23)$) = 7.900, P < 0.01; ***P < 0.001 Sidak's post-hoc; pooled 2 independent experiments). h, Circos plot showing the connectivity map derived from the pairwise comparison of transcriptome datasets. IFN-γ signature genes are over-represented in cortex of animals exposed to social aggregation and psychostimulants. The representations of IFN-γ, IL-4/IL-13, IL-17, and IL-

10/TGF-β dataset connectivity are shown in orange, green, blue, and purple, respectively. Each line represents a pairwise dataset overlap, which was determined using GSEA analysis and filtered by $P < 0.05$ and $NES > 1.5$. See for labels. Data from the 3-chamber test (a, b, g) were analyzed by applying a 2-way ANOVA for social behavior and genotype/treatment, followed by a post-hoc Sidak's test. Bars represent average mean times investigating ± s.e.m.

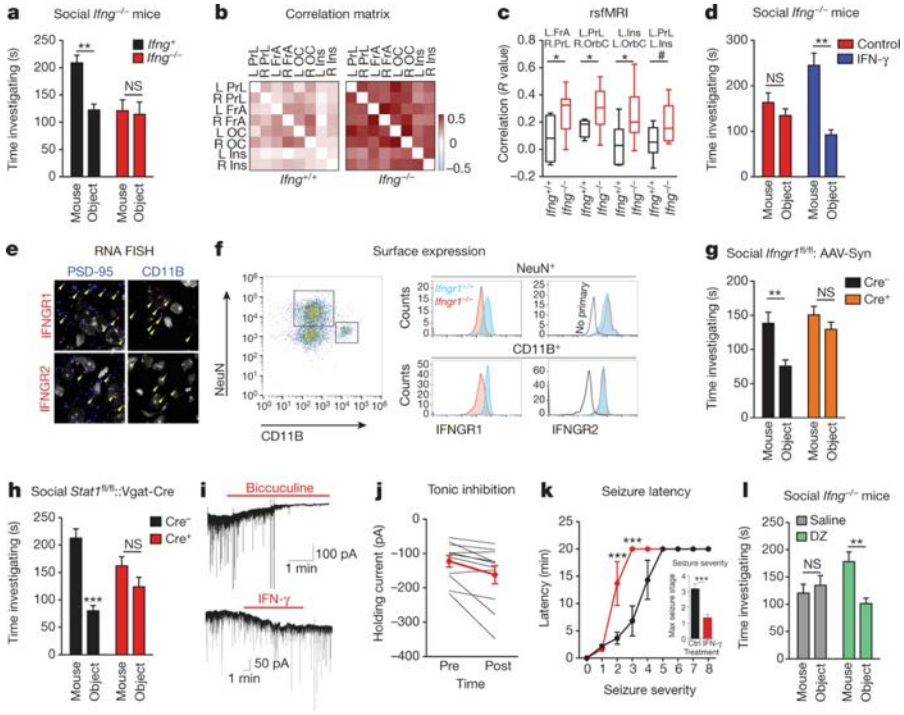

Figure III-2 IFN-γ supports proper neural connectivity and social behavior.
a**,** Ifng$^{-/-}$ mice exhibit social deficits (n = 16;12 mice per group; ANOVA for genotype (F(1, 52)) = 8.327, P < 0.01; **P < 0.01 Sidak's post-hoc; pooled 2 independent experiments). **b,** Correlation matrix from Ifng$^{+/+}$ and Ifng$^{-/-}$ mice. **c,** Box and whisker plots of correlation values (n = 8 mice per group; *P < 0.05; # P = 0.06 t-test; repeated 2 times). **d,** A single CSF injection of IFN-γ (20ng) was sufficient to rescue social deficits in Ifng$^{-/-}$ mice 24 hours post-injection (n = 14;11 mice per group; ANOVA for interaction (F (1, 46)) = 10.22 P < 0.01; ***P < 0.001 Sidak's post-hoc; pooled 2 independent experiments). **e,** Expression of IFN-γ receptor subunit mRNA by fluorescent in situ hybridization in slices from mouse PFC. RNA probes and corresponding colors: left:psd95-blue (neurons); right: CD11B-blue (microglia); top: IFNGR1-red; bottom: IFGR2-red. Yellow arrowheads denote co-localization. **f,** Expression of IFN-γ receptor subunit protein by flow cytometry. Cells were gated on Hoechst+/live/single then neurons and microglia were gated on NeuN and CD11B, respectively. Ifngr1$^{-/-}$ mice and no primary antibody for IFNGR2 were included as negative controls. **g,** Deleting Ifngr1from neurons in the PFC caused social deficits. Ifngr1$^{fl/fl}$ mice were injected with AAV-Syn-CRE-GFP into the PFC and tested for social behavior 3 weeks post injection (n = 11;12 mice per group; ANOVA for genotype (F (1, 21)) = 10.62, P < 0.01; *P < 0.05 Sidak's post-hoc; pooled 3 independent experiments). **h,** Vgat^{Cre}::Stat1$^{fl/fl}$ mice exhibit social deficits (n = 10;11 mice per group; ANOVA for interaction (F(1, 19)) = 10.30 < 0.01; ***P < 0.001 Sidak's post-hoc; pooled 3 independent experiments). **i,** Layer 2/3 neurons in slices from wild-type mice are held under tonic GABAergic inhibition (top), which is blocked by the GABA-A receptor antagonist bicuculline. IFN-γ increases tonic GABAergic inhibitory current (n = 11 cells from 4 mice; bottom). **j,** Holding current pre and during IFN-γ (P = 0.01 t-test). **k,** IFN-γ increased latency to reach each seizure stage (n = 6 mice per group; ANOVA with repeated measures < 0.001; ***P < 0.001 Sidak post-hoc) and (**inset**) reduced the maximum severity of seizures (***P < 0.001 t-test; repeated 2

times). **l,** Diazepam rescued social deficits in Ifng$^{-/-}$ mice (n = 12 mice per group; ANOVA for interaction (F (1, 22)) = 9.204 < 0.01; **P < 0.01 Sidak's post-hoc; repeated 2 times). Data from the 3-chamber test (**a**, **d**, **g**, **h**, **i**) were analyzed by applying a 2-way ANOVA for social behavior and genotype/treatment, followed by a Sidak's post-hoc test. Bars represent average mean times investigating ± s.e.m. All experiments were repeated at least once.

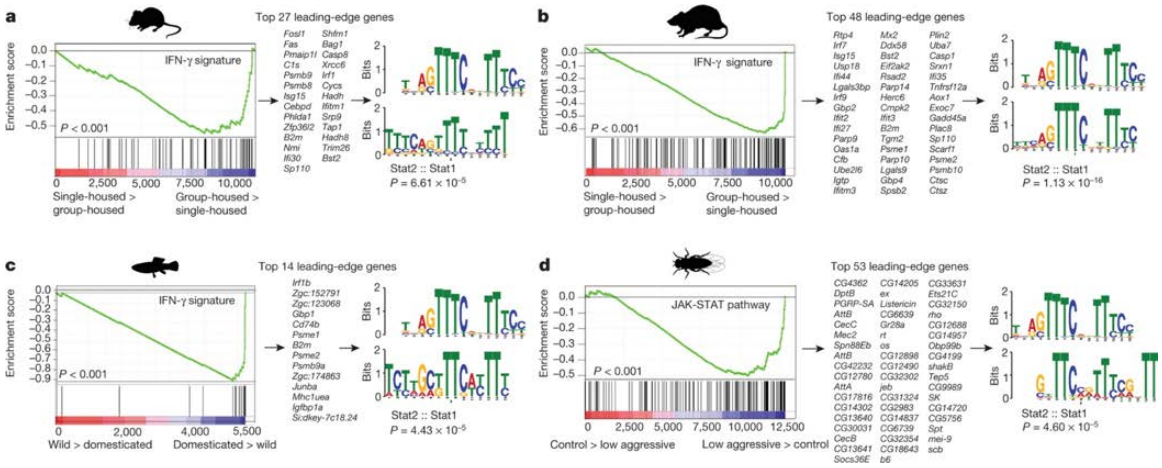

Figure III-3 Over-representation of IFN-γ transcriptional signature genes in social behavior-associated brain transcriptomes of rat, mouse, zebrafish, and drosophila.
GSEA plots demonstrate the over-representation of IFN-γ transcriptional signatures (derived from Molecular Signature Database C2, GSE33057, or Lopez-Munoz, A. et al) in brain transcriptomes of (a) mice and (b) rats subjected to social or isolated housing and in brain transcriptomes of (c) domesticated zebrafish compared to a wild zebrafish strain. (d) Over-representation of JAK/STAT pathway transcriptional signature genes (derived from GSE2828) in head transcriptomes of flies selected for low-aggressive behavior (behavioral readout for social behavior in flies (see methods section "Meta-data analysis" for more details)). Genes are ranked into an ordered list according to their differential expression. The middle part of the plot is a bar code demonstrating the distribution of genes in the IFN-γ transcriptional signature gene set against the ranked list of genes. The list on the right shows the top genes in the leading-edge subset. Promoter regions of these genes were scanned for transcription factor binding site (TFBS) using MEME suite. MEME output demonstrates significant STAT TFBS enrichment in cis-regulatory regions of leading edge genes up-regulated in a social context.

CHAPTER IV THE TREM2-APOE PATHWAY DRIVES THE TRANSCRIPTIONAL PHENOTYPE OF DYSFUNCTIONAL MICROGLIA IN NEURODEGENERATIVE DISEASES

The work presented in this chapter has been published as:

Susanne Krasemann, Charlotte Madore, Ron Cialic, Caroline Baufeld, Narghes Calcagno, Rachid El Fatimy, Lien Beckers, Elaine O`Loughlin, **Yang Xu**, Zain Fanek, David J. Greco, Scott T Smith, George Tweet, Zachary Humulock, Tobias Zrzavy, Patricia Conde-Sanroman, Mar Gacias, Zhiping Weng, Hao Chen, Emily Tjon, Fargol Mazaheri, Kristin Hartmann, Asaf Madi, Jason Ulrich, Markus Glatzel, Anna Worthmann, Joerg Heeren, Bogdan Budnik, Cynthia Lemere, Tsuneya Ikezu, Frank L. Heppner, Vladimir Litvak, David Holtzman, Hans Lassmann, Howard L. Weiner, Jordi Ochando, Christian Haass and Oleg Butovsky (2017). The TREM2-APOE pathway drives the transcriptional phenotype of dysfunctional microglia in neurodegenerative diseases. **Immunity** *47*,566-581

My contribution to this work include in-house RNA-seq analysis and meta-analysis of publicly available microglia transcriptomes in all diseases, promoter sequence analysis and construction of gene regulatory networks.

CHAPTER IV THE TREM2-APOE PATHWAY DRIVES THE TRANSCRIPTIONAL PHENOTYPE OF DYSFUNCTIONAL MICROGLIA IN NEURODEGENERATIVE DISEASES

Summary

Microglia play a pivotal role in the maintenance of brain homeostasis, but lose their homeostatic function during the course of neurodegenerative disorders. We identified a specific APOE-dependent molecular signature in microglia isolated from mouse models of amyotrophic lateral sclerosis, multiple sclerosis and Alzheimer's disease (SOD1, EAE and APP-PS1) and in microglia surrounding neuritic Aβ-plaques in human Alzheimer's disease brain. This is mediated by a switch from a (M0)-homeostatic to (MGnD)-neurodegenerative phenotype following phagocytosis of apoptotic neurons via the TREM2-APOE pathway. TREM2 induces APOE signaling which is a negative regulator of the transcription program in M0-homeostatic microglia. Targeting the TREM2-APOE pathway restores the M0-homeostatic signature of microglia in APP-PS1 and SOD1 mice and prevents neuronal loss in an acute model of neurodegeneration. Taken together, our work identifies the TREM2-APOE pathway as a major regulator of microglial functional phenotype in neurodegenerative diseases and serves as a novel target to restore homeostatic microglia.

Introduction

Neuronal injury and cell death are common hallmarks of neurodegenerative processes (Mattson et al., 1998). It remains unclear whether neuronal cell death is a cause or result of Alzheimer's disease (AD), especially when one considers that neurodegeneration is not an acute and rapid event but occurs gradually over a long period of time. However, apoptosis, as well as neuritic dystrophy leading to permanent central nervous system (CNS) damage, occurs in neurodegenerative diseases, including AD (Masliah et al., 1998) and amyotrophic lateral sclerosis (ALS) (Kostic et al., 1997), and in inflammatory autoimmune diseases such as multiple sclerosis (MS) (Ofengeim et al., 2015). Microglia are brain-resident immune cells that maintain CNS homeostasis, constantly survey their environment (Nimmerjahn et al., 2005), and react to homeostasis-perturbing elements by initiating an inflammatory reaction (Kreutzberg, 1996). In the healthy brain, they have a unique homeostatic molecular and functional signature (M0) (Butovsky et al., 2014, Gautier et al., 2012, Hickman et al., 2013), which is tightly controlled by transforming growth factor β (TGFβ) signaling (Butovsky et al., 2014, Gosselin et al., 2014). However, during the course of disease, microglia lose their homeostatic molecular signature and functions (Butovsky et al., 2015, Holtman et al., 2015) and become chronically inflammatory (Perry and Holmes, 2014). Recent studies identified a common disease-associated microglia signature (Chiu et al., 2013, Hickman et

al., 2013, Holtman et al., 2015, Keren-Shaul et al., 2017, Orre et al., 2014). However, the mechanisms that regulate the microglial phenotype in disease have not been identified. In this study, we identified a role for apolipoprotein E (APOE) in regulating a subset of microglia, which exhibit a common disease-associated phenotype. This neurodegenerative phenotypic switch is triggered by TREM2, leading to activation of APOE signaling and subsequent suppression of homeostatic microglial phenotype. A functional consequence of the activation of TREM2-APOE pathway is that microglia lose the ability to regulate brain homeostasis.

Methods

Mice

C57BL/6, SOD1, *Apoe*$^{-/-}$, mir155$^{-/-}$, *Cx3cr1*^{CreERT2} mice were purchased from Jaxmice. *Trem2*$^{-/-}$ mice were generously provided by Dr. Marco Colonna (Washington Univ.). APP-PS1 mice were kindly provided by Dr. Mathias Jucker (University of Tübingen). These mice develop amyloid plaque deposition approximately at six weeks of age in the neocortex. Deposits appear in the hippocampus at about three to four months, and in the striatum, thalamus, and brainstem at four to five months(Radde et al., 2006). APP-PS1/*Trem2*$^{-/-}$, were generated by crossing APP-PS1 mice with *Trem2*$^{-/-}$ mice. Generation of *Apoe*$^{fl/fl}$ mice have been described recently (Wagner et al., 2015) and these mice were used for microglia specific deletion of *Apoe*. If not otherwise stated, mice were 6-8 weeks of age at the beginning of the experiments. All mice were housed with food and water *ad libitum*. Mice were euthanized by CO_2 inhalation. The Institutional Animal Care and Use Committee at Harvard Medical School approved all experimental procedures involving animals.

Conditional genetic deletion of *Apoe* in microglia

To induce Cre recombinase expression(Sohal et al., 2001), a single dose of tamoxifen (75 mg/kg of body weight) in corn oil (Sigma) was injected i.p. for 5 consecutive days. For genetic depletion of APOE in microglia cells, *Apoe*$^{fl/fl}$ were crossed with tamoxifen-inducible *Cx3cr1*^{CreERT2} transgenic mice. Recombination

was induced in *Cx3cr1*^{CreERT2}*/Apoe*$^{fl/fl}$ adult mice and *Cx3cr1*$^{wt/w}$*/Apoe*$^{fl/fl}$ littermates were used as controls.

Immunohistochemistry

Following immersion fixation in 4% PFA, brains were dehydrated and embedded in paraffin. H&E staining was performed according to standard procedures. For immunohistochemical staining, frontal sections (2-5 µm) were collected on superfrost slides, deparaffinized in xylol and rehydrated. After heat induced antigen retrieval, the following primary antibodies were used for detection: Neurons, NeuN (clone A60, Millipore, 2 µg ml^{-1}), myelin/oligodendrocytes, CNPase (clone SMI91, Sternberger Monoclonals, 1.5 µg ml^{-1}), progenitor cells, NG2 (polyclonal, Millipore, 0.4 µg ml^{-1}, AB5320), microglia/macrophages/monocytes, Iba1 (polyclonal, #019-19741; WAKO Chemicals, 1 µg ml^{-1}), resident microglia, P2RY12 (polyclonal, 0.4 µg ml^{-1}, validated in ref. (Butovsky et al., 2015, Butovsky et al., 2014), APOE (polyclonal, AB947; Millipore, 5 µg ml^{-1}) phosphorylated neurofilament (pNF; (clone SMI31 Biolegend; 1:2,000), TMEM119 antibody (Sigma, HPA051870; 1:300) and activated caspase 3 CM1 (Indu Pharmaceuticals CM1; 1:50,000). Detection was performed with the respective secondary antibodies and diaminobenzidine. For immunofluorescence staining, antigen retrieval was performed for 30 min at 96°C in 10 mM citrate buffer pH 6.0. Subsequently, sections were permeabilized with 0.2% TritonX-100 (Roche) in TBS for 5 min. Tissues were blocked in Pierce Protein-Free T20 blocking buffer (Thermo Scientific) and treated with 1% Sudan

Black to reduce autofluorescence. Sections were stained at 4°C overnight, washed with TBS Tween (TBS-T) and incubated with secondary donkey anti-rabbit Alexa555 antibody (Life Technologies, 6 µg ml^{-1}) or chicken anti-rabbit Alexa488, anti-mouse Alexa647 (Life Technologies, 6 µg ml^{-1}) during 90 min. APOE was stained with goat anti-APOE (polyclonal, Millipore, 5 µg ml^{-1}) and detected with the superclonal rabbit anti-goat Alexa555 (Thermo Scientific, 1 µg ml^{-1}). Sections were washed again and slides were mounted with DAPI-Fluoromount-G (SouthernBiotech, Birmingham, USA). Staining and analyses of APP-PS1/Trem2$^{-/-}$ and APP-PS1 tissues were performed on cryo or floating sections and the following additional antibodies were used: mClec7a (clone R1-8g7, Invivogene, 1:30); Aβ (clone 6E10, Covance, 1:100 or Mob 410-05, Zytomed, 1:100); goat anti-mouse Alexa405; chicken anti-rat Alexa488 or Alexa647. Sections were permeabilized with 0.2% TritonX-100 as mentioned above with subsequent antibody incubations, respectively. Data acquisition and quantification was performed using a Leica TCS SP5 confocal microscope and Leica application suite software (LAS-AF-lite). Quantification of positive staining within microglia or amyloid-plaque region was performed using the LAS-AF quantification tool. Briefly, the region of interest was carefully selected and the sum of the values of the pixels in the selection was calculated. For quantification of APOE-signal in human microglia, only cells with fully visible cell bodies, away from plaques or astrocytes were used. Selected area was 300µm^2 and 30 cells were measured each (n=3 AD subjects vs. n=3 controls). For quantification of

CLEC7a signal within single plaque associated microglia in mouse brains, we measured an area of 250µm^2 from 10-14 plaques each (n=5 APP-PS1 versus n=5 APP-PS1/Trem2$^{-/-}$). Reduction of P2RY12 protein amount in plaque area associated microglia was measured in 3,000µm^2 from 15 plaques each (n=5 APP-PS1 versus n=5 APP-PS1/Trem2$^{-/-}$). For quantitative evaluation of P2ry12 and dystrophic axons in human AD brains, double staining for P2RY12 with Aß or phosphorylated neurofilament was performed on paraffin sections as described previously(Bauer and Lassmann, 2016). After deparaffinization heat induced epitope retrieval was performed in EDTA buffer (pH: 8.5). The primary antibodies (rabbit polyclonal anti-P2RY12; mouse monoclonal anti-Amyloid ß, Clone W02, Millipore and mouse monoclonal anti-phosporylated neurofilament, SMI31; Sternberger Monoclonals, Affiniti Res Prod.) were applied together overnight. Antibody binding was visualized with either alkaline phosphatase-conjugated anti-mouse antibodies or with biotinylated anti-rabbit secondary antibodies and peroxidase-conjugated streptavidin. Alkaline phosphatase or peroxidase reaction products were visualized by development with fast blue BB salt (blue) or amino ethyl carbazole (AEC; red), respectively.

Human cortical specimens

We examined the cortices (prefrontal cortex, Brodmann area 9-15) of brains deposited at Massachusetts Alzheimer Disease Research Center (MADRC; NIA P50 AG005134) at Massachusetts General Hospital. Brain tissue from the selected autopsies was accompanied by the reports generated by the

Neuropathology Core of the MADRC. These reports include neuropathology diagnosis of Alzheimer Disease (AD)-associated changes and descriptive clinical information on the severity of neurological signs and symptoms of AD-associated cognitive decline. AD subjects (n=3, 2 females and 1 male) and healthy controls (n=3) for laser capture microdissection with high fidelity mRNAs were age- and race-matched. Bioanalysis was performed a priori using the Agilent (Waldbronn GmbH) RNA 6000 Pico chip human tissue to assess the quality of RNA extracted. An independent set of AD-patients (n=3, 2 females and 1 male) versus healthy control (n=3, 3 males) was used for fluorescence microscopy. The Institutional Review Board at Massachusetts General Hospital provided an exemption for the protocol describing research on postmortem human brain tissue analyzed in this study.

RNA isolation, nanostring RNA counting, quantitative real-time PCR

Total RNA was extracted using mirVanaTM miRNA isolation kit (Ambion) according to the manufacturer's protocol. Nanostring nCounter technology (http://www.nanostring.com/) allows expression analysis of multiple genes from a single sample (Butovsky et al., 2014). We performed nCounter multiplexed target profiling of 400 to 542 microglial transcripts (MG400 and MG550, see MG custom-chip design). 100 ng of total RNA per sample were used in all described nCounter analyses according to the manufacturer's suggested protocol (Butovsky et al., 2014). Nanostring analysis was performed on RNA from human LCM

samples according to manufacturer's suggested protocol for Single cell Analysis. A third of the RNA sample was first retro-transcribed into cDNA using SuperScript VILO master mix (Invitrogen). A Multiple Target Enrichment (MTE) was performed with 70 selected primer pairs to linearly pre-amplify human LCM samples using Taqman PreAmp master mix (Applied Biosystems). Resulting amplified material was then directly hybridized with nCounter Codeset. Total RNA (30 ng) and 3 ng of RNA with specific miRNA probes (Applied Biosystems) were used for reverse transcription reaction according to the manufacturer (high-capacity cDNA Reverse Transcription Kit; Applied Biosystems). mRNA or miRNAs levels were normalized relative to GAPDH or U6, respectively. Real-time PCR reaction was performed using Vii7 (Applied Biosystems). All qRT-PCRs were performed in duplicate, and the data are presented as relative expression compared to GAPDH or U6 as mean ± s.e.m.

MG550 and human MG447 chip design

The MG550 Nanostring chip was designed using the quantitative Nanostring nCounter platform. Selection of genes is based on analyses that identified genes and proteins, which are specifically or highly expressed in adult mouse microglia plus 40 inflammation-related genes, which were significantly affected in EAE, APP-PS1 and SOD1 mice. Two other versions were done after MG400. MG468 contains an additional 48 inflammation/phagocytosis-related genes (Butovsky et al., 2015). Using this signature, we generated a new version of Nanostring-based microglia chip termed MG550 that encompasses 400 unique and enriched

microglial genes we have identified previously (Butovsky et al., 2014) and additional 150 inflammation-, inflammasome- and phagocytosis-related genes. The human MG447 chip was previously described in ref (Butovsky et al., 2015).

Induction of EAE

Female mice (6-8 weeks) were injected s.c. in both flanks with 100 μg myelin oligodendrocyte glycoprotein (MOG) 35–55 peptide dissolved in PBS and emulsified in an equal volume CFA (Difco) supplemented with 5 mg ml–1 Mycobacterium tuberculosis H37Ra and injected twice i.p. with 200 ng pertussis toxin (List Biological Laboratories) administered on the day of immunization and 48 h later. Clinical assessment of EAE was performed daily after disease induction according to the following criteria: 0, no signs of disease; 1, loss of tone in the tail; 2, hind limb paresis; 3, hind limb paralysis; 4, tetraplegia; 5, moribund, during the duration of the acute phase (15 d), or only during the progressive or chronic phase (days 30–50).

Heatmaps

Selected gene expression was averaged between the replicates (n = 3 for aging, APPPS1, SOD1, and n = 4 for EAE) for each disease score or time-point. For clustering, the z-scores were calculated using the mean of samples for all disease conditions and then subsequently clustered using K-means. A scree plot was used to assess the number of clusters, which suggested that four clusters were a suitable number to explain most of the variability in the data. Heatmaps were generated using R (version 3.2.0) and heatmap.2 from the gplots package.

Circos plot

The custom-made microglia transcriptional signatures (Figure IV-3I) were generated by retrieving genes upregulated at least 1.5-fold and p-value less than 0.01 (Student's T-test) in disease conditions from GSE43366, GSE60670, GSE62420, GSE66211, GSE66420, GSE71133, GSE55968, and GSE65067. All custom signatures were derived from publicly available transcriptomes downloaded from Gene Expression Omnibus (GEO). A GSEA algorithm was applied to identify the enrichment of phagocytic microglia signaling pathways in the microglia transcriptomes in various diseases conditions. This includes Aging, Mfp2-deficiency, Alzheimer's disease, ALS, neuropathic pain, chronic pain and Mecp2-deficiency. All custom signatures were derived from publically available rodent transcriptomes downloaded from Gene Expression Omnibus. Statistical significance of GSEA results was assessed using 1,000 sample permutations. A nominal P value less than 0.001 was used to determined pairwise transcriptome connectivity. A Circos graph was generated using Circos package 0.68.12.

Transcription factor binding site analysis

Web-based system for the detection of overrepresented conserved transcription factor binding sites, oPOSSUM (Ho Sui et al., 2007, Ho Sui et al., 2005, Kwon et al., 2012), was used to analyze promoter sequences of specific co-regulated gene sets. Promoter sequences (250bp) of APOE-induced and repressed gene sets in phagocytic conditions were analyzed. Transcription factor binding sites

were considered significant if either the z-score was above 10 or the Fisher score was above 5.

Promoter motif analysis

A GSEA algorithm was used to identify genes that are differentially expressed in microglia transcriptomes from lipid disorder (Mfp2–/–)(GSE66420), ALS (SOD1) (GSE43366), AD (5xFAD) (GSE65067) and aging(GSE62420), as compared with their control counterparts. High-scoring differentially expressed 'leading-edge' social genes were selected on the basis of their presence in the TREM2-responsive gene signature 5xFAD/Trem2$^{-/-}$ and SOD1/Trem2$^{-/-}$ mice. The statistics were determined using Euclidean distance.

Ingenuity Pathway Analysis (IPA)

Data were analyzed using Ingenuity software (Ingenuity Systems, http://www.ingenuity.com). Differentially expressed genes (with corresponding fold changes and P values) were incorporated in canonical pathways and bio-functions and were used to generate biological networks as described previously(Butovsky et al., 2014). Briefly, uploaded data set for analysis was filtered using the following cutoff definitions: fivefold change, $P < 0.01$.

Results

Reciprocal induction of APOE and suppression of TGFβ signaling in disease-associated microglia

To investigate the underlying molecular mechanisms that regulate dysfunction of microglial phenotype in neurodegenerative disease, we isolated microglia and analyzed transcriptomes during aging and disease progression in mouse models of ALS (SOD1 mice), Alzheimer's disease (AD, APP-PS1 mice) and multiple sclerosis (MS, EAE; experimental autoimmune encephalomyelitis). To identify common patterns of gene expression during aging and disease progression, we performed *k*-mean clustering and identified two major clusters (Figure IV-1A). Cluster 1 was associated with the loss of 68 homeostatic microglial genes, including *P2ry12, Tmem119, Gpr34, Jun, Olfml3, Csf1r, Hexb, Mertk, Rhob, Cx3Cr1, Tgfbr1* and *Tgfb1* and transcription factors such as *Mef2a, Mafb, Jun*, *Sall1* and *Egr1,* which are enriched in adult microglia (Butovsky et al., 2014, Matcovitch-Natan et al., 2016, Buttgereit et al., 2016). Cluster 2 was associated with upregulation of 28 inflammatory molecules including *Spp1, Itgax, Axl, Lilrb4, Clec7a, Ccl2, Csf1* and *Apoe*, which was one of the most upregulated genes (Figure IV-1A). We have termed this microglial neurodegenerative phenotype as MGnD, in contrast to M0-homeostatic adult microglia (Gautier et al., 2012, Hickman et al., 2013, Butovsky et al., 2014). Linear regression analysis showed a negative correlation of *Mef2a*, *Sall1* and *Tgfbr1* with disease progression in EAE, SOD1 and APP-PS1 mice (Figure IV-1B). In contrast, induction of *Apoe*

was positively correlated with disease progression (Figure IV-1B). Importantly, during acute and relapsing phases in EAE, microglia transcriptome profiling showed global suppression of the homeostatic molecules [e.g., *P2ry12, Tmem119, Tgfbr1, Mafb, Mef2a, Sall1* and *Egr1* (Butovsky et al., 2014, Gautier et al., 2012, Hickman et al., 2013, Matcovitch-Natan et al., 2016) and their restoration during the remission phase of EAE (Figure IV-1C). In contrast, *Apoe* was reciprocally upregulated (Figure IV-1C). Ingenuity pathway analysis (IPA) identified APOE and TGFβ as the major upstream regulators of the MGnD microglia (Figure IV-1D). Of note, among previously identified TGFβ-dependent homeostatic microglia genes (Butovsky et al., 2014), top-suppressed *Olfml3, P2ry12, Tmem119, Mef2a, Jun, Sall1* and -upregulated *Apoe* and *Axl* were similarly and significantly affected during disease progression (Figure IV-1E).

The MGnD-microglia subset is associated with neuritic Aβ-plaques and diffuse neuritic dystrophy in the AD cortex

In AD, brain pathology is characterized by a widespread neuritic dystrophy presenting with filamentous inclusions and a swollen appearance associated with neurite degeneration (Larner, 1995). These dystrophic axons are enlarged and show intense reactivity for phosphorylated neurofilaments (Sternberger et al., 1985). To address whether a microglial phenotype switch from M0-homeostatic to MGnD-neurodegenerative is specifically associated with neuritic dystrophy in AD, we analyzed brain specimens from APP-PS1 mice and human AD. We

found previously that P2ry12 is a microglia specific homeostatic molecule (Butovsky et al., 2015, Butovsky et al., 2014) and its expression is suppressed in MGnD microglia. In contrast, *Clec7a* gene expression was induced in MGnD microglia (Figure IV-1A). Thus, in order to distinguish M0- vs. MGnD-microglia we used a combination of P2ry12 and Clec7a mAbs, respectively. We found that Clec7a^{+}/P2ry12^{-} microglia were associated with Aβ-plaque in APP-PS1 mice (Figure IV-2A). We identified three microglial subsets based on P2ry12 and Clec7a expression: 1) Clec7a^{-}/P2ry12^{+} microglia (not associated with Aβ-plaques); 2) Clec7a^{Low}/P2ry12^{Low} microglia (in close proximity to Aβ-plaques); and 3) Clec7a^{+}/P2ry12^{-} microglia (associated with neuritic Aβ-plaques) (Figure IV-2A). Importantly, Clec7a^{+}/P2ry12^{-} microglia were associated specifically with phosphorylated neurofilaments (NF^{+}) in neuritic plaques in APP-PS1 mice (Figure IV-2B). In order to determine whether the Clec7a^{+}/P2ry12^{-} microglia subset exhibit the MGnD molecular signature, we sorted FCRLS^{+}/Clec7a^{+} vs. FCRLS^{+}/Clec7a^{-} microglia from 24-month old APP-PS1 mice. We detected significantly more FCRLS^{+}/Clec7a^{+} microglia in APP-PS1 compared to age-matched WT mice (data not shown). Nanostring transcriptome profiling of isolated microglia showed that the phenotype of Clec7a^{+} microglia was similar to MGnD microglia identified in SOD1, EAE and APP-PS1 mouse models and during aging (Figure IV-2C). Among suppressed key microglial homeostatic genes were *P2ry12, Tmem119, Olfml3, Csf1r, Rhob, Cx3Cr1, Tgfbr1, Tgfb1, Mef2a, Mafb, Sall1* and the upregulation of inflammatory molecules including

Spp1, Itgax, Axl, Lilrb4, Clec7a, Csf1 and *Apoe*, which was among the most upregulated genes (Figure IV-2C and 2D). Of note, transition of microglia from Clec7a^{-} to Clec7a^{Int} to Clec7a^{Hi} was correlated with increased expression of *Apoe* and suppression of the homeostatic molecules (Figure IV-2D). RNA-seq analysis of three microglial subsets validated the results of Nanostring analysis and showed that only FCRLS^{+}/Clec7a^{+} microglia acquired an MGnD signature (Figure IV-2E–F).

To investigate whether a microglial phenotype switch is specifically associated with neuritic plaques, we performed immunohistochemical analysis of human AD brains by double staining for P2RY12 with antibodies to amyloid □-peptide (Aβ) or phosphorylated neurofilaments (pNF). P2RY12^{+} homeostatic microglia were preserved in Aβ-diffuse plaques which are not associated with neuritic pathology and P2ry12 signal was lost in pNF^{+} neuritic plaques in human AD brains (Figure IV-2G). Loss of P2RY12^{+} microglia was significantly correlated with axonal dystrophy in AD brains, but not with the extent of Aβ deposition (Figure IV-2H). We confirmed by immunohistochemical analysis increased APOE expression in microglia in close proximity to Aβ-plaque in AD brains (data not shown).

Phagocytosis of apoptotic neurons suppresses homeostatic microglia

A common feature in neurodegeneration is the occurrence of synaptic, dendritic or axonal apoptosis and neuritic dystrophy (Mattson et al., 1998, Ofengeim et al.,

2015, Larner, 1995). To determine the mechanisms by which the MGnD-microglia are induced in neurodegeneration, we performed stereotaxic injections of fluorescently-labeled apoptotic neurons into the cortex and hippocampus of naïve mice. Apoptotic neurons induced the recruitment of P2ry12^{+} microglia towards the site of injection 16 h post-injection (Figure IV-3A). P2ry12^{+} microglia changed their morphology from an M0-homeostatic non-phagocytic (MG-nΦ phenotype to an amoeboid-phagocytic (MG-dNΦ phenotype at the vicinity of the site of injection (Figure IV-3A–C). Of note, induction of MGnD microglia was not detected in PBS injected brains. Apoptotic neurons and neuronal fractions were internalized by P2ry12^{+} microglia (Figure IV-3B). Induction of APOE was detected in MG-dNΦ microglia (Figure IV-3C). Increased expression of *Apoe* was detected as early as 3h post-injection and reached a peak by 16 h post-injection. Restoration of homeostatic P2ry12+/Clec7a- microglia were observed at 14 days post-injection (data not shown). Transcriptome profiling of sorted MG-dNΦ and MG-nΦ microglia (Figure IV-3D and 3E) showed that phagocytosis of apoptotic neurons induced a microglial molecular phenotype similar to MGnD disease-associated microglial phenotype. Unique microglial homeostatic genes including *Tmem119, Egr1, Hexb, Gpr34, P2ry12, Olfml3 and Tgfbr1* were suppressed in phagocytic microglia, whereas *Apoe* was the major upregulated gene among other inflammatory molecules (Figure IV-3F). This was confirmed by qPCR analysis of key microglial genes including upregulation of *Apoe* and miR-155, a regulator of inflammation in microglia (Butovsky et al., 2015) and suppression of

Tgfbr1 (TGFβ signaling), which is critical to maintain homeostatic microglia (Butovsky et al., 2014, Gosselin et al., 2014).

To confirm the phenotypic switch on the protein level, we performed quantitative mass spectrometry analysis of phagocytic vs. non-phagocytic microglia 16 h post-injection. Apoe and Lgals3 were highly expressed in phagocytic microglia. In contrast, both Rgs10 and Bin1, two homeostatic microglial proteins (Butovsky et al., 2014), were suppressed (Figure IV-3H). To determine whether the MG-dNΦ microglia is closely related to disease models, we used gene set enrichment analysis (GSEA) (Subramanian et al., 2005). GSEA assesses whether the expression of a previously defined group of related genes is enriched in one biological state. The disease models included previously identified microglia transcriptomes from mouse models of neuropathic pain (GSE60670), chronic pain (GSE71133), Rett syndrome (*Mecp2*$^{-/-}$) (GSE66211), lipid disorder (*Mfp2*$^{-/-}$) (GSE66420), ALS (SOD1) (GSE43366), AD (5xFAD) (GSE65067), brain irradiation (GSE55968), and aging (GSE62420). Circos plot network analysis presented an overlap of the phagocytic microglial phenotype with the microglia molecular signature during aging and in a model of brain irradiation. Most importantly, the MG-dNΦ microglia signature was significantly enriched in microglia transcriptomes from mouse models of Alzheimer's disease (5XFAD), ALS (SOD1) and MFP2 deficiency, which is associated with cerebellar degeneration (Verheijden et al., 2013). In contrast,

microglial changes associated with neuropathic and chronic pain models or in MECP2 deficiency were not connected (Figure IV-3I).

APOE regulates transcriptional and post-transcriptional programs of the MGnD phenotype and function

We previously reported that *Apoe* expression is downregulated in microglia during development, which correlates with the induction of M0-homeostatic microglial genes (Butovsky et al., 2014). Moreover, *Apoe* expression is markedly increased in microglia progenitors from CNS *Tgfb1*$^{-/-}$ mice (Butovsky et al., 2014). To assess the role of Apoe in the induction of MGnD microglia, when phagocyting apoptotic neurons, we performed RNA-Seq analysis on *Apoe*$^{-/-}$ vs. WT transcriptomes from MG-nΦ vs MG-dNΦ microglia. We defined clusters based on differentially expressed genes between WT non-phagocytic vs. phagocytic vs. *Apoe*$^{-/-}$ phagocytic microglia (Figure IV-4A). We defined clusters based on differentially expressed genes between WT non-phagocytic vs. phagocytic vs. *Apoe*$^{-/-}$ phagocytic microglia (Figure IV-4A). Clusters 1-3 show 446 genes induced in phagocytic microglia which were repressed in *Apoe*$^{-/-}$ microglia. Of note, 15 genes among commonly upregulated in disease were suppressed by APOE (Figure IV-4A). Figure IV-4B shows selected APOE-repressed genes. Clusters 4-7 show 483 suppressed genes in phagocytic microglia which were restored in *Apoe*$^{-/-}$ phagocytic microglia. Of note, among 68 genes commonly suppressed in disease, 19 genes were restored in *Apoe*$^{-/-}$

phagocytic microglia including *P2ry12*, *Tgfbr1* and *Mef2a* (Figure IV-4A). To assess an intrinsic role of APOE regulation in cell-specific manner, we specifically deleted *Apoe* in microglia from *Cx3cr1*$^{Cre/+}$/*Apoe*$^{fl/fl}$ mice. qPCR analysis confirmed *Apoe* deletion in *Cx3cr1*$^{Cre/+}$/*Apoe*$^{fl/fl}$ microglia as compared to *Cx3cr1*$^{wt/wt}$/*Apoe*$^{fl/fl}$ microglia. Moreover, gene expression of *Clec7a* was repressed and *Csf1r, Tgfb1, Tgfbr1* was restored in *Cx3cr1*$^{Cre/+}$/*Apoe*$^{fl/fl}$ microglia (Figure IV-4C). Conditional deletion of *Apoe* in phagocytic microglia showed similar pattern of expression of selected genes as was observed in phagocytic microglia from global *Apoe*$^{-/-}$ mice (Figure IV-4A).

We found that transcription factors *Cited2*, *Mef2a* and *Smad3* which are essential in TGFβ signaling (Quinn et al., 2001, Chou and Yang, 2006) were repressed in *Apoe*$^{-/-}$ phagocytic microglia (Figure IV-4D). Moreover, *Spi1* (PU.1) a lineage-determining transcription factor for myeloid cells was suppressed by APOE (Figure IV-4A). On the opposite, APOE induced *Tfec* and specifically *Bhlhe40,* which is essential for pathogenicity in neuroinflammation (Lin et al., 2014, Sun et al., 2001) (Figure IV-4D). To investigate the mechanisms of APOE regulation in microglia, we performed a Transcription Factor Binding Site (TFBS) analysis in genes that were differentially regulated in phagocytic *Apoe*$^{-/-}$ microglia. Transcription factor binding site over-representation analysis using oPOSSUM, showing that the promoter regions (250bp upstream of TSS) of 28 APOE-induced and 39 APOE-repressed genes are enriched for predicted binding sites (Figure IV-4E). MEF2A and SPI-B (Spi-1/PU.1 related binding motifs) were

significantly enriched in genes repressed by APOE, implying a major role of these transcription factors in the APOE-dependent gene regulation (Figure IV-4E). Figure IV-4F shows major APOE–induced and –repressed transcription factors and their direct targets. Gene-regulatory network orchestrates two distinct pathways in phagocytic microglia. Both regulators function in concerted ways to activate appropriate genes.

These results show that APOE signaling has dual actions on microglia regulation in neurodegeneration: 1) suppression of microglia transcriptional homeostatic program including *Mef2a, Mafb, Smad3, PU.1* and 2) induction of inflammatory program including transcription factor *Bhlhe40* and *Tfec*.

Genetic targeting of *Trem2* suppresses APOE pathway and restores the homeostatic microglia in APP-PS1 and SOD1 mice

Recently, Wang et al. showed that TREM2 is a sensor of membrane-associated lipids including phosphatidylserine (PS) focally exposed on apoptotic cells and processes or synapses of damaged neurons (Wang et al., 2015). We found that blocking phosphatidylserine on apoptotic neurons with Annexin V protein, which specifically binds and blocks phosphatidylserine (Koopman et al., 1994), reduced microglial phagocytosis by 88% (Figure IV-5A). As shown in Figure IV-3, apoptotic neurons suppress homeostatic genes in microglia. Thus, we asked whether apoptotic neurons activate APOE pathway via TREM2 on microglia by comparing *Trem2*$^{-/-}$ and WT mice. We found that the expression of homeostatic

genes including *P2ry12, Gpr34, Tmem119, Tgfbr1* and *Csf1r* were restored in *Trem2*$^{-/-}$ phagocytic microglia as compared to WT phagocytic microglia (Figure IV-5B), whereas *Apoe* and miR-155 were suppressed in *Trem2*$^{-/-}$ phagocytic microglia (Figure IV-5C). To confirm whether TREM2 induces MGnD in disease, we genetically ablated *Trem2* in APP/PS1 and SOD1 mice. Nanostring transcriptome profiling of brain microglia isolated from APP-PS1/*Trem2*$^{-/-}$ mice showed suppression of 6 inflammatory molecules including *Axl, Clec7a, Csf1, Itgax, Cd34* and *Apoe,* which were among the most upregulated genes in common disease-associated signature (Figure IV-5D). Among 108 restored genes in APP-PS1/*Trem2*$^{-/-}$ mice, 54 were commonly suppressed homeostatic microglial genes in disease including *P2ry12, Tmem119, Gpr34, Olfml3, Csf1r, Mertk, Rhob, Cx3Cr1, Tgfbr1* and *Tgfb1* and transcriptional factors such as *Mef2a, Mafb* and *Sall1* (Figure IV-5D). Moreover, we confirmed by protein level restoration of P2ry12 and suppression of Clec7a in microglia associated with Aβ-plaque in APP-PS1/*Trem2*$^{-/-}$ mice as compared to APP-PS1 mice (Figure IV-5E–G). In SOD1/*Trem2*$^{-/-}$ microglia, among 36 downregulated inflammatory genes, 11 genes were common to disease-associated signature. Among 240 restored genes in SOD1/*Trem2*$^{-/-}$ mice, 66 were commonly suppressed homeostatic microglial genes in disease (Figure IV-5H). Of note, *P2ry12* and *Fabp5* gene targets of Mef2a and Bhlhe40 transcription factors, shown in Figure IV-4F, were restored and downregulated respectively, by *Trem2* genetic ablation in disease. Importantly, transcription factors including *Mef2a, Mafb* and *Sall1* and

TGFβ signaling (*Tgfb* and *Tgfbr1*), which were restored in *Trem2*$^{-/-}$ microglia in disease, were similarly restored in *Apoe*$^{-/-}$ phagocytic microglia. Immunohistological analysis of P2ry12 and Clec7a expression in spinal cords from SOD1/*Trem2*$^{+/-}$ at 115d of age showed appearance of Clec7a^{+}/P2ry12^{-} microglia. At this stage, Clec7a^{+}/P2ry12^{-} microglia were not detected in SOD1/*Trem2*$^{-/-}$ (Figure IV-5I). Importantly, Clec7a^{-}/P2ry12^{+} homeostatic microglia were preserved in SOD1/*Trem2*$^{-/-}$ mice (Figure IV-5I). Statistical analysis showed restoration of P2ry12 and suppression of Clec7a in microglia from SOD1/*Trem2*$^{-/-}$ mice as compared to SOD1/*Trem2*$^{+/-}$ mice (Figure IV-5J and 5K). To validate the role of TREM2 in regulation of the microglial phenotype switch in disease, we analyzed publicly available rodent microglia transcriptomes under degenerative conditions, which includes: 5XFAD, SOD1, *Mfp2*$^{-/-}$ and aged 22-month old mice. Using GSEA, our analysis showed that rodent microglia under neurodegenerative/aging conditions were enriched in TREM2 transcriptional signature (Figure IV-6A–D). Among all four-disease models, TREM2-induced common genes including *Clec7a, Gpnmb, Fabp5, Lgals3, Csf1* and *Ch25h* which were also induced by APOE.

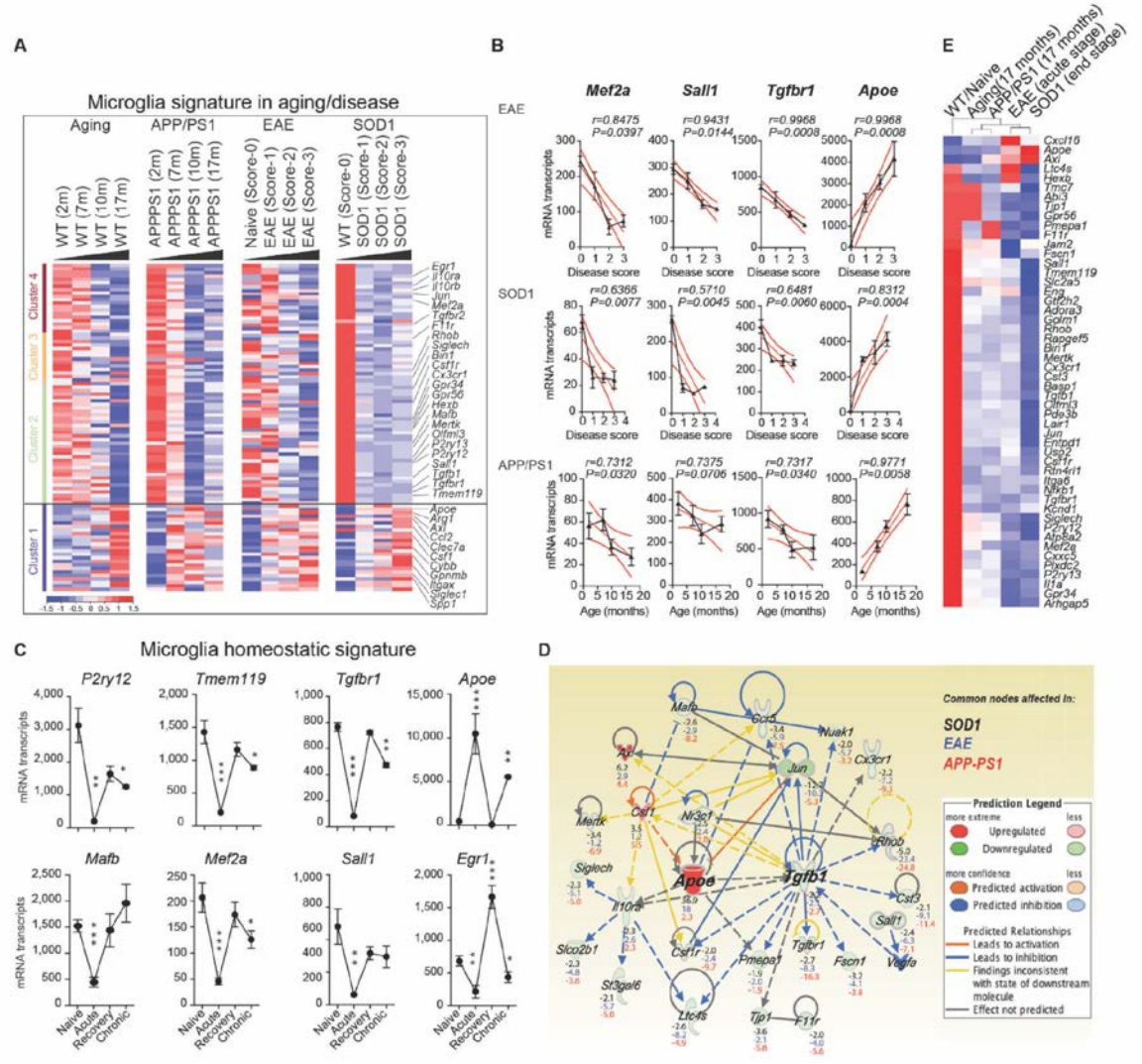

Figure IV-1 Reciprocal induction of APOE and suppression of TGFβ signaling in disease-associated microglia

(A) K-means clustering of 95 significantly affected common genes in FCRLS^{+} microglia during aging and disease progression as determined by Nanostring MG550 microglial chip analysis. Vertical lanes represent mean of biological replicates per disease stage/condition in WT (n = 12), EAE (n = 18), SOD1 (n = 11) and APP-PS1 (n = 12) mice. Cluster 1 represents upregulated genes and clusters 2-4 represents suppressed homeostatic genes. (B) Linear regression curve of *Mef2a*, *Sall1*, *Tgfbr1* and *Apoe* expressions in spinal cord microglia from EAE and SOD1 mice with different disease scores and brain microglia during disease course in APP-PS1. Thick line indicates 95% confidence interval of the regression line. (C) Nanostring transcriptome analysis of selected homeostatic and disease-associated microglial genes during disease stages in EAE. Data are presented as mean ± s.e.m. *p < 0.05, **p < 0.01, ***p < 0.001 by one-way ANOVA followed by Dunnett´s multiple-comparison *post-hoc* test. (D) Ingenuity pathway analysis (IPA)

shows common nodes significantly affected in microglia in all three-mouse models in disease. For each molecule in the data set, the expression fold change compared to normal, healthy microglia is presented. The legend shows prediction state and relationships. Solid lines represent a direct and dotted lines an indirect interaction between the two genes. (E) Heatmap (Pearson correlation; average linkage) of significantly affected genes dysregulated in all three diseases as determined by Nanostring microglial chip analysis.

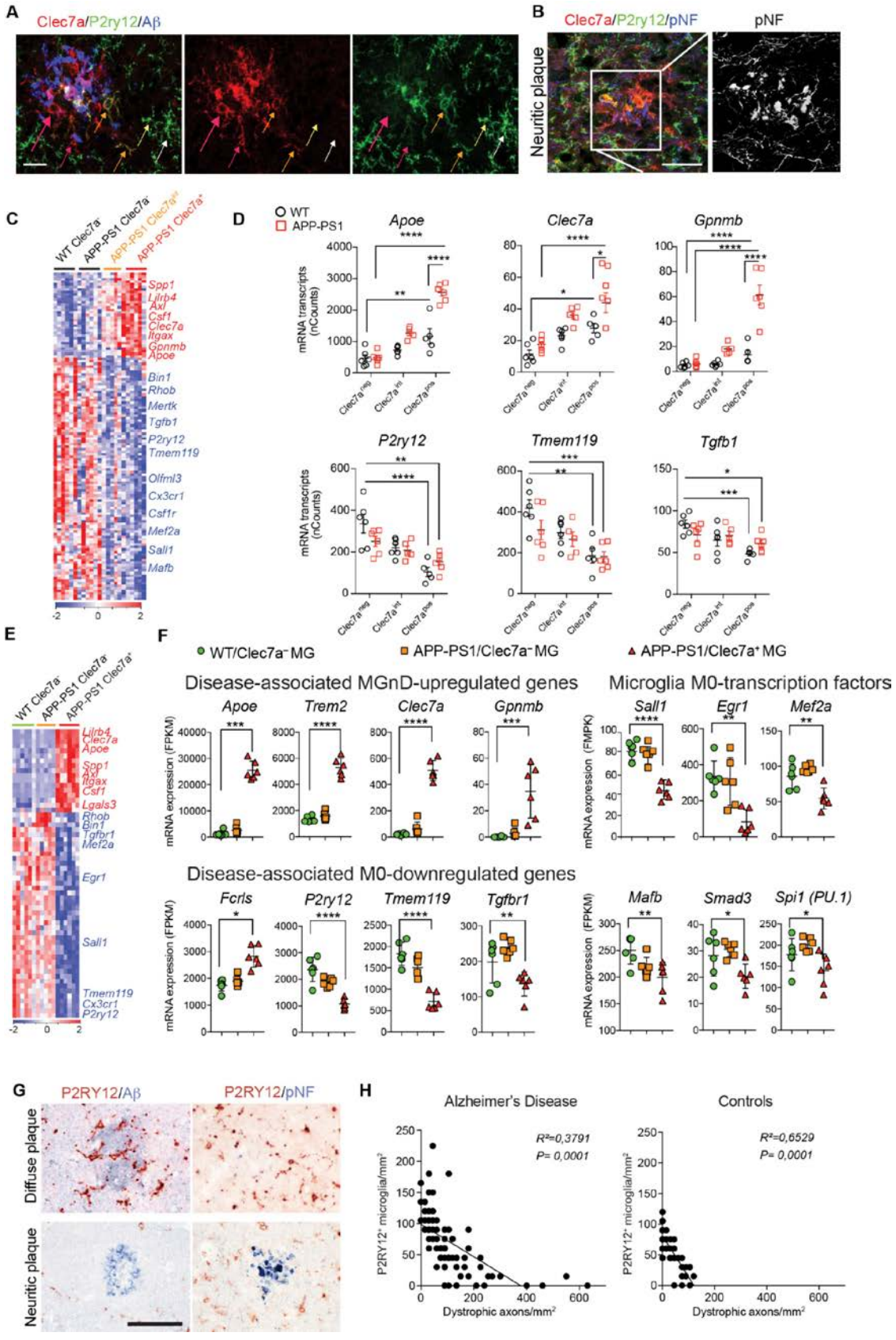
A
Clec7a/P2ry12/Aβ
B
Clec7a/P2ry12/pNF
pNF
Neuritic plaque
C
WT Clec7a⁻
APP-PS1 Clec7a⁻
APP-PS1 Clec7a⁺
Spp1
Lilrb4
Axl
Csf1
Clec7a
Itgax
Gpnmb
Apoe
Bin1
Rhob
Mertk
Tgfb1
P2ry12
Tmem119
Olfml3
Cx3cr1
Csf1r
Mef2a
Sall1
Mafb
D
WT
APP-PS1
Apoe
Clec7a
Gpnmb
P2ry12
Tmem119
Tgfb1
mRNA transcripts (nCounts)
E
Lilrb4
Clec7a
Apoe
Spp1
Axl
Itgax
Csf1
Lgals3
Rhob
Bin1
Tgfbr1
Mef2a
Egr1
Sall1
Tmem119
Cx3cr1
P2ry12
F
WT/Clec7a⁻ MG
APP-PS1/Clec7a⁻ MG
APP-PS1/Clec7a⁺ MG
Disease-associated MGnD-upregulated genes
Apoe
Trem2
Clec7a
Gpnmb
Microglia M0-transcription factors
Sall1
Egr1
Mef2a
mRNA expression (FPKM)
mRNA expression (FMPK)
Disease-associated M0-downregulated genes
Fcrls
P2ry12
Tmem119
Tgfbr1
Mafb
Smad3
Spi1 (PU.1)
G
P2RY12/Aβ
P2RY12/pNF
Diffuse plaque
Neuritic plaque
H
Alzheimer's Disease
Controls
R²=0,3791
P= 0,0001
R²=0,6529
P= 0,0001
P2RY12⁺ microglia/mm²
Dystrophic axons/mm²

Figure IV-2 MGnD-microglia are associated with neuritic Aβ-plaques.
(A) Representative immunohistochemical staining for P2ry12^{+} and Clec7a^{+} in microglia at the vicinity of Aβ-plaque in APP-PS1 mice (24 months). MGnD microglia around the plaque (red arrows). MGnD transitioning to the plaque (yellow arrows). M0-homeostatic microglia (white arrows). Scale bar, 20 μm. (B) Representative immunohistochemical staining for P2ry12^{+} and Clec7a^{+} in microglia associated with neuritic plaque (phosphorylated neurofilament; pNF) in APP-PS1 mice (24 months). Scale bar, 20 μm. (C) Heatmap of significantly affected genes in Clec7a^{+} vs. Clec7a^{int} vs. Clec7a^{-} FCRLS^{+} microglia in APP-PS1 vs. WT mice (n = 5 per group; 24 months). Selected homeostatic and inflammatory genes are highlighted in blue and red, respectively. (D) Selected genes shown in (C). Dot plots show mRNAs transcripts (mean ± s.e.m). *p < 0.05, **p < 0.01, ***p < 0.001, ****p< 0.0001 by one-way ANOVA followed by Tukey´s multiple-comparison *post-hoc* test. (E) Heatmap of selected significantly affected genes in Clec7a^{+} vs. Clec7a^{-} FCRLS^{+} microglia in APP-PS1 vs. WT mice (n = 5 per group; 9 months). Selected homeostatic and inflammatory genes are highlighted in blue and red, respectively. (F) Selected genes shown in (E). Dot plots show FPKM (mean ± s.e.m). *p < 0.05, **p < 0.01, ***p < 0.001, ****p< 0.0001 by one-way ANOVA followed by Tukey´s multiple-comparison *post-hoc* test. (G) Representative immunohistochemical staining for P2ry12 (red) with Aß (left figures) or phosphorylated neurofilament (pNF) in diffuse vs. neuritic plaques in human AD brain. Scale bar, 100 μm. (H) Linear regression curve of P2ry12^{+} microglia with dystrophic axons in the temporal cortex of control and AD patients defined by CERAD criteria and Braak stages (n = 14) and age matched controls (n = 10).

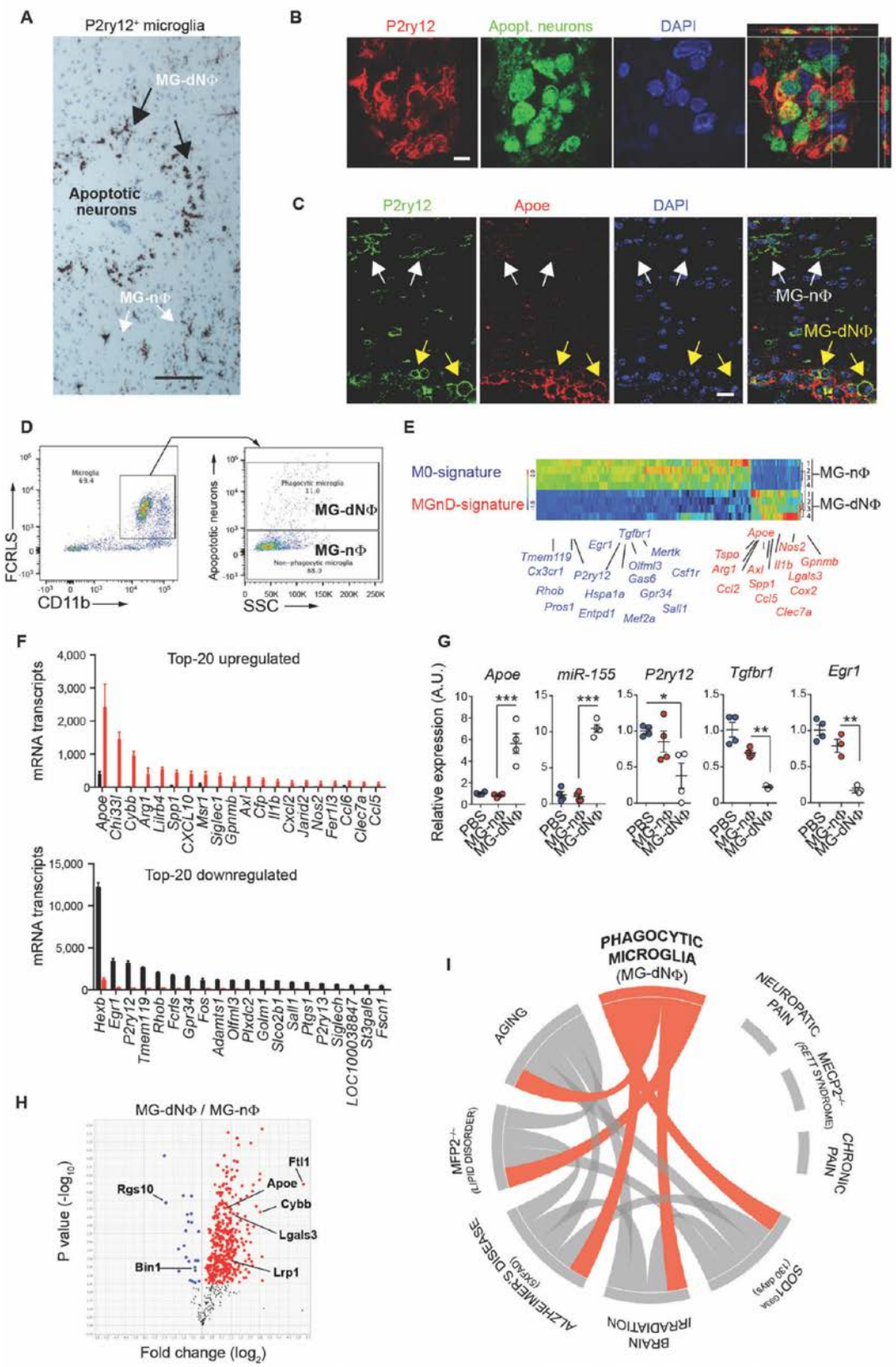
A
P2ry12+ microglia
MG-dNΦ
Apoptotic neurons
MG-nΦ
B
P2ry12
Apopt. neurons
DAPI
C
P2ry12
Apoe
DAPI
MG-nΦ
MG-dNΦ
D
FCRLS
CD11b
Microglia 69.4
Apoptotic neurons
SSC
Phagocytic microglia 11.0
MG-dNΦ
MG-nΦ
Non-phagocytic microglia 88.9
E
M0-signature
MGnD-signature
MG-nΦ
MG-dNΦ
Tmem119
Cx3cr1
Rhob
Pros1
Egr1
P2ry12
Entpd1
Tgfbr1
Hspa1a
Mef2a
Olfml3
Gas6
Gpr34
Mertk
Csf1r
Sall1
Apoe
Tspo
Arg1
Ccl2
Axl
Spp1
Ccl5
Nos2
Il1b
Lgals3
Cox2
Gpnmb
Clec7a
F
Top-20 upregulated
mRNA transcripts
Apoe
Chi3l1
Cybb
Arg1
Lilrb4
Spp1
CXCL10
Msr1
Siglec1
Gpnmb
Axl
Cfp
Il1b
Cxcl2
Jarid2
Nos2
Fer1l3
Ccl6
Clec7a
Ccl5
Top-20 downregulated
mRNA transcripts
Hexb
Egr1
P2ry12
Tmem119
Rhob
Fcrls
Gpr34
Fos
Adamts1
Olfml3
Plxdc2
Golm1
Slco2b1
Sall1
Ptgs1
P2ry13
Siglech
LOC100038847
St3gal6
Fscn1
G
Relative expression (A.U.)
Apoe
miR-155
P2ry12
Tgfbr1
Egr1
PBS
MG-nΦ
MG-dNΦ
H
MG-dNΦ / MG-nΦ
P value (-log10)
Fold change (log2)
Ftl1
Apoe
Cybb
Lgals3
Lrp1
Bin1
Rgs10
I
PHAGOCYTIC MICROGLIA (MG-dNΦ)
AGING
NEUROPATIC PAIN
MECP2-/+ (RETT SYNDROME)
CHRONIC PAIN
SOD1G93A (130 days)
BRAIN IRRADIATION
ALZHEIMER'S DISEASE (5XFAD)
MFP2-/+ (LIPID DISORDER)

Figure IV-3 Phagocytosis of apoptotic neurons suppresses homeostatic microglia.
(A) Representative immunohistochemical staining for P2ry12^{+} microglia in the site of injection of apoptotic neurons (n = 6) in C57BL/6 WT mice. MG-dNΦ and MG-nΦ represent phagocytic and non-phagocytic microglia respectively. Scale bar, 80 μm. (B) Orthogonal projections of confocal z-stacks show intracellular apoptotic neurons (labeled before injection with Alexa488; green) in P2ry12^{+} microglia (n = 6), 16 h post-injection. Scale bar, 5 μm. Data show one of two individual experiments. (C) Representative immunohistochemical staining for Apoe in P2ry12^{+} phagocytic microglia. White arrows point to non-phagocytic Apoe^{-} microglia; yellow arrows point to Apoe^{+} phagocytic microglia (n = 3). Scale bar, 15 μm. (D) Phagocytic CD11b^{+}/FCRLS^{+} microglia containing Alexa488^{+} apoptotic neurons and non-phagocytic microglia from the same injection site 16 h later. (E) Heatmap of significantly affected genes in phagocytic (n = 4) vs. non-phagocytic (*n* = 4) microglia 16 h post-injection with apoptotic neurons. Selected homeostatic and inflammatory genes are highlighted in blue and red, respectively. Data show one of two individual experiments. (F) Top-20 significantly affected genes shown in (E). Bars show mRNA transcript numbers (ncounts) (mean ± s.e.m) detected in 100 ug total RNA. *p < 0.05 by Student *t* test, 2-tailed. (G) qPCR validation of selected genes. Gene expression level was normalized against *Gapdh* using ΔCt (n = 3-4 per group). Data are presented as mean normalized expression ± s.e.m. *p < 0.05, **p < 0.01, ***p < 0.001 by one-way ANOVA followed by Tukey's multiple-comparison *post hoc* test. (H) Volcano plot of 552 TMT-mass spectrometry-identified proteins highlighting significant changes in phagocytic vs. non-phagocytic microglia. p < 0.05 by Student t test, 2-tailed. (I) Circos plot showing the connectivity map derived from the pairwise comparison of transcriptome data sets. The representations of MG-dNΦ phagocytic microglia RNAseq data set connectivity with RNAseq transcriptome datasets of microglia from mouse models of AD, ALS and MFP2 deficiency, aging and irradiation is shown in orange. Each line represents a pairwise data set overlap, which was determined using GSEA analysis and filtered by p < 0.001.

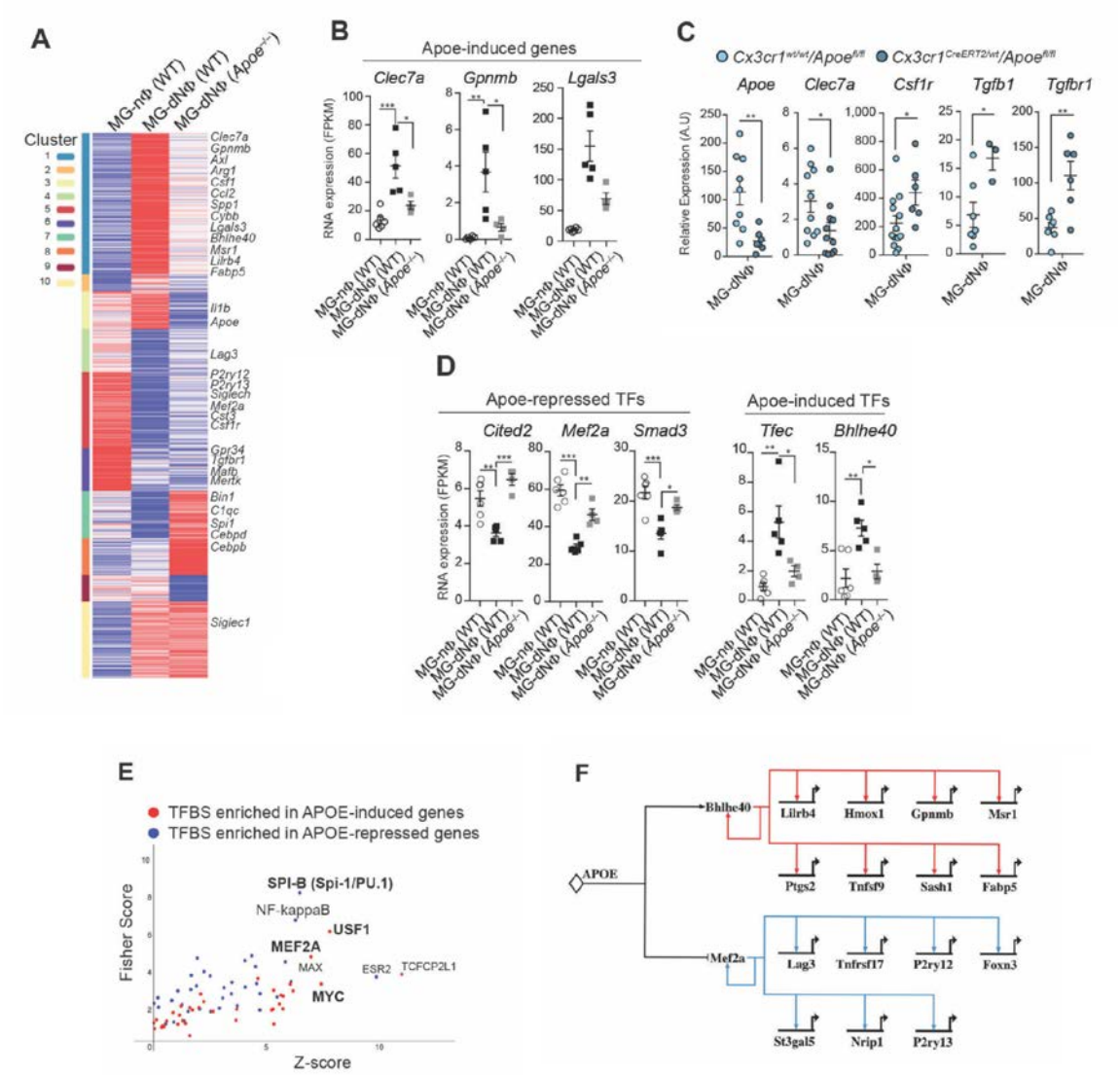

Figure IV-4 APOE regulates transcriptional and post-transcriptional program of MGnD phenotype.

(A) K-means clustering (k = 4) of 1,249 significantly affected genes in bulk microglia (1,000 cells per animal) from WT and Apoe$^{-/-}$ mice. Each vertical lane represents mean of biological replicates per condition in WT non-phagocytic (n = 6), WT phagocytic (n = 5) and Apoe$^{-/-}$ phagocytic (n = 4) mice. Microglia were isolated 16 h post-injection of apoptotic neurons. (B) Selected APOE-induced genes from WT and Apoe$^{-/-}$ mice 16 h post-injection of apoptotic neurons. Data are presented as mean ± s.e.m. *p < 0.05, **p < 0.01, ***p < 0.001 by one-way ANOVA followed by Tukey´s multiple-comparison post-hoc test. (C) qPCR validation of selected genes in phagocytic (MG-dNΦ) microglia from Cx3cr1^{CreERT2}/Apoe$^{fl/fl}$ vs. Cx3cr1$^{wt/}$Apoe$^{fl/fl}$ controls. Gene expression level was normalized against Gapdh using ΔCt (n =

6-10 per group). Data are presented as mean normalized expression ± s.e.m. *p < 0.05, **p < 0.01, by Student t test, 2-tailed. (D) Selected APOE-repressed and induced Transcription Factors (TFs) from WT and $Apoe^{-/-}$ mice 16 h post-injection of apoptotic neurons. Data are presented as mean ± s.e.m. *p < 0.05, **p < 0.01, ***p < 0.001 by one-way ANOVA followed by Tukey´s multiple-comparison post-hoc test. (E) Transcription factor binding site (TFBS) over-representation analysis using oPOSSUM, showing that the promoter regions (250bp upstream of TSS) of 28 APOE-induced and 39 APOE-repressed genes are enriched for predicted binding sites. (F) Target analysis shows gene-regulatory networks orchestrates two distinct pathways in phagocytic microglia. Both regulators function in concerted ways to activate appropriate genes. Red lines, gene activation inputs; Blue lines, gene repression inputs.

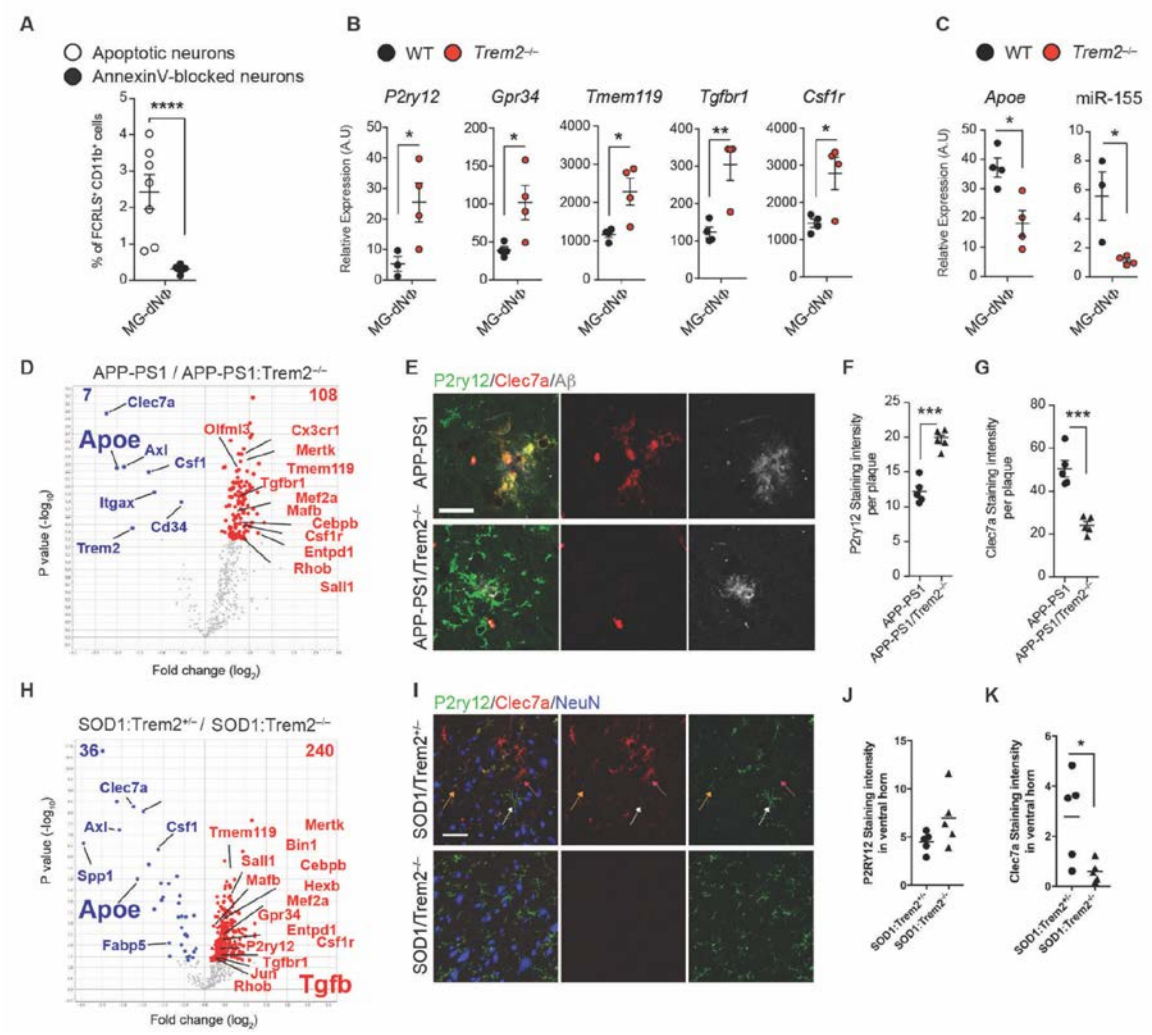

Figure IV-5 Genetic targeting of *Trem2* suppresses APOE pathway and restores the homeostatic microglia in APP-PS1 and SOD1 mice.

(A) Quantification of phagocytosis efficiency of apoptotic vs. Annexin V-pretreated apoptotic neurons (n = 5 per group). Bars show relative fold change (mean ± s.e.m) (****p < 0.001 by Student t test, 2-tailed). (B) qPCR analysis of selected homeostatic genes in phagocytic (MG-dNΦ microglia from Trem2$^{-/-}$ vs. WT mice (n = 4 per group). Data are presented as mean ± s.e.m. *p < 0.05, **p < 0.01 by one way ANOVA. (C) qPCR analysis of *Apoe* and miR-155 expression in phagocytic (MG-dNΦ) microglia from Trem2$^{-/-}$ vs. WT mice (n = 3-4 per group). Data are presented as mean ± s.e.m normalized against *Gapdh* and U6 expression using ΔCt. *p < 0.05, by Student t test, 2-tailed. (D) Volcano plot based on significant differentially expressed genes in microglia from APP-PS1 (n = 4) vs. APP-PS1:Trem2$^{-/-}$ (n = 5) mice at 120 days. p < 0.05 by Student t test, 2-tailed. Selected restored homeostatic and suppressed inflammatory genes are highlighted in red and blue, respectively. (E) Representative immunohistochemical staining for P2ry12, Clec7a and Aβ in APP-PS1 vs. APP-PS1:Trem2$^{-/-}$ mice (120 days). Scale bar, 20 μm.

(F and G) Quantification of P2ry12 and Clec7a intensity per Amyloidβ plaque in APP-PS1 vs. APP-PS1:Trem2$^{-/-}$ mice (120 days).***$p < 0.001$, by Student t test, 2-tailed. (I) Volcano plot based on significant differentially expressed genes in microglia from SOD1:Trem2$^{+/-}$ (n = 9) vs. SOD1:Trem2$^{-/-}$ (n = 13) mice at 115 days (neurological score 1). *$p < 0.05$ by Student t test, 2-tailed. Selected restored homeostatic and suppressed inflammatory genes are highlighted in red and blue, respectively. (J) Representative immunohistochemical staining for P2ry12, Clec7a and NeuN in SOD1:Trem2$^{+/-}$ vs. SOD1:Trem2$^{-/-}$ mice (lumbar section, 115 days). Red arrows point to MGnD microglia at the epicenter of the ventral horn. Yellow arrows point to MGnD transitioning to the ventral horn. White arrows point to M0-homeostatic microglia. Scale bar, 50 μm. (K and L) Quantification of P2ry12 and Clec7a intensity in ventral horn of spinal cord from SOD1:Trem2$^{+/-}$ (n = 5) vs. SOD1:Trem2$^{-/-}$ (n = 5) mice (lumbar section, 115 days). **$p < 0.001$, ***$p < 0.001$ by Student t test, 2-tailed.

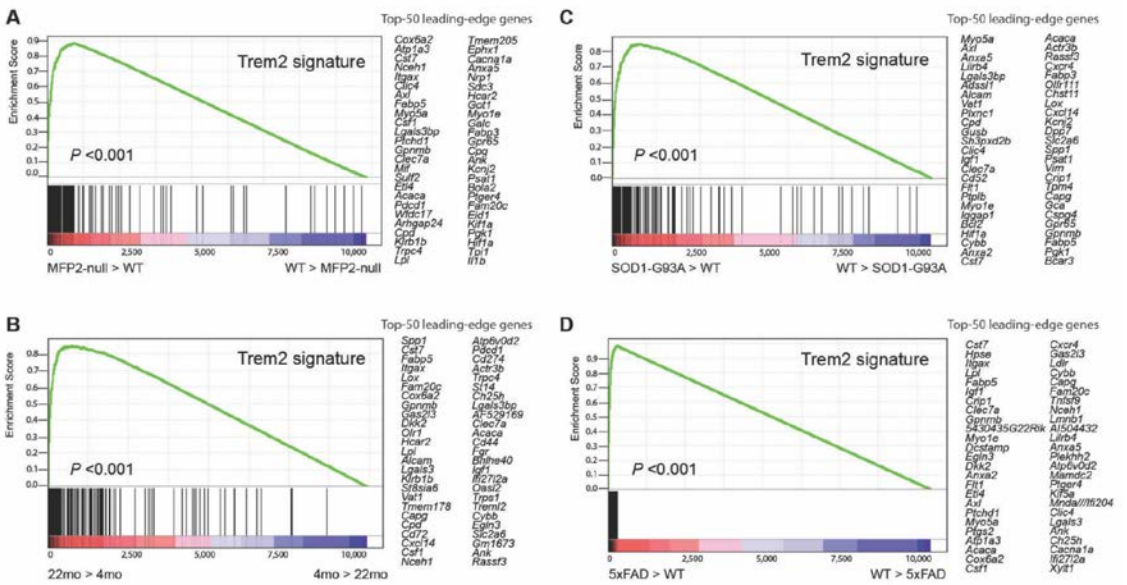

Figure IV-6 Over-representation of TREM2 transcriptional signature genes in aging and disease.

(A-D), GSEA plots demonstrate the over-representation of TREM2 signature in microglia transcriptomes of (A) MFP$^{-/-}$mice; (B) aged mice; (C) SOD1 mice; and (D) 5xFAD mice compared with WT microglia. Genes are ranked into an ordered list according to their differential expression. The middle part of the plot is a bar code demonstrating the distribution of genes in the TREM2 transcriptional signature gene set against the ranked list of genes. The list on the right shows the top genes in the leading-edge subset.

CHAPTER V GSEA-DRIVEN META-ANALYSIS TO UNEARTH IMMUNE-GENE-REGULATORY NETWORKS IN THE MODULATION OF BRAIN FUNCTION

Introduction

The immune system has been recently recognized as a key player in supporting CNS functions. Immune system dysfunction is associated with many neurological disorders, ranging from neurodevelopmental disorders to neurodegenerative diseases. Immune responses and development are tightly controlled by signaling and transcriptional pathways and associated gene regulatory networks. Gene regulatory networks consist of transcriptional factors (TFs), chromatin modifiers, miRNAs, and long noncoding RNAs (Singh et al., 2014). Herein, we focused on TFs and their coordinately activated and repressed gene expression in immune cells to study gene regulatory network-mediated cellular and molecular responses. The objective of this work is a) to delineate the immune gene regulatory networks and pathways underlying the regulation of brain behavior, and 2) to explore the activation and perturbation of these pathways in neurological disorders. In this chapter, I will illustrate how we implemented gene set enrichment analysis (GSEA), a pathway analysis tool to analyze gene expression data, to identify 1) immune signaling pathways disturbed in Rett-like mouse macrophages, 2) T-cell mediated cytokine pathways in the regulation of social behavior, and 3) gene-regulatory networks governing microglia phenotype switching in neurodegenerative diseases.

GSEA was first developed (Subramanian et al. 2005; Tian et al. 2005; Mootha et al. 2003) as an alternative approach to the over-representation approach (ORA) using Gene Ontology (GO) categories to identify biological

pathways and functional processes in gene expression datasets. ORA focuses on lists of differentially expressed genes and uses a statistical analysis to identify whether any GO categories are over-represented in the input list. GSEA, on the other hand, represents a different approach that takes into account all the genes in an experiment and performs a functional class scoring (FCS), thereby allowing for adjustments for gene correlations (Draghici et al., 2007, Pavlidis et al., 2004). GSEA is a more complex and robust analysis as it not only includes the differential expression of genes but it also considers the ranking of the gene expression correlating with the phenotype, thus it preserves the pattern in gene expression data.

Three key outputs are generated by GSEA for interpreting gene expression data: enrichment score (ES), nominal *P* value (Nom-*P*), and false discovery rate (FDR). First, ES reflects the degree to which a given gene set is over-represented at the top or bottom of all ranked genes. It is computed by comparing the distribution of gene ranks from the given gene set against the distribution for the rest of the genes using a one-sided Kolmogorov-Smirnov statistic (Tian et al., 2005). From the GSEA plot, the ES is the magnitude of maximum deviation from zero. Second, the Nom-*P* value is the statistical significance of the ES is. To calculate the Nom-*P*, GSEA adopts an empirical phenotype-based permutation test procedure to regenerate an ES with the permutated data (Subramanian et al., 2005). This not only allows the software to generate a null distribution of ES, but also it preserves the complex correlation

structure of the gene expression data. The Nom-*P* value of the observed ES is computed for the top-ranking gene set by comparison with the null distribution of the ES from each permutation (Tian et al., 2005). Last, FDR is estimated after adjustment for multiple hypothesis testing. In this step, multiple hypothesis testing first yields the normalized enrichment score (NES), which is perhaps more valuable in interpreting GSEA results to predict a particular pathway enrichment than ES, as it normalizes the ES for each gene set to account for the size of the set. The FDR is then computed by comparing the tails of the observed and null distribution of NES. Hence, it is defined as the estimated probability of a given NES to be a false positive (Subramanian et al., 2005).

GSEA queries gene expression data by using a collection of gene sets in the Molecular Signature Database (MSigDB). The original MSigDB was originally built in 2005 and had a collection of 1,325 gene sets that have been under constant changing and expansion. Currently, MSigDB has a catalogue of 17,779 gene sets and consists of 8 major collections, with much broader applicability covering gene sets from chromosome location to upstream *cis* motifs, and can be applied to other data sets such as genotyping information and metabolite profiles.

The real power of GSEA lies in its flexibility. Despite the large resources that GSEA employs, researchers can also use GSEA's powerful and sensitive algorithm for their own manually curated gene sets, allowing them to test the impact of gene expression changes in specific pathways. This GSEA features can be particularly helpful in the following scenarios: 1) If the gene expression

data are of good quality, i.e. the noise from the sequencing technology is low and the experiment design is well thought, one can expect to see only small variations within technical replicates and perhaps a substantial long list of differential expressed genes in the biological condition under study. GSEA results from such transcriptome can then yield tens or hundreds of pathways that fall below the cut offs of statistical significance due to the large database the software employs. Interpretation and identification of the relevant, important biological pathways to the underlying biological phenomena can be daunting and ad hoc; 2) if the transcriptome outcome is poor, with a short list of differentially expressed genes meeting the statistically significant cutoff, the GSEA test may have only a few non-relevant pathways barely meeting the statistical significance. Under either of the above situations, one can curate different functional gene sets from publicly available databases such as the ArrayExpress and Gene Expression Omnibus (GEO). Curating the gene sets not only allows you to eliminate the noise that masks the moderate effect that is relevant to the biological condition of study, but also confirms the finding by curating multiple gene sets derived from independent studies.

We employed the GSEA method to analyze in-house and publicly available transcriptomes for three neuroimmunology projects. In each project, we used the GSEA results to generate relevant experimental testable hypotheses, along with other bioinformatics tools to analyze regulatory regions of TFs. By doing so, we were able to provide key insights into the transcriptional regulation

and gene regulatory network underlying immune cell phenotypic changes in response to different brain stimuli.

Project 1: Dysfunctional microglia and macrophages in MeCP2-null mice

Mutations in methyl-CPG-binding protein 2 (MECP2) lead to over 95% of classical Rett syndrome, a neurodevelopment disorder with both neurological and somatic impairments (Guy et al., 2001). Studies over the past decade on genetic mouse models of Rett syndrome have expanded our knowledge on the genetics and etiology of the disease and provided valuable insights on the underlying mechanism of the pathogenesis observed in Rett patients (Amir et al., 1999, Cronk et al., 2015, Dunn and MacLeod, 2001, Lioy et al., 2011, Yasui et al., 2013, Derecki et al., 2012).

Deletion of MeCP2 gene in mice leads to a breadth of symptoms that recapitulate symptoms in Rett patients (Guy et al., 2001). Studies of MeCP2 null mice have revealed that the immune system plays an important role in the pathogenesis of the symptoms (Derecki et al., 2012, Jiang et al., 2014, Li et al., 2014a). Of note, engraftment of wild-type microglia into MeCP2-null mice via bone-marrow transplantation was shown to arrest disease progress and pathology (Derecki et al., 2012). This has prompted us to examine microglia and its development-related peripheral monocytes and macrophages population in great detail. Using flow cytometry, we found that three macrophages populations, microglia, meningeal macrophages and intestinal macrophages, were reduced in

Mecp2-null mice. In order to define the functional role of MeCP2 and uncover the mechanism of macrophages loss Mecp2-null mice, we performed RNA-seq profiling on microglia and peritoneal macrophage derived from wild-type and Mecp2-null mice. Using GSEA, we first tested the enrichment of biological pathways in Mecp2-null microglia and peritoneal macrophages using MSigDB C_2, which contains curated gene sets (~4738) from various sources such as literature and online pathway databases. We performed the analysis with phenotype permutation (N=1000) and this yielded more than 50 informative sets that met the statistical cutoffs, namely Nom-*P*< 0.001. Glucocorticoid signaling was ranked top among the list of significantly overrepresented pathways (Nom-*P*<0.001) in both Mecp2-null microglia and peritoneal macrophages. The glucocorticoid signaling pathway was particularly interesting to us as *Fkbp5*, which is a canonical target of glucocorticoid pathway, was highly upregulated in transcriptomes of Mecp2-null microglia and peritoneal macrophages. Of note, a previous study (Braun et al., 2012) showed that blocking glucocorticoid signaling using a pharmacological drug-RU486 could ameliorate symptoms and increase life spans of the otherwise Mecp2-null mice. Collectively, these results led us to hypothesize that MeCP2 represses the glucocorticoid signaling pathway and that over-production of glucocorticoid contributes to pathologies of Mecp2-null mice. We validated the functional role of Mecp2 in the regulation of glucocorticoid signaling using *in vitro* experiments. Our chromatin immunoprecipitation (ChIP) experiments confirmed that MeCP2 is bound to the promoters of *Fkbp5* gene,

suggesting MeCP2 directly controls glucocorticoid signaling pathway. In the absence of MeCP2, there was increased acetylation of histone H4 level, which corresponded to increased *Fkbp5* transcription in Mecp2-null microglia and peritoneal macrophages transcriptome. To further investigate the role of MeCP2 in the regulation of glucocorticoid pathway, we performed glucocorticoid signaling stimulation in vitro using glucocorticoid receptor agonist- dexamethasone. We found that there was increased transcription of *fkbp5* gene in Mecp2-null bone marrow derived macrophages (BMDMs) as compared with wild-type counterparts under low doses of dexamethasone stimuli, and the difference in fkbp5 transcription between wild-type and Mecp2-null BMDMs disappeared as dexamethasone doses increased. This result suggests that MeCP2 controls the sensitivity of glucocorticoid signaling pathway.

Secondly, we noticed that a subset of the glucocorticoid pathway signature that was up-regulated in Mecp2-null microglia and macrophages transcriptome, contains a subset of hypoxia-inducible genes. Correspondingly, GSEA results from the MSigDB C_2 database also demonstrated a moderate correlation of hypoxia-induced genes with Mecp2-null microglia induced transcripts, though the NES and Nom-*P* value corresponding to hypoxia pathway were not as significant as the values corresponding to glucocorticoid pathway. To confirm the hypoxia pathway prediction from the GSEA results using MSigDB C_2, we curated our own hypoxia gene sets from the GEO database, where we found most of the publicly available gene expression datasets (RNA_seq and

microarrays). When curating gene sets for a biological pathway, GSEA requires the input length of the gene sets to be greater than 15 and less than 500 in order for the program to run. To accommodate the maximum number of transcriptomes we downloaded from the GEO database, we derived hypoxia-induced gene signatures by selecting differentially expressed genes that are upregulated under hypoxia conditions at least 2-fold by average function. We curated 32 independent gene sets for hypoxia pathways and found that 25 out of 32 curated hypoxia gene sets were significantly enriched in Mecp2-null microglia. We then validated this hypothesis *in vitro* using BMDMs under normoxia and hypoxia conditions.

A third pathway revealed by our GSEA result was the Tnf-mediated inflammatory pathway: there were multiple statistical significant Tnf transcriptional signatures overrepresented in transcriptomes of Mecp2-null microglia and macrophages using MSigDB C_2. Moreover, transcriptome profiles of Mecp2-null microglia and macrophages demonstrated increased expression of a subset of inflammatory genes such as Tnf, IL6, Cxcl2 etc. Thus, we hypothesized that MeCP2 restrains inflammatory response and MeCP2 deficiency leads to dysregulation of Tnf-mediated inflammatory responses. We validated this hypothesis *in vitro* using Tnf-stimulation in BMDMs, and *in vivo* using Tnf (intraperitoneal injection) challenge. It is worth mentioning that one of the Tnf pathway target, *csf3*, was overexpressed in Mecp2-null macrophages both *in vitro* and *in vivo*. Since *csf3* encodes the protein granulocyte-colony

stimulating (GCSF), which is well-known for its function in stimulating neutrophil production, this led us to examine the GCSF levels in the serum and neutrophil population in the blood of wild-type and Mecp2-null mice. We found that the serum GCSF levels were increased in Mecp2-null mice without any manipulation in comparison with wild-type mice. Using flow cytometry method, we found neutrophil population was significantly increased (~5 fold) in Mecp2-null mice compared with wild-type mice. To determine whether severe neutrophilia contributes to pathologies in Mecp2-null mice, we treated wild-type and Mecp2-null mice with antibodies against GCSF. We found that neutralizing GCSF could moderately increase the life span of Mecp2-null mice, suggesting that Mecp2-mediated inflammatory pathway contributes to pathologies in Mecp2-null mice.

Taken all together, we have demonstrated that MeCP2 is required for macrophage responses to three stimuli (glucocorticoid, hypoxia and Tnf-mediated inflammatory responses). We have provided evidence for these using a combination of RNA-seq analysis using GSEA software and *in vitro* as well as *in vivo* validations of the pathways. Our transcriptome analysis exemplifies the use of GSEA analysis in generating a hypothesis to guide bench-side experiments and uncover the fundamental mechanism underlying a biological phenomenon.

Project 2: T-cell secreted IFNγ in regulating social behavior

Recent seminal work demonstrated that adaptive immunity (primarily T-cell and its secreted molecules) is essential for proper brain functions such as cognition

and learning (Derecki et al., 2010, Brynskikh et al., 2008, Kipnis et al., 2004). T-cell dysfunction or overall immune deficiency is associated with several neurological and psychiatric disorders that present with social withdrawal (Ashwood et al., 2011, Gupta et al., 1998). Social behavior is crucial for the survival of an organism, and for higher-order species, mental-health (Filiano et al., 2016, Kennedy and Adolphs, 2012). Our preliminary results showed that mice lacking the adaptive immunity (SCID mice) have social behavior deficits. Specifically, meningeal T cells support social behavior as their partial depletion results in social deficiency observed in SCID mice. Though meningeal T cells are located in proximity to the brain parenchyma, they do not enter into the brain tissue under physiological conditions. Thus, we hypothesized that meningeal T cells support social behavior through its secreted molecules-such as cytokines.

To identify which T-cell secreted cytokines/mediated-pathways are involved in regulating social behavior, we used a systems approach and performed meta-analysis of available transcriptomes representing various T-cell pathways and brain responses (Figure V-1). We downloaded and used most of the gene expression datasets from GEO and we implemented the GSEA as our main tool to integrate available transcriptomes. Specifically, transcriptomes of mice and rats brain cortices exposed to various stimuli were downloaded and analyzed (Figure V-1a). Brain responses transcriptional signatures were generated from the downloaded transcriptomes by retrieving genes upregulated at least twofold by average function following a brain stimuli. Similarly, T-cell

responses transcriptomes and signatures were downloaded and generated (Figure V-1b). Subsequently, we used GSEA to identify T-cell-mediated transcriptional signatures (IFN-γ, IL-4/IL-13, IL17, IL-10, TGF-β) in brain cortex transcriptomes of mice and rats exposed to different stimuli (social aggregation, sleep deprivation, stress, psychostimulants, antipsychotics and antidepressants) (Figure V-1c). To further validate the connectivity between any T-cell-mediated pathways and brain responses, we also performed GSEA using brain cortex transcriptional signatures and immune response transcriptomes (Figure V-1c). The connectivity between a T-cell-mediated pathway and a brain response was determined by the statistical significance of the GSEA output. Specifically, the following criteria were used to determine a pairwise connection: NES≥1.5 and a $P<0.05$. We then plotted all the connections between T-cell-mediated pathways and brain responses using circos plots, whose layout allows for exploring and uncovering novel interactions (Figure V-1d). We found that transcriptomes from cortices of rats exposed to social aggregation (group housing condition) were exclusively enriched in IFN-γ-mediated transcriptional signatures. This led us to hypothesize that T-cell secreted IFN-γ supports social behavior. We validated this hypothesis through behavioral assays using *Ifng*$^{-/-}$ mice. Greater details on the mechanism of how meningeal T-cell secreted IFN-γ alter neural circuit and control social behavior are provided in (Filiano et al. 2016).

The reason we used the GSEA method in this context is two-fold: 1) to integrate and group available transcriptomes by shared pathways; 2) to

uncover any interactions between T-cell-mediated pathways and brain responses. Implementing GSEA as a means to integrate available transcriptomes represents a novel approach of meta-analysis.

IFN-γ is thought to be an important cytokine secreted by immune cells mediated anti-pathogen response. We recently showed that T-cell secreted IFN-γ can have a profound role in maintaining proper social behavior in mice. Since social behavior is crucial for the survival of a species, and increased social behavior increased the likelihood of spreading pathogens, we hypothesized that there was a co-evolutionary pressure that as sociability increases, anti-pathogen response also increases; IFN-γ pathway may have increased this co-evolution (Filiano et al., 2016). To test this hypothesis, we turned to the GEO database and searched for available brain transcriptomes in various organisms that were shown or indicated to represent distinctive social behavior. We identified brain transcriptomes of group-housing versus single-housing rats, domesticated versus wild-strain zebrafish and low versus high aggressive drosophila strains. In addition to the publicly available transcriptomes, we also conducted our own RNA-seq experiments on group-housing versus single-housing mice. We first used the GSEA to assess whether these brain transcriptomes exposed to various social stimuli were enriched in IFN-γ transcriptional signatures; it turned out that both transcriptomes of socially experienced rats and mice (acute group housing) were enriched in IFN-γ response signatures. Similarly, the transcriptome of a domesticated zebrafish strain, which demonstrated higher social interaction

(Barba-Escobedo and Gould, 2012), exhibited enrichment for an IFN-γ transcriptional signature derived from (López-Muñoz et al. 2009). Though drosophila lack T cells or IFN-γ, they contain JAK-STAT pathway which is canonically downstream of IFN-γ receptor signaling in higher species. We found that transcriptome of low-aggressive drosophila strains, which is a physiological correlate with socially experienced flies (Wang et al., 2008), was highly enriched with an anti-pathogen JAK/STAT-dependent transcriptional signature derived from GSE54833 and GSE2828. In conclusion, GSEA results demonstrated that IFN-γ transcriptional signatures are over-represented in social behavior-associated brain transcriptomes ranging from insects to mammals, suggesting that the IFN-γ-mediated pro-social behavior effect is evolutionarily conserved.

To reaffirm that social aggregation upregulates IFN-γ responsive gene signatures, we examined the promoter regions of the highly upregulated 'social' genes in the aforementioned social-behavior-associated transcriptomes of mice, rats, zebrafish, and drosophila. Given our GSEA results, we hypothesized that these highly-regulated 'social' transcripts are controlled by the transcriptional factor STAT1, which is downstream of IFN-γ receptor signaling controlling IFN-γ target genes. Specifically, top ranking 'social' genes were identified by selecting the leading-edge genes contributing to the enrichment of IFN-γ pathways and their differential expressions in social behavior-associated mice, rat, zebrafish and drosophila. Next, we extracted the promoter sequences (~200bp) of the 'social' genes using UCSC Genome Browser (https://genome.ucsc.edu/). Using a

de novo motif discovery tool (MEME), we generated the over-represented transcriptional factor binding site (TFBS) motifs in the input promoter sequences. Subsequently, a motif comparison tool, namely Tomtom, was used to compare the top *de novo* generated motifs to a motif database (JASPER) containing TFBS motifs *in vivo* and *in silico*. A statistical significance (p-value) is calculated by the motif similarity analysis tool (Tomtom) by comparing the de novo motif to a known TFBS sequence. We found that the promoter regions of the 'social' transcripts in mice, rat, zebrafish and drosophila were enriched in STAT1 TFBS motifs, indicating that the social behavior upregulated genes were bona fide IFN-γ targets. Taken together, we have shown that social aggregation/enrichment can upregulate an IFN-γ or anti-pathogen immune program even in the absence of an infection. This is in line with our hypothesis that IFN-γ pathway can mediate the co-evolution of the dynamic interaction between social behavior and anti-pathogen response.

In conclusion, we have presented a novel GSEA-driven approach of meta-analysis to integrate large numbers of transcriptomes. Using this approach, we showed that T-cell secreted IFN-γ is important in maintaining proper social behavior, and this dynamic interaction between the immune and nervous systems is evolutionarily conserved.

Project 3: Microglia phenotype switching in neurodegenerative diseases

Microglia are the brain resident immune cells and play a pivotal role in maintaining brain homeostasis (Butovsky et al., 2014, Matcovitch-Natan et al., 2016). They are constantly surveying the environment and react to homeostasis-perturbing elements by initiating an inflammatory response (Wake et al. 2013). Previous studies revealed a unique molecular and functional transcriptional signature of microglia under homeostasis in the healthy brain (Butovsky et al. 2013; Gautier et al. 2012; Hickman et al. 2013). The homeostatic microglia transcriptional signature is controlled by TGFβ signaling. It is well known that microglia are sensitive to the microenvironment stimuli and change phenotypes (i.e. transcriptional signature) during the course of CNS diseases (Chiu et al., 2013, Holtman et al., 2015, Keren-Shaul et al., 2017, Kreutzberg, 1996, Orre et al., 2014, Perry and Holmes, 2014, Wang et al., 2015). Microglia lose homeostatic transcriptional signature and adopt an inflammatory phenotype in CNS diseases (Orre et al., 2014). Recent studies taking advantages of sequencing technologies have revealed a common-disease-associated microglia signature in neurodegenerative diseases (Chiu et al., 2013, Hickman et al., 2013, Holtman et al., 2015, Keren-Shaul et al., 2017, Orre et al., 2014). However, there were discrepancies in the common disease-associated microglia signatures, as each study was focused on a different disease model. Whether different microglia signatures in neurodegenerative diseases share a common transcriptional signature, and what is the underlying mechanism governing such

changes in transcription still remains unknown. To address these two questions, we followed an approach similar to the one established in Project 2 above. In particular, we used GSEA to perform a meta-analysis of microglia transcriptomes in different neurodegenerative diseases. Microglia transcriptomes from the following neurological disease were downloaded from GEO and re-analyzed: mouse models of neuropathic pain (GSE60670), chronic pain (GSE71133), Rett syndrome (*Mecp2*$^{-/-}$) (GSE66211), lipid disorder (*Mfp2*$^{-/-}$) (GSE66420), ALS (SOD1) (GSE433660), Alzheimer's disease (5x FAD) (GSE65067), brain irradiation (GSE55968), and aging (GSE62420). Subsequently, microglia transcriptional signatures were generated by retrieving genes upregulated at least 1.5-fold by average function with a p value less than 0.01 (Student's t-test) in disease conditions. The GSEA algorithm was applied to assess the overlap of microglia transcriptional signatures in various diseases. Our preliminary data using NanoString analysis suggest that phagocytic microglia shared similar transcriptional signature with microglia signatures in neurodegenerative diseases. To further validate our preliminary data, we conducted an RNA-seq experiment on phagocytic microglia and used GSEA to access phagocytic microglia signature enrichment in available microglia transcriptome of various neurodegenerative diseases. A Nom-*P* value less than 0.001 was used to determine pairwise transcriptome connectivity. We used circos plots to present our meta-analysis results and found that microglia transcriptomes in mouse models of aging, *MFP2*$^{-/-}$, Alzheimer's disease and brain irradiation shared a

common transcriptional signature. Of note, the common disease-associated microglia signature showed statistical significant overlap with a transcriptional signature of phagocytic microglia. Taken together, these data suggest that microglia share a common transcriptional signature in neurodegenerative diseases which is induced by microglia phagocytosis.

Our NanoString analysis in three disease models (SOD1, EAE, APP-PS1) suggest that APOE pathway is significantly induced in microglia signatures in diseases. To explore the APOE signaling regulating microglia phenotype switching in neurodegenerative diseases, we performed RNA-seq on WT versus *Apoe*$^{-/-}$ microglia under both phagocytic and non-phagocytic conditions. We analyzed 1) APOE induced targets by selecting genes that were induced in phagocytic microglia but repressed in *Apoe*$^{-/-}$ phagocytic microglia, and 2) APOE repressed targets by selecting genes that were suppressed in phagocytic microglia but were restored in *Apoe*$^{-/-}$ phagocytic microglia. We then analyzed the promoter regions (~250bp upstream of transcriptional start site) of selected APOE induced- and repressed genes using a TFBS over-representation analysis tool oPOSSUM (Ho Sui et al., 2007). We found that APOE signaling represses homeostatic microglia signatures by suppressing transcriptional factor including *Mef2a* and *Mafb*; APOE signaling induces microglia signature in diseases by inducing transcriptional factors involving *Bhlhe40* and *Tfec*.

Recent findings suggest that TREM2-pathway is activated in apoptotic neurons (Wang et al., 2015) that can induce microglia phagocytosis. As APOE

signaling activation is a hallmark of phagocytic/neurodegenerative microglia, we hypothesized that activation of APOE signaling in disease-associated microglia is TREM2-pathway dependent. To test this hypothesis, we derived Trem2-mediated transcriptional signature derived from GSE65067 (5XFAD/Trem2$^{-/-}$), and used GSEA to determine the enrichment of Trem2-mediated transcriptional signature in microglia transcriptomes of various neurodegenerative models. We found that Trem2 pathway is enriched in microglia transcriptomes of aging, ALS, Alzheimer's disease and lipid disorder (*Mfp2*$^{-/-}$). In combination with APOE signaling activation in phagocytic microglia, our results suggest that microglia phenotype switching in neurodegenerative diseases is dependent on the TREM2-APOE pathway.

In summary, we used the GSEA method to perform meta-analysis of microglia transcriptomes and identified a unique microglia molecular signature that is common to several neurodegenerative models. A combination of pathway analysis and promoter sequence analysis revealed that the APOE-mediated gene regulatory networks regulate microglia phenotype switching in neurodegenerative diseases.

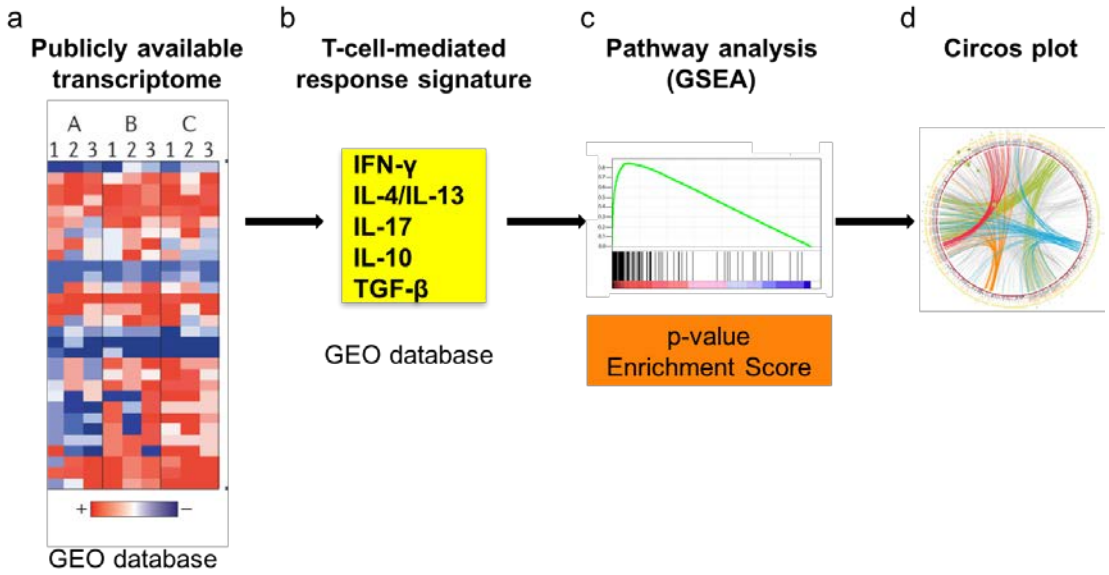

Figure V-1.Steps undertaken to perform the meta-analysis of T-cell mediated pathways in regulating brain responses.

a. Rats and mice cortices transcriptomes were downloaded from GEO. b. Transcriptomes of T-cell responses were downloaded from GEO and T-cell mediated pathway signatures were generated by retrieving genes upregulated at least twofold by average function following a cytokine stimulus. c. GSEA was implemented to integrate transcriptomes and determine the enrichment of T-cell response signatures in brain responses transcriptomes and vice versa. The connectivity between a T-cell pathway and a brain response is determined by NES ≥ 1.5 and Nom-*P* < 0.05. d. Circos plots were used to present the results of the meta-analysis of transcriptomes.

CHAPTER VI DISCUSSION

Dysfunctional microglia and macrophages in MeCP2-null mice

Increasing evidence has been demonstrating that non-neuron cells, such as brain resident microglia (Cronk et al., 2015, Derecki et al., 2012), astrocytes (Ballas et al., 2009), and oligodendrocytes (Nguyen et al., 2013), contribute significantly to the pathologies of Rett Syndrome. In Chapter II, we demonstrated that MeCP2 is broadly expressed in various peripheral macrophages populations, and its global loss leads to transcription impairment and reduced number of specific macrophage populations: microglia, perivascular meningeal macrophages, and intestinal macrophages. Re-expression of MeCP2 in Cx3CR1-expressing macrophages when administering tamoxifen in $Cx3cr1^{creER/+}MeCP2^{lox\text{-}stop/y}$ mice resulted in attenuation of weight loss and increased lifespan. This result corroborates with earlier findings that MeCP2-deficient myeloid-derived cells, including macrophages and microglia, are dysfunctional, and introduction of wild-type macrophages and microglia in otherwise null background can arrest pathologies in Rett Syndrome (Derecki et al., 2012). We have further provided the underlying mechanism of MeCP2-deficient macrophage phenotypes through RNA-seq analysis of whole-brain microglia and peritoneal macrophages isolated from wild type and MeCP2-null mice, and in vitro and in vivo validations of pathways identified through RNA-seq.

We found that both microglia and peritoneal macrophages displayed impairment to three stimuli: glucocorticoid signaling, hypoxia response, and inflammatory response. These data implicate macrophage as a novel player in Rett Syndrome pathology. Our data also emphasize that, in addition to canonical nervous system cell types, MeCP2 expression is specific and important for the function of macrophage populations.

Our findings suggest both malfunction and loss of macrophages likely to be important contributors to somatic impairments in Rett Syndrome across multiple organ systems. However, the contribution to the neurological deficits is unclear, as MeCP2 itself plays a critical role in nervous systems function and global loss of MeCP2 results in serious general organ impairment. Therefore, dysfunctional neurons might increase the cellular stress and further activate MeCP2-deficient microglia and macrophages, aggravating their loss and maladaptive responses to the aforementioned stimuli. Such a positive feedback loop involving multiple cells types might explain the progressive worsening of systemic symptoms. These results are in line with a recent report that specific deletion of MeCP2 in Cx3cr1-expressing cells did not yield significant symptoms of Rett Syndrome (Schafer et al., 2016). We propose a model that neurons initiate and drive pathology, MeCP2-deficient microglia and macrophages further amplify neuronal-driven phenotypes, forming a positive feedback loop which progressively leads to death. Therefore, introduction of wild-type non-neuronal

cells could stop the vicious cycle and therefore arrest or blunt the progressive phenotype.

We have demonstrated that subsets of macrophage populations are particular venerable to MeCP2 deficiency, one of which are intestinal resident macrophages. It is well known that Rett patients also suffer from gastrointestinal abnormalities such as distension and constipation dysfunction (Chahrour and Zoghbi, 2007, Dunn, 2001). It is possible that the intestinal macrophages, which make up a significant proportion of the intestinal immune cells, could contribute to the gastrointestinal pathology due to either loss of favorable resident macrophages and/or dysfunction of macrophages in the absence of MeCP2. Our results on functional defects and loss of tissue-resident macrophages connect with previous findings on insulin-like growth factor (IGF-1) in increasing the lifespan of MeCP2-null mice (Tropea et al., 2009) as macrophages have been indicated as one of the two largest sources of IGF-1 (Gow et al., 2010). Importantly, recombinant human IGF-1 has shown promising results in clinical trials (Khwaja et al., 2014). Therefore, it is conceivable that MeCP2-deficient macrophage contribute to overall pathology via loss of critical growth factor IGF1.

We found dysregulation of multiple gene expression programs being common in both microglia and a peripheral macrophage population-peritoneal macrophage. Given that macrophages throughout the body are very diverse given variation in location, context, and functions, this result suggests a more global role for MeCP2 in macrophage transcription regulation. These gene

expression programs might act alone or in concert depending on the exact stimuli present to the macrophage. For example, we found that many glucocorticoid-induced transcripts were also hypoxia targets. Such transcripts might represent independent stimulus or synergic combination of both stimuli, which leads to complex transcriptional dysregulation.

Our validation studies confirmed a macrophage-intrinsic role for MeCP2 in the transcription regulation of inflammatory-, hypoxia- and glucocorticoid signaling pathways. We validated the role of MeCP2 on restraining glucocorticoid response in vitro using MeCP2-deficient BMDMs. MeCP2-deficient macrophages produced excessive responses when stimulated with low-dose of glucocorticoid, which have been previously shown to contribute to pathology in MeCP2-null mice (Braun et al., 2012). Furthermore, we showed that MeCP2 controls glucocorticoid target, Fkbp5, via binding directly to macrophage genome, supporting a direct role for MeCP2 in epigenetic regulation of macrophage response.

It is worth mentioning that MeCP2-null mice developed an activation of inflammatory program as disease progressed. This is exhibited by increased level of serum GCSF, which subsequently leads to severe neutrophilia. In addition, peritoneal macrophages and BMDM stimulated with TNF in vivo and in vitro, respectively, demonstrated dysregulated transcriptional response. These results implicated MeCP2 as a master regulator of TNF-mediated inflammatory responses in macrophages. Interestingly, TNF has been implicated as a non-inflammatory cytokine and play an important role in development, homeostasis in

both CNS and outside CNS (Stellwagen and Malenka, 2006, Wheeler et al., 2014). Maladaptive response to TNF in neurons or other brain cells types might lead to defective brain development in the absence of MeCP2.

In summary, we have provided evidence that MeCP2 is a master epigenetic regulator in macrophages responses. Our study augments our understanding of the broad range of effects of MeCP2 on non-neuronal cell types, especially outside the CNS, a largely unexplored aspect in the studies of Rett Syndrome. We concluded that macrophages response in three signaling pathways were defective in the absence of MeCP2: glucocorticoid, hypoxia and inflammation via RNA-Seq studies. Our transcriptome analysis was an exemplar of using 'omics' data to generate effective and verifiable hypotheses and to guide bench-side experiments for studying the mechanisms underlying presenting biological phenomena. Given the diversity of macrophages populations throughout the body, we cannot predict the exact function in specific macrophage population. Future work on examining transcription regulation of unique macrophage populations' response should consider the role of MeCP2 in macrophage activation. Provided the above, we implicate macrophages as a potentially therapeutic target for future Rett Syndrome therapies.

'Arms race' between host and pathogens

Despite being 'immune privileged', the CNS uses the help from the immune system under homeostasis and in diseases. The immune system, particularly

through T-cell and its secreted molecules, controls CNS development and function. In Chapter III, we demonstrated a novel role of cytokine IFN-γ in maintaining normal social behavior via meta-analysis of publicly available transcriptomes. Furthermore, we demonstrated that CNS neurons directly respond to IFN-γ derived from meningeal T cells to maintain an IFN-γ induced tonic inhibition. Lack of IFN-γ can lead to disinhibition of the PFC neurons and subsequently cause social deficits in mice. These data suggest IFN-γ acts as a rheostat to keep in check the baseline activation of neural circuits in supporting proper social behavior.

Earlier work on examining T-cell influences in the healthy brain has uncovered a vital role of a unique population, meningeal T cells, with respect to different effects on circuits and behaviors. However, how meningeal T cells influence brain behavior remains unknown as, though located in proximity of the brain tissue, they do not enter the brain parenchyma under non-pathological conditions. One of the hypotheses is that meningeal T cells affect brain behavior through one of their secreted molecules, such as cytokines. Identifying which cytokine affects which behavior is a challenging task, as meningeal T cells produce a myriad of cytokines having coinciding and/or synergic responses, although each can have a distinctive function. To identify specific cytokines effect on most brain behaviors, we carried out a meta-analysis of immune cell (and fibroblast) transcriptomes stimulated with different cytokines or a combination of cytokines, as well as rodent brain transcriptome exposed to different stimuli and

conditions. Using GSEA analysis and circus plot layout, we grouped transcriptomes into clusters based on experiments settings and transcriptome connectivity. Our analysis demonstrated that rodents which experience social environment induced transcriptional changes similar to those triggered by IFN-γ stimulation. We validated this result with mice lacking T cells or IFN-γ using three-chamber sociability assay. This result indicated a link between T-cell secreted cytokine IFN-γ and social behavior.

A number of studies have reported altered IFN-γ levels in individuals with neurological disorders that present with social withdraw, such as depression and Autism Spectrum Disorders (ASD) (Dahl et al., 2014, Gupta et al., 1998). In the collected studies of depression, one study reported reduced IFN-γ levels in the post-mortem ventrolateral PFC region of people diagnosed with depression (Clark et al., 2016), while another study described contrasting results that the circulating IFN-γ levels were increased in individuals suffer from depression (Dahl et al., 2014). It is possible that these conflicting results are due to differential expression of IFN-γ in the blood versus in the CNS. Similarly, variations regarding immune dysfunction and reported IFN-γ levels can also be seen in ASD studies. Reduced number of terminally differentiated T cells was reported in autistic children (Saresella et al., 2009) . These T cells produced lower amounts of IFN-γ when isolated and stimulated in vitro with phorbol myristate acetate and ionomycin (Gupta et al., 1998). In contrast, other studies reported increased levels of IFN-γ detected both in the brain (Li et al., 2009) and blood (Masi et al.,

2015). Collectively, these results indicate ASD as a heterogeneous disorder, with both too much and too little IFN-γ or immune disruption in any direction could lead to disease.

Social behavior is crucial not only for survival and reproduction of a species (host) but also for the transmission and evolution of pathogens. Our transcriptome analysis using public data source demonstrated that the brain transcriptome of rat, mice, zebrafish and flies exhibited enrichments of IFN-γ-induced transcriptional signatures even in the absence of any infection. Of particular note, brain transcriptome of flies demonstrated increased expression of primordial Janus kinase (JAK)-STAT-induced transcripts, though flies lack IFN-γ itself and adaptive immunity. These results implied a conceivable theory: IFN-γ drives pro-social genes to increase social interactions of the host and its conspecifics, which also benefits the pathogen to spread. Higher species may have evolved IFN-γ to combat pathogen more efficiently as sociability increases. Furthermore, in combination with the well-studied sickness behavior, one of which is pathogen-induced social withdraw, we proposed a plausible hypothesis that the complex social behavior (pathogen-induced pro-social versus host-induced social withdraw) may have evolved as a result of an “arm race’ between pathogens and hosts (Filiano et al., 2017, Filiano et al., 2016, Kipnis, 2016). Our discovery on the novel role of IFN-γ in promoting social behavior fits this dynamic interaction between the pathogens and hosts.

Taken together, our results indicate that impaired immunity may cause numerous neurological and psychiatric disorders present with social behavior deficits. We provided a detailed mechanism on how immune cell-derived molecules can alter neural circuit and affect brain behavior. Given the vast number of cytokines or cytokine-like molecules secreted by the immune system, and the growing appreciation that the immune and nervous system interact closely, these immune agents constitute a promising target reservoir for the therapeutical intervention of neurological disorders.

Disease-associated microglia

It is known that microglia adopt a different phenotype in CNS diseases. In Chapter IV, we identified a unique population of disease-associated microglia (MGnD) that is commonly found in several neurodegenerative conditions in mouse models. Pathway analysis of these transcriptome revealed that MGnD phenotype was induced by activation of the TREM2-APOE pathway. Our studies showed that phagocytic microglia following injecting apoptotic neurons and neuronal filaments also induced MGnD by suppressing TGFβ-mediated homeostatic signature. Our results suggest a novel role of APOE in the regulation of newly identified microglia population (MGnD) and implicate the APOE-TREM2 pathway as a potential therapeutic target to restore homeostatic microglia function in Alzheimer and related diseases.

We have demonstrated that APOE-dependent MGnD are located in close proximity to amyloid plaques in a mouse model and patients' brain of Alzheimer's disease. Moreover, APOE-mediated MGnD and dystrophic neuritis form a complex around amyloid plaques, forming a unique microenvironment. Our results are in line with literature reports on the positive role of APOE in promoting amyloid plaques formation in Alzheimer's disease (Huang et al., 2017, Kim et al., 2012, Liao et al., 2014a). Moreover, we showed that the APOE-suppressed homeostatic microglia signature is inversely correlated with AD pathology in human. Therefore, it is conceivable that APOE-mediated MGnD may contribute to AD pathology via promoting amyloid plaque formation.

Our promoter analysis of APOE targets revealed that APOE induces MGnD signature via *Bhlhe40*, and suppresses homeostatic signature via *PU.1* and *Mef2a*. Therefore, it forms bifurcate gene regulatory networks to induce MGnD and suppresses homeostatic signature. Promoter analysis using oPOSSUM demonstrated that upstream promoter regions of APOE-repressed genes were enriched with PU.1 and MEF2 transcription factor binding sites, and our in-house motif analysis using TRANSFAC database also confirmed that (data not shown). Interestingly, previous studies found that PU.1 binding sites are enriched in the enhancer regions of microglia; PU.1 can cooperate with Mef2a family to drive gene expressions specific in microglia. These results suggest that APOE signaling may suppress homeostatic signature by inhibiting Mef2a binding to the promoters and/or enhancers of microglia genes. Of note, we also

observed that transcription factor smad3 is repressed by APOE. Given that smad3 is primarily induced by TGFb signaling pathway, it is likely that APOE represses TGFb-mediated homeostatic signature via smad3. Our promoter analysis also proposed a novel transcriptional factor Bhlhe40 in mediating APOE-induced MGnD transcriptional signature. This result will be validated in future studies.

The role of TREM2 protein, one of the major risk factors for AD, has been hotly debated in the context of neurodegenerative diseases. Our pathway analysis of microglia transcriptomes under several diseased conditions, including Alzheimer's disease (5xFAD), ALS (SOD1 model), cerebellar degeneration (MFP2 deficiency) and aged mice, showed that neurodegenerative conditions induced changes in gene expression that are similar to those triggered by activation of TREM2 pathway. We have further provided experimental validation through genetically deleting Trem2 in both APP-PS1 and SOD1 mice. We found that deletion of Trem2 in these mice restored homeostatic microglia signature via suppressing APOE pathway.

All in all, these results provided evidence that the APOE-TREM2 pathway plays an important role in microglia phenotype switch in diseases, and implicate microglia as therapeutic targets in AD and related conditions. Importantly, we identified a unique population of microglia subset (MGnD) that is common to neurodegenerative diseases like AD and ALS and present in aged brains. The mechanism for such microglia phenotype switch is possibly attributed to neuronal

apoptosis and activation of APOE-TREM2 pathway. Restoration of microglia homeostatic function by targeting APOE-TREM2 may be beneficial in AD and other neurodegenerative conditions. However, this possibility should be approached with caution as it will be important to take into consideration the different APOE genotypes and TREM2 polymorphism in AD patients.

CHAPTER VII REFERENCES

AJAMI, B., BENNETT, J. L., KRIEGER, C., TETZLAFF, W. & ROSSI, F. M. 2007. Local self-renewal can sustain CNS microglia maintenance and function throughout adult life. *Nat Neurosci,* 10**,** 1538-43.

AMIR, R. E., VAN DEN VEYVER, I. B., WAN, M., TRAN, C. Q., FRANCKE, U. & ZOGHBI, H. Y. 1999. Rett syndrome is caused by mutations in X-linked MECP2, encoding methyl-CpG-binding protein 2. *Nat Genet,* 23**,** 185-8.

ASHBURNER, M., BALL, C. A., BLAKE, J. A., BOTSTEIN, D., BUTLER, H., CHERRY, J. M., DAVIS, A. P., DOLINSKI, K., DWIGHT, S. S., EPPIG, J. T., HARRIS, M. A., HILL, D. P., ISSEL-TARVER, L., KASARSKIS, A., LEWIS, S., MATESE, J. C., RICHARDSON, J. E., RINGWALD, M., RUBIN, G. M. & SHERLOCK, G. 2000. Gene ontology: tool for the unification of biology. The Gene Ontology Consortium. *Nat Genet,* 25**,** 25-9.

ASHWOOD, P., KRAKOWIAK, P., HERTZ-PICCIOTTO, I., HANSEN, R., PESSAH, I. N. & VAN DE WATER, J. 2011. Altered T cell responses in children with autism. *Brain Behav Immun,* 25**,** 840-9.

AVANTS, B. B., DUDA, J. T., KILROY, E., KRASILEVA, K., JANN, K., KANDEL, B. T., TUSTISON, N. J., YAN, L., JOG, M., SMITH, R., WANG, Y., DAPRETTO, M. & WANG, D. J. 2015. The pediatric template of brain perfusion. *Sci Data,* 2**,** 150003.

AVANTS, B. B., TUSTISON, N. J., SONG, G., COOK, P. A., KLEIN, A. & GEE, J. C. 2011. A reproducible evaluation of ANTs similarity metric performance in brain image registration. *Neuroimage,* 54**,** 2033-44.

BAILEY, T. L., BODEN, M., BUSKE, F. A., FRITH, M., GRANT, C. E., CLEMENTI, L., REN, J., LI, W. W. & NOBLE, W. S. 2009. MEME SUITE: tools for motif discovery and searching. *Nucleic Acids Res,* 37**,** W202-8.

BAIN, C. C., SCOTT, C. L., URONEN-HANSSON, H., GUDJONSSON, S., JANSSON, O., GRIP, O., GUILLIAMS, M., MALISSEN, B., AGACE, W. W. & MOWAT, A. M. 2013. Resident and pro-inflammatory macrophages in the colon represent alternative context-dependent fates of the same Ly6Chi monocyte precursors. *Mucosal Immunol,* 6**,** 498-510.

BALLAS, N., LIOY, D. T., GRUNSEICH, C. & MANDEL, G. 2009. Non-cell autonomous influence of MeCP2-deficient glia on neuronal dendritic morphology. *Nat Neurosci,* 12**,** 311-7.

BARBA-ESCOBEDO, P. A. & GOULD, G. G. 2012. Visual social preferences of lone zebrafish in a novel environment: strain and anxiolytic effects. *Genes Brain Behav,* 11**,** 366-73.

BAUER, J. & LASSMANN, H. 2016. Neuropathological Techniques to Investigate Central Nervous System Sections in Multiple Sclerosis. *Methods Mol Biol,* 1304**,** 211-29.

BEHZADI, Y., RESTOM, K., LIAU, J. & LIU, T. T. 2007. A component based noise correction method (CompCor) for BOLD and perfusion based fMRI. *Neuroimage,* 37**,** 90-101.

BENDALL, L. J. & BRADSTOCK, K. F. 2014. G-CSF: From granulopoietic stimulant to bone marrow stem cell mobilizing agent. *Cytokine Growth Factor Rev,* 25**,** 355-67.

BLUTHE, R. M., MICHAUD, B., POLI, V. & DANTZER, R. 2000. Role of IL-6 in cytokine-induced sickness behavior: a study with IL-6 deficient mice. *Physiol Behav,* 70**,** 367-73.

BOURKE, A. F. 2014. Hamilton's rule and the causes of social evolution. *Philos Trans R Soc Lond B Biol Sci,* 369**,** 20130362.

BRAUN, S., KOTTWITZ, D. & NUBER, U. A. 2012. Pharmacological interference with the glucocorticoid system influences symptoms and lifespan in a mouse model of Rett syndrome. *Hum Mol Genet,* 21**,** 1673-80.

BRYNSKIKH, A., WARREN, T., ZHU, J. & KIPNIS, J. 2008. Adaptive immunity affects learning behavior in mice. *Brain Behav Immun,* 22**,** 861-9.

BUTOVSKY, O., JEDRYCHOWSKI, M. P., CIALIC, R., KRASEMANN, S., MURUGAIYAN, G., FANEK, Z., GRECO, D. J., WU, P. M., DOYKAN, C. E., KINER, O., LAWSON, R. J., FROSCH, M. P., POCHET, N., FATIMY, R. E., KRICHEVSKY, A. M., GYGI, S. P., LASSMANN, H., BERRY, J., CUDKOWICZ, M. E. & WEINER, H. L. 2015. Targeting miR-155 restores abnormal microglia and attenuates disease in SOD1 mice. *Ann Neurol,* 77**,** 75-99.

BUTOVSKY, O., JEDRYCHOWSKI, M. P., MOORE, C. S., CIALIC, R., LANSER, A. J., GABRIELY, G., KOEGLSPERGER, T., DAKE, B., WU, P. M., DOYKAN, C. E., FANEK, Z., LIU, L., CHEN, Z., ROTHSTEIN, J. D., RANSOHOFF, R. M., GYGI, S. P., ANTEL, J. P. & WEINER, H. L. 2014. Identification of a unique TGF-

beta-dependent molecular and functional signature in microglia. *Nat Neurosci,* 17**,** 131-43.

BUTTGEREIT, A., LELIOS, I., YU, X., VROHLINGS, M., KRAKOSKI, N. R., GAUTIER, E. L., NISHINAKAMURA, R., BECHER, B. & GRETER, M. 2016. Sall1 is a transcriptional regulator defining microglia identity and function. *Nat Immunol,* 17**,** 1397-1406.

CACIOPPO, S., CAPITANIO, J. P. & CACIOPPO, J. T. 2014. Toward a neurology of loneliness. *Psychol Bull,* 140**,** 1464-504.

CHAHROUR, M. & ZOGHBI, H. Y. 2007. The story of Rett syndrome: from clinic to neurobiology. *Neuron,* 56**,** 422-37.

CHEN, S. K., TVRDIK, P., PEDEN, E., CHO, S., WU, S., SPANGRUDE, G. & CAPECCHI, M. R. 2010. Hematopoietic origin of pathological grooming in Hoxb8 mutant mice. *Cell,* 141**,** 775-85.

CHIU, I. M., MORIMOTO, E. T., GOODARZI, H., LIAO, J. T., O'KEEFFE, S., PHATNANI, H. P., MURATET, M., CARROLL, M. C., LEVY, S., TAVAZOIE, S., MYERS, R. M. & MANIATIS, T. 2013. A neurodegeneration-specific gene-expression signature of acutely isolated microglia from an amyotrophic lateral sclerosis mouse model. *Cell Rep,* 4**,** 385-401.

CHO, R. J., HUANG, M., CAMPBELL, M. J., DONG, H., STEINMETZ, L., SAPINOSO, L., HAMPTON, G., ELLEDGE, S. J., DAVIS, R. W. & LOCKHART, D. J. 2001. Transcriptional regulation and function during the human cell cycle. *Nat Genet,* 27**,** 48-54.

CHOU, Y. T. & YANG, Y. C. 2006. Post-transcriptional control of Cited2 by transforming growth factor beta. Regulation via Smads and Cited2 coding region. *J Biol Chem,* 281**,** 18451-62.

CLARK, S. M., POCIVAVSEK, A., NICHOLSON, J. D., NOTARANGELO, F. M., LANGENBERG, P., MCMAHON, R. P., KLEINMAN, J. E., HYDE, T. M., STILLER, J., POSTOLACHE, T. T., SCHWARCZ, R. & TONELLI, L. H. 2016. Reduced kynurenine pathway metabolism and cytokine expression in the prefrontal cortex of depressed individuals. *J Psychiatry Neurosci,* 41**,** 386-394.

COHEN, H., ZIV, Y., CARDON, M., KAPLAN, Z., MATAR, M. A., GIDRON, Y., SCHWARTZ, M. & KIPNIS, J. 2006. Maladaptation to mental stress mitigated by the adaptive immune system via depletion of naturally occurring regulatory CD4+CD25+ cells. *J Neurobiol,* 66**,** 552-63.

CRONK, J. C., DERECKI, N. C., JI, E., XU, Y., LAMPANO, A. E., SMIRNOV, I., BAKER, W., NORRIS, G. T., MARIN, I., CODDINGTON, N., WOLF, Y., TURNER, S. D., ADEREM, A., KLIBANOV, A. L., HARRIS, T. H., JUNG, S., LITVAK, V. & KIPNIS, J. 2015. Methyl-CpG Binding Protein 2 Regulates Microglia and Macrophage Gene Expression in Response to Inflammatory Stimuli. *Immunity,* 42**,** 679-91.

DAHL, J., ORMSTAD, H., AASS, H. C., MALT, U. F., BENDZ, L. T., SANDVIK, L., BRUNDIN, L. & ANDREASSEN, O. A. 2014. The plasma levels of various cytokines are increased during ongoing depression and are reduced to normal levels after recovery. *Psychoneuroendocrinology,* 45**,** 77-86.

DAI, X. M., RYAN, G. R., HAPEL, A. J., DOMINGUEZ, M. G., RUSSELL, R. G., KAPP, S., SYLVESTRE, V. & STANLEY, E. R. 2002. Targeted disruption of the mouse colony-stimulating factor 1 receptor gene results in osteopetrosis, mononuclear phagocyte deficiency, increased primitive progenitor cell frequencies, and reproductive defects. *Blood,* 99**,** 111-20.

DANTZER, R. 2009. Cytokine, sickness behavior, and depression. *Immunol Allergy Clin North Am,* 29**,** 247-64.

DAVIES, L. C., JENKINS, S. J., ALLEN, J. E. & TAYLOR, P. R. 2013. Tissue-resident macrophages. *Nat Immunol,* 14**,** 986-95.

DAVIS, M. M., TATO, C. M. & FURMAN, D. 2017. Systems immunology: just getting started. *Nat Immunol,* 18**,** 725-732.

DERECKI, N. C., CARDANI, A. N., YANG, C. H., QUINNIES, K. M., CRIHFIELD, A., LYNCH, K. R. & KIPNIS, J. 2010. Regulation of learning and memory by meningeal immunity: a key role for IL-4. *J Exp Med,* 207**,** 1067-80.

DERECKI, N. C., CRONK, J. C., LU, Z., XU, E., ABBOTT, S. B., GUYENET, P. G. & KIPNIS, J. 2012. Wild-type microglia arrest pathology in a mouse model of Rett syndrome. *Nature,* 484**,** 105-9.

DOBIN, A., DAVIS, C. A., SCHLESINGER, F., DRENKOW, J., ZALESKI, C., JHA, S., BATUT, P., CHAISSON, M. & GINGERAS, T. R. 2013. STAR: ultrafast universal RNA-seq aligner. *Bioinformatics,* 29**,** 15-21.

DRAGHICI, S., KHATRI, P., TARCA, A. L., AMIN, K., DONE, A., VOICHITA, C., GEORGESCU, C. & ROMERO, R. 2007. A systems biology approach for pathway level analysis. *Genome Res,* 17**,** 1537-45.

DUNN, H. G. 2001. Importance of Rett syndrome in child neurology. *Brain Dev,* 23 Suppl 1**,** S38-43.

DUNN, H. G. & MACLEOD, P. M. 2001. Rett syndrome: review of biological abnormalities. *Can J Neurol Sci,* 28**,** 16-29.

EBERT, D. H., GABEL, H. W., ROBINSON, N. D., KASTAN, N. R., HU, L. S., COHEN, S., NAVARRO, A. J., LYST, M. J., EKIERT, R., BIRD, A. P. & GREENBERG, M. E. 2013. Activity-dependent phosphorylation of MeCP2 threonine 308 regulates interaction with NCoR. *Nature,* 499**,** 341-5.

EDEN, E., NAVON, R., STEINFELD, I., LIPSON, D. & YAKHINI, Z. 2009. GOrilla: a tool for discovery and visualization of enriched GO terms in ranked gene lists. *BMC Bioinformatics,* 10**,** 48.

ELMORE, M. R., NAJAFI, A. R., KOIKE, M. A., DAGHER, N. N., SPANGENBERG, E. E., RICE, R. A., KITAZAWA, M., MATUSOW, B., NGUYEN, H., WEST, B. L. & GREEN, K. N. 2014. Colony-stimulating factor 1 receptor signaling is necessary for microglia viability, unmasking a microglia progenitor cell in the adult brain. *Neuron,* 82**,** 380-97.

ENGESZER, R. E., PATTERSON, L. B., RAO, A. A. & PARICHY, D. M. 2007. Zebrafish in the wild: a review of natural history and new notes from the field. *Zebrafish,* 4**,** 21-40.

FILIANO, A. J., GADANI, S. P. & KIPNIS, J. 2017. How and why do T cells and their derived cytokines affect the injured and healthy brain? *Nat Rev Neurosci,* 18**,** 375-384.

FILIANO, A. J., MARTENS, L. H., YOUNG, A. H., WARMUS, B. A., ZHOU, P., DIAZ-RAMIREZ, G., JIAO, J., ZHANG, Z., HUANG, E. J., GAO, F. B., FARESE, R. V., JR. & ROBERSON, E. D. 2013. Dissociation of frontotemporal dementia-related deficits and neuroinflammation in progranulin haploinsufficient mice. *J Neurosci,* 33**,** 5352-61.

FILIANO, A. J., XU, Y., TUSTISON, N. J., MARSH, R. L., BAKER, W., SMIRNOV, I., OVERALL, C. C., GADANI, S. P., TURNER, S. D., WENG, Z., PEERZADE, S. N., CHEN, H., LEE, K. S., SCOTT, M. M., BEENHAKKER, M. P., LITVAK, V. & KIPNIS, J. 2016. Unexpected role of interferon-gamma in regulating neuronal connectivity and social behaviour. *Nature,* 535**,** 425-9.

GAUTIER, E. L., SHAY, T., MILLER, J., GRETER, M., JAKUBZICK, C., IVANOV, S., HELFT, J., CHOW, A., ELPEK, K. G., GORDONOV, S., MAZLOOM, A. R., MA'AYAN, A., CHUA, W. J., HANSEN, T. H., TURLEY, S. J., MERAD, M., RANDOLPH, G. J. & IMMUNOLOGICAL GENOME, C. 2012. Gene-expression profiles and transcriptional regulatory pathways that underlie the identity and diversity of mouse tissue macrophages. *Nat Immunol,* 13**,** 1118-28.

GINHOUX, F., GRETER, M., LEBOEUF, M., NANDI, S., SEE, P., GOKHAN, S., MEHLER, M. F., CONWAY, S. J., NG, L. G., STANLEY, E. R., SAMOKHVALOV, I. M. & MERAD, M. 2010. Fate mapping analysis reveals that adult microglia derive from primitive macrophages. *Science,* 330**,** 841-5.

GOEMAN, J. J., VAN DE GEER, S. A., DE KORT, F. & VAN HOUWELINGEN, H. C. 2003. A global test for groups of genes: testing association with a clinical outcome. *Bioinformatics,* 20**,** 93-99.

GOLDMANN, T., WIEGHOFER, P., MULLER, P. F., WOLF, Y., VAROL, D., YONA, S., BRENDECKE, S. M., KIERDORF, K., STASZEWSKI, O., DATTA, M., LUEDDE, T., HEIKENWALDER, M., JUNG, S. & PRINZ, M. 2013. A new type of microglia gene targeting shows TAK1 to be pivotal in CNS autoimmune inflammation. *Nat Neurosci,* 16**,** 1618-26.

GOMEZ PERDIGUERO, E., KLAPPROTH, K., SCHULZ, C., BUSCH, K., AZZONI, E., CROZET, L., GARNER, H., TROUILLET, C., DE BRUIJN, M. F., GEISSMANN, F. & RODEWALD, H. R. 2015. Tissue-resident macrophages originate from yolk-sac-derived erythro-myeloid progenitors. *Nature,* 518**,** 547-51.

GOSSELIN, D., LINK, V. M., ROMANOSKI, C. E., FONSECA, G. J., EICHENFIELD, D. Z., SPANN, N. J., STENDER, J. D., CHUN, H. B., GARNER, H., GEISSMANN, F. & GLASS, C. K. 2014. Environment drives selection and function of enhancers controlling tissue-specific macrophage identities. *Cell,* 159**,** 1327-40.

GOW, D. J., SESTER, D. P. & HUME, D. A. 2010. CSF-1, IGF-1, and the control of postnatal growth and development. *J Leukoc Biol,* 88**,** 475-81.

GUPTA, S., AGGARWAL, S., RASHANRAVAN, B. & LEE, T. 1998. Th1- and Th2-like cytokines in CD4+ and CD8+ T cells in autism. *J Neuroimmunol,* 85**,** 106-9.

GUY, J., CHEVAL, H., SELFRIDGE, J. & BIRD, A. 2011. The role of MeCP2 in the brain. *Annu Rev Cell Dev Biol,* 27**,** 631-52.

GUY, J., HENDRICH, B., HOLMES, M., MARTIN, J. E. & BIRD, A. 2001. A mouse Mecp2-null mutation causes neurological symptoms that mimic Rett syndrome. *Nat Genet,* 27**,** 322-6.

HART, B. L. 1988. Biological basis of the behavior of sick animals. *Neurosci Biobehav Rev,* 12**,** 123-37.

HERZ, J., FILIANO, A. J., SMITH, A., YOGEV, N. & KIPNIS, J. 2017. Myeloid Cells in the Central Nervous System. *Immunity,* 46**,** 943-956.

HICKMAN, S. E., KINGERY, N. D., OHSUMI, T. K., BOROWSKY, M. L., WANG, L. C., MEANS, T. K. & EL KHOURY, J. 2013. The microglial sensome revealed by direct RNA sequencing. *Nat Neurosci,* 16**,** 1896-905.

HO SUI, S. J., FULTON, D. L., ARENILLAS, D. J., KWON, A. T. & WASSERMAN, W. W. 2007. oPOSSUM: integrated tools for analysis of regulatory motif over-representation. *Nucleic Acids Res,* 35**,** W245-52.

HO SUI, S. J., MORTIMER, J. R., ARENILLAS, D. J., BRUMM, J., WALSH, C. J., KENNEDY, B. P. & WASSERMAN, W. W. 2005. oPOSSUM: identification of over-represented transcription factor binding sites in co-expressed genes. *Nucleic Acids Res,* 33**,** 3154-64.

HOFFMANN, A. A. 1987. A laboratory study of male territoriality in the sibling species Drosophila melanogaster and D. simulans. *Animal Behaviour,* 35**,** 807-818.

HOLTMAN, I. R., RAJ, D. D., MILLER, J. A., SCHAAFSMA, W., YIN, Z., BROUWER, N., WES, P. D., MOLLER, T., ORRE, M., KAMPHUIS, W., HOL, E. M., BODDEKE, E. W. & EGGEN, B. J. 2015. Induction of a common microglia gene expression signature by aging and neurodegenerative conditions: a co-expression meta-analysis. *Acta Neuropathol Commun,* 3**,** 31.

HONG, S. & STEVENS, B. 2016. Microglia: Phagocytosing to Clear, Sculpt, and Eliminate. *Dev Cell,* 38**,** 126-8.

HOSHIKO, M., ARNOUX, I., AVIGNONE, E., YAMAMOTO, N. & AUDINAT, E. 2012. Deficiency of the microglial receptor CX3CR1 impairs postnatal functional development of thalamocortical synapses in the barrel cortex. *J Neurosci,* 32**,** 15106-11.

HUANG DA, W., SHERMAN, B. T. & LEMPICKI, R. A. 2009. Systematic and integrative analysis of large gene lists using DAVID bioinformatics resources. *Nat Protoc,* 4**,** 44-57.

HUANG, Y. A., ZHOU, B., WERNIG, M. & SUDHOF, T. C. 2017. ApoE2, ApoE3, and ApoE4 Differentially Stimulate APP Transcription and Abeta Secretion. *Cell,* 168**,** 427-441 e21.

IDEKER, T., GALITSKI, T. & HOOD, L. 2001. A new approach to decoding life: systems biology. *Annu Rev Genomics Hum Genet,* 2**,** 343-72.

JIANG, S., LI, C., MCRAE, G., LYKKEN, E., SEVILLA, J., LIU, S. Q., WAN, Y. & LI, Q. J. 2014. MeCP2 reinforces STAT3 signaling and the generation of effector

CD4+ T cells by promoting miR-124-mediated suppression of SOCS5. *Sci Signal,* 7**,** ra25.

JOHNSON, G. A., BADEA, A., BRANDENBURG, J., COFER, G., FUBARA, B., LIU, S. & NISSANOV, J. 2010. Waxholm space: an image-based reference for coordinating mouse brain research. *Neuroimage,* 53**,** 365-72.

JUNG, S., ALIBERTI, J., GRAEMMEL, P., SUNSHINE, M. J., KREUTZBERG, G. W., SHER, A. & LITTMAN, D. R. 2000. Analysis of fractalkine receptor CX(3)CR1 function by targeted deletion and green fluorescent protein reporter gene insertion. *Mol Cell Biol,* 20**,** 4106-14.

KAMYSHEV, N. G., SMIRNOVA, G. P., KAMYSHEVA, E. A., NIKIFOROV, O. N., PARAFENYUK, I. V. & PONOMARENKO, V. V. 2002. Plasticity of social behavior in Drosophila. *Neurosci Behav Physiol,* 32**,** 401-8.

KELLEY, K. W., BLUTHE, R. M., DANTZER, R., ZHOU, J. H., SHEN, W. H., JOHNSON, R. W. & BROUSSARD, S. R. 2003. Cytokine-induced sickness behavior. *Brain Behav Immun,* 17 Suppl 1**,** S112-8.

KENNEDY, D. P. & ADOLPHS, R. 2012. The social brain in psychiatric and neurological disorders. *Trends Cogn Sci,* 16**,** 559-72.

KEREN-SHAUL, H., SPINRAD, A., WEINER, A., MATCOVITCH-NATAN, O., DVIR-SZTERNFELD, R., ULLAND, T. K., DAVID, E., BARUCH, K., LARA-ASTAISO, D., TOTH, B., ITZKOVITZ, S., COLONNA, M., SCHWARTZ, M. & AMIT, I. 2017. A Unique Microglia Type Associated with Restricting Development of Alzheimer's Disease. *Cell,* 169**,** 1276-1290.e17.

KHATRI, P. & DRAGHICI, S. 2005. Ontological analysis of gene expression data: current tools, limitations, and open problems. *Bioinformatics,* 21**,** 3587-95.

KHATRI, P., DRAGHICI, S., OSTERMEIER, G. C. & KRAWETZ, S. A. 2002. Profiling gene expression using onto-express. *Genomics,* 79**,** 266-70.

KHWAJA, O. S., HO, E., BARNES, K. V., O'LEARY, H. M., PEREIRA, L. M., FINKELSTEIN, Y., NELSON, C. A., 3RD, VOGEL-FARLEY, V., DEGREGORIO, G., HOLM, I. A., KHATWA, U., KAPUR, K., ALEXANDER, M. E., FINNEGAN, D. M., CANTWELL, N. G., WALCO, A. C., RAPPAPORT, L., GREGAS, M., FICHOROVA, R. N., SHANNON, M. W., SUR, M. & KAUFMANN, W. E. 2014. Safety, pharmacokinetics, and preliminary assessment of efficacy of mecasermin (recombinant human IGF-1) for the treatment of Rett syndrome. *Proc Natl Acad Sci U S A,* 111**,** 4596-601.

KIERDORF, K., ERNY, D., GOLDMANN, T., SANDER, V., SCHULZ, C., PERDIGUERO, E. G., WIEGHOFER, P., HEINRICH, A., RIEMKE, P., HOLSCHER, C., MULLER, D. N., LUCKOW, B., BROCKER, T., DEBOWSKI, K., FRITZ, G., OPDENAKKER, G., DIEFENBACH, A., BIBER, K., HEIKENWALDER, M., GEISSMANN, F., ROSENBAUER, F. & PRINZ, M. 2013. Microglia emerge from erythromyeloid precursors via Pu.1- and Irf8-dependent pathways. *Nat Neurosci,* 16**,** 273-80.

KIM, J., ELTORAI, A. E., JIANG, H., LIAO, F., VERGHESE, P. B., KIM, J., STEWART, F. R., BASAK, J. M. & HOLTZMAN, D. M. 2012. Anti-apoE immunotherapy inhibits amyloid accumulation in a transgenic mouse model of Abeta amyloidosis. *J Exp Med,* 209**,** 2149-56.

KIPNIS, J. 2016. Multifaceted interactions between adaptive immunity and the central nervous system. *Science,* 353**,** 766-71.

KIPNIS, J., COHEN, H., CARDON, M., ZIV, Y. & SCHWARTZ, M. 2004. T cell deficiency leads to cognitive dysfunction: implications for therapeutic vaccination for schizophrenia and other psychiatric conditions. *Proc Natl Acad Sci U S A,* 101**,** 8180-5.

KITANO, H. 2002. Systems biology: a brief overview. *Science,* 295**,** 1662-4.

KOOPMAN, G., REUTELINGSPERGER, C. P., KUIJTEN, G. A., KEEHNEN, R. M., PALS, S. T. & VAN OERS, M. H. 1994. Annexin V for flow cytometric detection of phosphatidylserine expression on B cells undergoing apoptosis. *Blood,* 84**,** 1415-20.

KOSTIC, V., JACKSON-LEWIS, V., DE BILBAO, F., DUBOIS-DAUPHIN, M. & PRZEDBORSKI, S. 1997. Bcl-2: prolonging life in a transgenic mouse model of familial amyotrophic lateral sclerosis. *Science,* 277**,** 559-62.

KRAUSE, J., BUTLIN, R. K., PEUHKURI, N. & PRITCHARD, V. L. 2000. The social organization of fish shoals: a test of the predictive power of laboratory experiments for the field. *Biol Rev Camb Philos Soc,* 75**,** 477-501.

KREUTZBERG, G. W. 1996. Microglia: a sensor for pathological events in the CNS. *Trends Neurosci,* 19**,** 312-8.

KRZYWINSKI, M., SCHEIN, J., BIROL, I., CONNORS, J., GASCOYNE, R., HORSMAN, D., JONES, S. J. & MARRA, M. A. 2009. Circos: an information aesthetic for comparative genomics. *Genome Res,* 19**,** 1639-45.

KUNIS, G., BARUCH, K., ROSENZWEIG, N., KERTSER, A., MILLER, O., BERKUTZKI, T. & SCHWARTZ, M. 2013. IFN-gamma-dependent activation of

the brain's choroid plexus for CNS immune surveillance and repair. *Brain,* 136**,** 3427-40.

KWON, A. T., ARENILLAS, D. J., WORSLEY HUNT, R. & WASSERMAN, W. W. 2012. oPOSSUM-3: advanced analysis of regulatory motif over-representation across genes or ChIP-Seq datasets. *G3 (Bethesda),* 2**,** 987-1002.

LARNER, A. J. 1995. The cortical neuritic dystrophy of Alzheimer's disease: nature, significance, and possible pathogenesis. *Dementia,* 6**,** 218-24.

LEVINE, J. D., FUNES, P., DOWSE, H. B. & HALL, J. C. 2002. Resetting the circadian clock by social experience in Drosophila melanogaster. *Science,* 298**,** 2010-2.

LI, C., JIANG, S., LIU, S. Q., LYKKEN, E., ZHAO, L. T., SEVILLA, J., ZHU, B. & LI, Q. J. 2014a. MeCP2 enforces Foxp3 expression to promote regulatory T cells' resilience to inflammation. *Proc Natl Acad Sci U S A,* 111**,** E2807-16.

LI, X., CHAUHAN, A., SHEIKH, A. M., PATIL, S., CHAUHAN, V., LI, X. M., JI, L., BROWN, T. & MALIK, M. 2009. Elevated immune response in the brain of autistic patients. *J Neuroimmunol,* 207**,** 111-6.

LI, Z., HALL, A. M., KELINSKE, M. & ROBERSON, E. D. 2014b. Seizure resistance without parkinsonism in aged mice after tau reduction. *Neurobiol Aging,* 35**,** 2617-2624.

LIAO, F., HORI, Y., HUDRY, E., BAUER, A. Q., JIANG, H., MAHAN, T. E., LEFTON, K. B., ZHANG, T. J., DEARBORN, J. T., KIM, J., CULVER, J. P., BETENSKY, R., WOZNIAK, D. F., HYMAN, B. T. & HOLTZMAN, D. M. 2014a. Anti-ApoE antibody given after plaque onset decreases Abeta accumulation and improves brain function in a mouse model of Abeta amyloidosis. *J Neurosci,* 34**,** 7281-92.

LIAO, Y., SMYTH, G. K. & SHI, W. 2014b. featureCounts: an efficient general purpose program for assigning sequence reads to genomic features. *Bioinformatics,* 30**,** 923-30.

LIENERT, F., LOHMUELLER, J. J., GARG, A. & SILVER, P. A. 2014. Synthetic biology in mammalian cells: next generation research tools and therapeutics. *Nat Rev Mol Cell Biol,* 15**,** 95-107.

LIN, C. C., BRADSTREET, T. R., SCHWARZKOPF, E. A., SIM, J., CARRERO, J. A., CHOU, C., COOK, L. E., EGAWA, T., TANEJA, R., MURPHY, T. L., RUSSELL, J. H. & EDELSON, B. T. 2014. Bhlhe40 controls cytokine production

by T cells and is essential for pathogenicity in autoimmune neuroinflammation. *Nat Commun,* 5**,** 3551.

LIOY, D. T., GARG, S. K., MONAGHAN, C. E., RABER, J., FOUST, K. D., KASPAR, B. K., HIRRLINGER, P. G., KIRCHHOFF, F., BISSONNETTE, J. M., BALLAS, N. & MANDEL, G. 2011. A role for glia in the progression of Rett's syndrome. *Nature,* 475**,** 497-500.

LITVAK, V., RAMSEY, S. A., RUST, A. G., ZAK, D. E., KENNEDY, K. A., LAMPANO, A. E., NYKTER, M., SHMULEVICH, I. & ADEREM, A. 2009. Function of C/EBPdelta in a regulatory circuit that discriminates between transient and persistent TLR4-induced signals. *Nat Immunol,* 10**,** 437-43.

LITVAK, V., RATUSHNY, A. V., LAMPANO, A. E., SCHMITZ, F., HUANG, A. C., RAMAN, A., RUST, A. G., BERGTHALER, A., AITCHISON, J. D. & ADEREM, A. 2012. A FOXO3-IRF7 gene regulatory circuit limits inflammatory sequelae of antiviral responses. *Nature,* 490**,** 421-5.

LOPEZ-MUNOZ, A., ROCA, F. J., MESEGUER, J. & MULERO, V. 2009. New insights into the evolution of IFNs: zebrafish group II IFNs induce a rapid and transient expression of IFN-dependent genes and display powerful antiviral activities. *J Immunol,* 182**,** 3440-9.

LOVE, M. I., HUBER, W. & ANDERS, S. 2014. Moderated estimation of fold change and dispersion for RNA-seq data with DESeq2. *Genome Biol,* 15**,** 550.

LYST, M. J., EKIERT, R., EBERT, D. H., MERUSI, C., NOWAK, J., SELFRIDGE, J., GUY, J., KASTAN, N. R., ROBINSON, N. D., DE LIMA ALVES, F., RAPPSILBER, J., GREENBERG, M. E. & BIRD, A. 2013. Rett syndrome mutations abolish the interaction of MeCP2 with the NCoR/SMRT co-repressor. *Nat Neurosci,* 16**,** 898-902.

MAERE, S., HEYMANS, K. & KUIPER, M. 2005. BiNGO: a Cytoscape plugin to assess overrepresentation of gene ontology categories in biological networks. *Bioinformatics,* 21**,** 3448-9.

MAEZAWA, I. & JIN, L. W. 2010. Rett syndrome microglia damage dendrites and synapses by the elevated release of glutamate. *J Neurosci,* 30**,** 5346-56.

MAN, M. Z., WANG, X. & WANG, Y. 2000. POWER_SAGE: comparing statistical tests for SAGE experiments. *Bioinformatics,* 16**,** 953-9.

MASI, A., QUINTANA, D. S., GLOZIER, N., LLOYD, A. R., HICKIE, I. B. & GUASTELLA, A. J. 2015. Cytokine aberrations in autism spectrum disorder: a systematic review and meta-analysis. *Mol Psychiatry,* 20**,** 440-6.

MASLIAH, E., MALLORY, M., ALFORD, M., TANAKA, S. & HANSEN, L. A. 1998. Caspase dependent DNA fragmentation might be associated with excitotoxicity in Alzheimer disease. *J Neuropathol Exp Neurol,* 57**,** 1041-52.

MATCOVITCH-NATAN, O., WINTER, D. R., GILADI, A., VARGAS AGUILAR, S., SPINRAD, A., SARRAZIN, S., BEN-YEHUDA, H., DAVID, E., ZELADA GONZALEZ, F., PERRIN, P., KEREN-SHAUL, H., GURY, M., LARA-ASTAISO, D., THAISS, C. A., COHEN, M., BAHAR HALPERN, K., BARUCH, K., DECZKOWSKA, A., LORENZO-VIVAS, E., ITZKOVITZ, S., ELINAV, E., SIEWEKE, M. H., SCHWARTZ, M. & AMIT, I. 2016. Microglia development follows a stepwise program to regulate brain homeostasis. *Science,* 353**,** aad8670.

MATTSON, M. P., KELLER, J. N. & BEGLEY, J. G. 1998. Evidence for synaptic apoptosis. *Exp Neurol,* 153**,** 35-48.

MERY, F., VARELA, S. A., DANCHIN, E., BLANCHET, S., PAREJO, D., COOLEN, I. & WAGNER, R. H. 2009. Public versus personal information for mate copying in an invertebrate. *Curr Biol,* 19**,** 730-4.

MILLER, N. & GERLAI, R. 2007. Quantification of shoaling behaviour in zebrafish (Danio rerio). *Behav Brain Res,* 184**,** 157-66.

MOOTHA, V. K., LINDGREN, C. M., ERIKSSON, K. F., SUBRAMANIAN, A., SIHAG, S., LEHAR, J., PUIGSERVER, P., CARLSSON, E., RIDDERSTRALE, M., LAURILA, E., HOUSTIS, N., DALY, M. J., PATTERSON, N., MESIROV, J. P., GOLUB, T. R., TAMAYO, P., SPIEGELMAN, B., LANDER, E. S., HIRSCHHORN, J. N., ALTSHULER, D. & GROOP, L. C. 2003. PGC-1alpha-responsive genes involved in oxidative phosphorylation are coordinately downregulated in human diabetes. *Nat Genet,* 34**,** 267-73.

MORETZ, J. A., MARTINS, E. P. & ROBISON, B. D. 2007. Behavioral syndromes and the evolution of correlated behavior in zebrafish. *Behavioral ecology,* 18**,** 556-562.

MOY, S. S., NADLER, J. J., PEREZ, A., BARBARO, R. P., JOHNS, J. M., MAGNUSON, T. R., PIVEN, J. & CRAWLEY, J. N. 2004. Sociability and preference for social novelty in five inbred strains: an approach to assess autistic-like behavior in mice. *Genes Brain Behav,* 3**,** 287-302.

NELSON, S. B. & VALAKH, V. 2015. Excitatory/Inhibitory Balance and Circuit Homeostasis in Autism Spectrum Disorders. *Neuron,* 87**,** 684-98.

NGUYEN, M. V., FELICE, C. A., DU, F., COVEY, M. V., ROBINSON, J. K., MANDEL, G. & BALLAS, N. 2013. Oligodendrocyte lineage cells contribute unique features to Rett syndrome neuropathology. *J Neurosci,* 33**,** 18764-74.

NIMMERJAHN, A., KIRCHHOFF, F. & HELMCHEN, F. 2005. Resting microglial cells are highly dynamic surveillants of brain parenchyma in vivo. *Science,* 308**,** 1314-8.

NING, S., PAGANO, J. S. & BARBER, G. N. 2011. IRF7: activation, regulation, modification and function. *Genes Immun,* 12**,** 399-414.

NUBER, U. A., KRIAUCIONIS, S., ROLOFF, T. C., GUY, J., SELFRIDGE, J., STEINHOFF, C., SCHULZ, R., LIPKOWITZ, B., ROPERS, H. H., HOLMES, M. C. & BIRD, A. 2005. Up-regulation of glucocorticoid-regulated genes in a mouse model of Rett syndrome. *Hum Mol Genet,* 14**,** 2247-56.

NUSSER, Z. & MODY, I. 2002. Selective modulation of tonic and phasic inhibitions in dentate gyrus granule cells. *J Neurophysiol,* 87**,** 2624-8.

OFENGEIM, D., ITO, Y., NAJAFOV, A., ZHANG, Y., SHAN, B., DEWITT, J. P., YE, J., ZHANG, X., CHANG, A., VAKIFAHMETOGLU-NORBERG, H., GENG, J., PY, B., ZHOU, W., AMIN, P., BERLINK LIMA, J., QI, C., YU, Q., TRAPP, B. & YUAN, J. 2015. Activation of necroptosis in multiple sclerosis. *Cell Rep,* 10**,** 1836-49.

OLAH, S., FULE, M., KOMLOSI, G., VARGA, C., BALDI, R., BARZO, P. & TAMAS, G. 2009. Regulation of cortical microcircuits by unitary GABA-mediated volume transmission. *Nature,* 461**,** 1278-81.

ORRE, M., KAMPHUIS, W., OSBORN, L. M., JANSEN, A. H. P., KOOIJMAN, L., BOSSERS, K. & HOL, E. M. 2014. Isolation of glia from Alzheimer's mice reveals inflammation and dysfunction. *Neurobiol Aging,* 35**,** 2746-2760.

OSHLACK, A., ROBINSON, M. D. & YOUNG, M. D. 2010. From RNA-seq reads to differential expression results. *Genome Biol,* 11**,** 220.

PALOP, J. J., MUCKE, L. & ROBERSON, E. D. 2011. Quantifying biomarkers of cognitive dysfunction and neuronal network hyperexcitability in mouse models of Alzheimer's disease: depletion of calcium-dependent proteins and inhibitory hippocampal remodeling. *Methods Mol Biol,* 670**,** 245-62.

PAOLICELLI, R. C., BOLASCO, G., PAGANI, F., MAGGI, L., SCIANNI, M., PANZANELLI, P., GIUSTETTO, M., FERREIRA, T. A., GUIDUCCI, E., DUMAS, L., RAGOZZINO, D. & GROSS, C. T. 2011. Synaptic pruning by microglia is necessary for normal brain development. *Science,* 333**,** 1456-8.

PARKHURST, C. N., YANG, G., NINAN, I., SAVAS, J. N., YATES, J. R., 3RD, LAFAILLE, J. J., HEMPSTEAD, B. L., LITTMAN, D. R. & GAN, W. B. 2013. Microglia promote learning-dependent synapse formation through brain-derived neurotrophic factor. *Cell,* 155**,** 1596-609.

PAVLIDIS, P., QIN, J., ARANGO, V., MANN, J. J. & SIBILLE, E. 2004. Using the gene ontology for microarray data mining: a comparison of methods and application to age effects in human prefrontal cortex. *Neurochem Res,* 29**,** 1213-22.

PERRY, V. H. & HOLMES, C. 2014. Microglial priming in neurodegenerative disease. *Nat Rev Neurol,* 10**,** 217-24.

POWER, J. D., BARNES, K. A., SNYDER, A. Z., SCHLAGGAR, B. L. & PETERSEN, S. E. 2012. Spurious but systematic correlations in functional connectivity MRI networks arise from subject motion. *Neuroimage,* 59**,** 2142-54.

PRIETO, J. J., PETERSON, B. A. & WINER, J. A. 1994. Morphology and spatial distribution of GABAergic neurons in cat primary auditory cortex (AI). *J Comp Neurol,* 344**,** 349-82.

PRINZ, M., PRILLER, J., SISODIA, S. S. & RANSOHOFF, R. M. 2011. Heterogeneity of CNS myeloid cells and their roles in neurodegeneration. *Nat Neurosci,* 14**,** 1227-35.

QUINN, Z. A., YANG, C. C., WRANA, J. L. & MCDERMOTT, J. C. 2001. Smad proteins function as co-modulators for MEF2 transcriptional regulatory proteins. *Nucleic Acids Res,* 29**,** 732-42.

QUINNIES, K. M., COX, K. H. & RISSMAN, E. F. 2015. Immune deficiency influences juvenile social behavior and maternal behavior. *Behav Neurosci,* 129**,** 331-8.

RADDE, R., BOLMONT, T., KAESER, S. A., COOMARASWAMY, J., LINDAU, D., STOLTZE, L., CALHOUN, M. E., JAGGI, F., WOLBURG, H., GENGLER, S., HAASS, C., GHETTI, B., CZECH, C., HOLSCHER, C., MATHEWS, P. M. & JUCKER, M. 2006. Abeta42-driven cerebral amyloidosis in transgenic mice reveals early and robust pathology. *EMBO Rep,* 7**,** 940-6.

RADJAVI, A., SMIRNOV, I. & KIPNIS, J. 2014. Brain antigen-reactive CD4+ T cells are sufficient to support learning behavior in mice with limited T cell repertoire. *Brain Behav Immun,* 35**,** 58-63.

RAMSEY, S. A., KLEMM, S. L., ZAK, D. E., KENNEDY, K. A., THORSSON, V., LI, B., GILCHRIST, M., GOLD, E. S., JOHNSON, C. D., LITVAK, V., NAVARRO,

G., ROACH, J. C., ROSENBERGER, C. M., RUST, A. G., YUDKOVSKY, N., ADEREM, A. & SHMULEVICH, I. 2008. Uncovering a macrophage transcriptional program by integrating evidence from motif scanning and expression dynamics. *PLoS Comput Biol,* 4**,** e1000021.

RATTAZZI, L., PIRAS, G., ONO, M., DEACON, R., PARIANTE, C. M. & D'ACQUISTO, F. 2013. CD4(+) but not CD8(+) T cells revert the impaired emotional behavior of immunocompromised RAG-1-deficient mice. *Transl Psychiatry,* 3**,** e280.

REIBER, C., SHATTUCK, E. C., FIORE, S., ALPERIN, P., DAVIS, V. & MOORE, J. 2010. Change in human social behavior in response to a common vaccine. *Ann Epidemiol,* 20**,** 729-33.

REIMAND, J., ARAK, T., ADLER, P., KOLBERG, L., REISBERG, S., PETERSON, H. & VILO, J. 2016. g:Profiler-a web server for functional interpretation of gene lists (2016 update). *Nucleic Acids Res,* 44**,** W83-9.

RICKLIN, D., HAJISHENGALLIS, G., YANG, K. & LAMBRIS, J. D. 2010. Complement: a key system for immune surveillance and homeostasis. *Nat Immunol,* 11**,** 785-97.

ROUMIER, A., BECHADE, C., PONCER, J. C., SMALLA, K. H., TOMASELLO, E., VIVIER, E., GUNDELFINGER, E. D., TRILLER, A. & BESSIS, A. 2004. Impaired synaptic function in the microglial KARAP/DAP12-deficient mouse. *J Neurosci,* 24**,** 11421-8.

RUAN, H. & WU, C. F. 2008. Social interaction-mediated lifespan extension of Drosophila Cu/Zn superoxide dismutase mutants. *Proc Natl Acad Sci U S A,* 105**,** 7506-10.

SARESELLA, M., MARVENTANO, I., GUERINI, F. R., MANCUSO, R., CERESA, L., ZANZOTTERA, M., RUSCONI, B., MAGGIONI, E., TINELLI, C. & CLERICI, M. 2009. An autistic endophenotype results in complex immune dysfunction in healthy siblings of autistic children. *Biol Psychiatry,* 66**,** 978-84.

SARIN, S. & DUKAS, R. 2009. Social learning about egg-laying substrates in fruitflies. *Proc Biol Sci,* 276**,** 4323-8.

SAVERINO, C. & GERLAI, R. 2008. The social zebrafish: behavioral responses to conspecific, heterospecific, and computer animated fish. *Behav Brain Res,* 191**,** 77-87.

SCHAFER, D. P., HELLER, C. T., GUNNER, G., HELLER, M., GORDON, C., HAMMOND, T., WOLF, Y., JUNG, S. & STEVENS, B. 2016. Microglia contribute

to circuit defects in Mecp2 null mice independent of microglia-specific loss of Mecp2 expression. *Elife,* 5.

SCHAFER, D. P., LEHRMAN, E. K., KAUTZMAN, A. G., KOYAMA, R., MARDINLY, A. R., YAMASAKI, R., RANSOHOFF, R. M., GREENBERG, M. E., BARRES, B. A. & STEVENS, B. 2012. Microglia sculpt postnatal neural circuits in an activity and complement-dependent manner. *Neuron,* 74**,** 691-705.

SCHOGGINS, J. W., MACDUFF, D. A., IMANAKA, N., GAINEY, M. D., SHRESTHA, B., EITSON, J. L., MAR, K. B., RICHARDSON, R. B., RATUSHNY, A. V., LITVAK, V., DABELIC, R., MANICASSAMY, B., AITCHISON, J. D., ADEREM, A., ELLIOTT, R. M., GARCIA-SASTRE, A., RACANIELLO, V., SNIJDER, E. J., YOKOYAMA, W. M., DIAMOND, M. S., VIRGIN, H. W. & RICE, C. M. 2014. Pan-viral specificity of IFN-induced genes reveals new roles for cGAS in innate immunity. *Nature,* 505**,** 691-5.

SCHULZ, C., GOMEZ PERDIGUERO, E., CHORRO, L., SZABO-ROGERS, H., CAGNARD, N., KIERDORF, K., PRINZ, M., WU, B., JACOBSEN, S. E., POLLARD, J. W., FRAMPTON, J., LIU, K. J. & GEISSMANN, F. 2012. A lineage of myeloid cells independent of Myb and hematopoietic stem cells. *Science,* 336**,** 86-90.

SCHWARTZ, M. & KIPNIS, J. 2011. A conceptual revolution in the relationships between the brain and immunity. *Brain Behav Immun,* 25**,** 817-9.

SHAHBAZIAN, M. D., ANTALFFY, B., ARMSTRONG, D. L. & ZOGHBI, H. Y. 2002. Insight into Rett syndrome: MeCP2 levels display tissue- and cell-specific differences and correlate with neuronal maturation. *Hum Mol Genet,* 11**,** 115-24.

SHAKHAR, K. & SHAKHAR, G. 2015. Why Do We Feel Sick When Infected--Can Altruism Play a Role? *PLoS Biol,* 13**,** e1002276.

SHECHTER, R., LONDON, A. & SCHWARTZ, M. 2013. Orchestrated leukocyte recruitment to immune-privileged sites: absolute barriers versus educational gates. *Nat Rev Immunol,* 13**,** 206-18.

SHEN, H. H. 2015. Core Concept: Resting-state connectivity. *Proc Natl Acad Sci U S A,* 112**,** 14115-6.

SICA, A. & MANTOVANI, A. 2012. Macrophage plasticity and polarization: in vivo veritas. *J Clin Invest,* 122**,** 787-95.

SILVERMAN, J. L., YANG, M., LORD, C. & CRAWLEY, J. N. 2010. Behavioural phenotyping assays for mouse models of autism. *Nat Rev Neurosci,* 11**,** 490-502.

SINGH, H., KHAN, A. A. & DINNER, A. R. 2014. Gene regulatory networks in the immune system. *Trends Immunol,* 35**,** 211-8.

SOHAL, D. S., NGHIEM, M., CRACKOWER, M. A., WITT, S. A., KIMBALL, T. R., TYMITZ, K. M., PENNINGER, J. M. & MOLKENTIN, J. D. 2001. Temporally regulated and tissue-specific gene manipulations in the adult and embryonic heart using a tamoxifen-inducible Cre protein. *Circ Res,* 89**,** 20-5.

SOKOLOWSKI, M. B. 2010. Social interactions in "simple" model systems. *Neuron,* 65**,** 780-94.

STELLWAGEN, D. & MALENKA, R. C. 2006. Synaptic scaling mediated by glial TNF-alpha. *Nature,* 440**,** 1054-9.

STERNBERGER, N. H., STERNBERGER, L. A. & ULRICH, J. 1985. Aberrant neurofilament phosphorylation in Alzheimer disease. *Proc Natl Acad Sci U S A,* 82**,** 4274-6.

SUBRAMANIAN, A., TAMAYO, P., MOOTHA, V. K., MUKHERJEE, S., EBERT, B. L., GILLETTE, M. A., PAULOVICH, A., POMEROY, S. L., GOLUB, T. R., LANDER, E. S. & MESIROV, J. P. 2005. Gene set enrichment analysis: a knowledge-based approach for interpreting genome-wide expression profiles. *Proc Natl Acad Sci U S A,* 102**,** 15545-50.

SUN, H., LU, B., LI, R. Q., FLAVELL, R. A. & TANEJA, R. 2001. Defective T cell activation and autoimmune disorder in Stra13-deficient mice. *Nat Immunol,* 2**,** 1040-7.

SUNDERKOTTER, C., NIKOLIC, T., DILLON, M. J., VAN ROOIJEN, N., STEHLING, M., DREVETS, D. A. & LEENEN, P. J. 2004. Subpopulations of mouse blood monocytes differ in maturation stage and inflammatory response. *J Immunol,* 172**,** 4410-7.

SUPEKAR, K., UDDIN, L. Q., KHOUZAM, A., PHILLIPS, J., GAILLARD, W. D., KENWORTHY, L. E., YERYS, B. E., VAIDYA, C. J. & MENON, V. 2013. Brain hyperconnectivity in children with autism and its links to social deficits. *Cell Rep,* 5**,** 738-47.

TIAN, L., GREENBERG, S. A., KONG, S. W., ALTSCHULER, J., KOHANE, I. S. & PARK, P. J. 2005. Discovering statistically significant pathways in expression profiling studies. *Proc Natl Acad Sci U S A,* 102**,** 13544-9.

TING, J. T., DAIGLE, T. L., CHEN, Q. & FENG, G. 2014. Acute brain slice methods for adult and aging animals: application of targeted patch clamp analysis and optogenetics. *Methods Mol Biol,* 1183**,** 221-42.

TROPEA, D., GIACOMETTI, E., WILSON, N. R., BEARD, C., MCCURRY, C., FU, D. D., FLANNERY, R., JAENISCH, R. & SUR, M. 2009. Partial reversal of Rett Syndrome-like symptoms in MeCP2 mutant mice. *Proc Natl Acad Sci U S A,* 106**,** 2029-34.

URDINGUIO, R. G., LOPEZ-SERRA, L., LOPEZ-NIEVA, P., ALAMINOS, M., DIAZ-URIARTE, R., FERNANDEZ, A. F. & ESTELLER, M. 2008. Mecp2-null mice provide new neuronal targets for Rett syndrome. *PLoS One,* 3**,** e3669.

VAROL, C., VALLON-EBERHARD, A., ELINAV, E., AYCHEK, T., SHAPIRA, Y., LUCHE, H., FEHLING, H. J., HARDT, W. D., SHAKHAR, G. & JUNG, S. 2009. Intestinal lamina propria dendritic cell subsets have different origin and functions. *Immunity,* 31**,** 502-12.

VERHEIJDEN, S., BOTTELBERGS, A., KRYSKO, O., KRYSKO, D. V., BECKERS, L., DE MUNTER, S., VAN VELDHOVEN, P. P., WYNS, S., KULIK, W., NAVE, K. A., RAMER, M. S., CARMELIET, P., KASSMANN, C. M. & BAES, M. 2013. Peroxisomal multifunctional protein-2 deficiency causes neuroinflammation and degeneration of Purkinje cells independent of very long chain fatty acid accumulation. *Neurobiol Dis,* 58**,** 258-69.

VILLOSLADA, P., MORENO, B., MELERO, I., PABLOS, J. L., MARTINO, G., UCCELLI, A., MONTALBAN, X., AVILA, J., RIVEST, S., ACARIN, L., APPEL, S., KHOURY, S. J., MCGEER, P., FERRER, I., DELGADO, M., OBESO, J. & SCHWARTZ, M. 2008. Immunotherapy for neurological diseases. *Clin Immunol,* 128**,** 294-305.

WAGNER, T., BARTELT, A., SCHLEIN, C. & HEEREN, J. 2015. Genetic Dissection of Tissue-Specific Apolipoprotein E Function for Hypercholesterolemia and Diet-Induced Obesity. *PLoS One,* 10**,** e0145102.

WAISMAN, A., LIBLAU, R. S. & BECHER, B. 2015. Innate and adaptive immune responses in the CNS. *Lancet Neurol,* 14**,** 945-55.

WANG, L., DANKERT, H., PERONA, P. & ANDERSON, D. J. 2008. A common genetic target for environmental and heritable influences on aggressiveness in Drosophila. *Proc Natl Acad Sci U S A,* 105**,** 5657-63.

WANG, X., ZHAO, L., ZHANG, J., FARISS, R. N., MA, W., KRETSCHMER, F., WANG, M., QIAN, H. H., BADEA, T. C., DIAMOND, J. S., GAN, W. B., ROGER, J. E. & WONG, W. T. 2016. Requirement for Microglia for the Maintenance of Synaptic Function and Integrity in the Mature Retina. *J Neurosci,* 36**,** 2827-42.

WANG, Y., CELLA, M., MALLINSON, K., ULRICH, J. D., YOUNG, K. L., ROBINETTE, M. L., GILFILLAN, S., KRISHNAN, G. M., SUDHAKAR, S.,

ZINSELMEYER, B. H., HOLTZMAN, D. M., CIRRITO, J. R. & COLONNA, M. 2015. TREM2 lipid sensing sustains the microglial response in an Alzheimer's disease model. *Cell,* 160**,** 1061-71.

WHEELER, M. A., HEFFNER, D. L., KIM, S., ESPY, S. M., SPANO, A. J., CLELAND, C. L. & DEPPMANN, C. D. 2014. TNF-alpha/TNFR1 signaling is required for the development and function of primary nociceptors. *Neuron,* 82**,** 587-602.

YASUI, D. H., XU, H., DUNAWAY, K. W., LASALLE, J. M., JIN, L. W. & MAEZAWA, I. 2013. MeCP2 modulates gene expression pathways in astrocytes. *Mol Autism,* 4**,** 3.

YEDNOCK, T. A., CANNON, C., FRITZ, L. C., SANCHEZ-MADRID, F., STEINMAN, L. & KARIN, N. 1992. Prevention of experimental autoimmune encephalomyelitis by antibodies against alpha 4 beta 1 integrin. *Nature,* 356**,** 63-6.

YONA, S., KIM, K. W., WOLF, Y., MILDNER, A., VAROL, D., BREKER, M., STRAUSS-AYALI, D., VIUKOV, S., GUILLIAMS, M., MISHARIN, A., HUME, D. A., PERLMAN, H., MALISSEN, B., ZELZER, E. & JUNG, S. 2013. Fate mapping reveals origins and dynamics of monocytes and tissue macrophages under homeostasis. *Immunity,* 38**,** 79-91.

ZALA, S. M., MÄÄTTÄNEN, I. & PENN, D. J. 2012. Different social-learning strategies in wild and domesticated zebrafish, Danio rerio. *Animal Behaviour,* 83**,** 1519-1525.

ZHAN, Y., PAOLICELLI, R. C., SFORAZZINI, F., WEINHARD, L., BOLASCO, G., PAGANI, F., VYSSOTSKI, A. L., BIFONE, A., GOZZI, A., RAGOZZINO, D. & GROSS, C. T. 2014. Deficient neuron-microglia signaling results in impaired functional brain connectivity and social behavior. *Nat Neurosci,* 17**,** 400-6.